

Preserving the Integrity of the Highly Dynamic Bacterial Replisome

McGill University

Doctoral Thesis

Author

Nicolas Soubry

Supervisor

Dr. Rodrigo Reyes-Lamothe

December 2020

*A thesis submitted to McGill University in partial fulfillment of the requirements of the degree of
Doctor of Philosophy*

Nicolas Soubry 2020

Department of Biology

*I dedicate this thesis to all my family, friends and McGill Lacrosse for all their
support*

Acknowledgements

First, I need to thank my supervisor, Dr. Rodrigo Reyes-Lamothe, for helping me navigate these past six years of my life. I still remember calling Rodrigo, visiting Montréal, and him calling me back to tell me he wanted me in his lab. I remember listening to the song *You & Me* by *Disclosure* on the way to work that day, so glad I was leaving the retail store I worked at, going to study science at the same university my mother had attended. It is a moment I will never forget. Rodrigo helped me curve my obsessive tendencies to get out of roadblocks and focus on why I hit a roadblock more than trying to get past a roadblock by brute force. He helped me push my curiosity and try new things I had never done, letting me figure it out. That process helped me develop problem-fixing skills I did not know I had. He also let me follow my passions outside of the lab, which has led me to be the head coach for the McGill Redbirds varsity lacrosse team.

Second, I want to thank all the past and current members of the Reyes Lab. We became a family, though we all had different backgrounds. They helped me get out of my little nest and explore the world a bit. I would like to give special thanks to Thomas Beattie and Ziad El Hajj. Both postdoctoral fellows helped me learn the wet lab aspect of my work. They were very patient with me and taught me that there are many ways to make strains, even when the first does not work. Lab work is like an ever-changing puzzle. It sounds complex, but once you have the rhythm, things just work. Their patience is something I have learnt is essential in teaching others. I would also like to thank Ziad for sharing his tea obsession with me. I am sad we never opened a David's Tea bar in the office. I would also like to thank Nitin Kapadia and Baljot Parmar for teaching me how to write code. I do not think the success of my Ph.D. would have been possible without that skill.

I would like to thank my committee members, Prof. Richard Roy and Prof. Gonzalo Cosa. Their feedback has helped me grow as a scientist. It also pushed me to think outside the box and communicate my ideas to others who are not in the same field. Specifically, the skill of not knowing an answer, not panic and speculating to the best of my ability.

None of this work would be possible without help from my partner in crime, Camille Bodnar. She has been a sounding board for my wild ideas from the start. She had dealt with my excitement when things worked and my disappointment when things did not. I am sure at first, she did not know what I was talking about, but she let me say what I had to say and, with time, learnt precisely what I was doing. Her enthusiasm helped me write this thesis during COVID when I just wanted to push it off and keep writing helpful code for the lab. She and our dog Luna have been my co-pilots during this ride!

Next, I would like to thank my friends and family, especially my parents, Mark and Sonia. As with most family members of Ph.D. students, they never fully understood what my Ph.D. was all about, but they were always there to encourage me because they knew I was passionate about my work and science in general and what it meant to me. Both of my parents are not scientists, but they motivated me in their own ways. My mother for her constant support, dropping off goodie bags at the house during COVID, helping me by being around. My father, for the long calls, asking me where I was in my thesis and wanting to know more information. Hopefully, I will have told them enough to understand it a bit when they read this.

Lastly, I would like to thank the McGill Lacrosse family. I feel like the luckiest man alive for being able to accomplish two dreams at once. I would like to thank my mentor Tim Murdoch for his constant positive attitude and the players for their trust in me.

Statement of Originality

Nicolas Soubry claims the following parts of the thesis are distinct contributions of original knowledge and original scholarship.

- Observed the replication slowdown of the DNA polymerase after UV irradiation. Observed the binding of replication forks away from the replication fork via a clamp loader subunit χ . Developed analysis methods to quantify bound molecules (Chapter 3). Published in Soubry et al. *Proceedings of the National Academy of Sciences* 2019; 201819297
- Characterization of the clamp loader subunit χ in the maintenance of the dynamic replisome (Chapter 4). Manuscript in preparation: Soubry, N., et al. 2020.

Contribution of Authors

This thesis is manuscript-based. Chapters 3-4 are based on manuscripts

Chapter 3

I collected and analyzed all of the data. I developed the analysis for the bound proportions and replication speed measurement. I also created most of the strains. Andrea Wang started the project and contributed to the findings. R. Reyes-Lamothe made the simulations, wrote the manuscript and supervised the project.

Chapter 4

I conducted some of the single-molecule experiments, developed the rebinding analysis, analyzed the data, wrote MATLAB code for image analysis and wrote the manuscript. C.V Lopez Jauregui & J.P. Rascon Perez did all of the snapshot images and some of the single-molecule experiments. R. Reyes-Lamothe supervised the project.

Abstract

The replication of DNA is a critical step that every cell needs to complete once every cell cycle. Repercussions from errors in DNA replication can be very costly to the cell, from simple DNA repair to cell death. The multi-protein complex known as the replisome is responsible for completing DNA replication faithfully. Recent data have refuted the belief that the replisome is a stable assembly in *Escherichia coli* (*E. coli*); instead, it is highly dynamic. However, it is unclear in this new model how the replisome maintains its integrity when some of its subunits turnover every few seconds. To address this question, I used fluorescent microscopy to directly assess what happens to replisome components when they encounter DNA damage and identify factors required for the replisome's dynamic behaviour.

In this work, I first investigate the effect of DNA damage caused by ultraviolet (UV) light on the replisome. I reveal that the activity of the replisome continues after UV irradiation, albeit at a reduced rate. The active DNA polymerase may stall at the site of DNA damage, but because of its dynamicity, another DNA polymerase continues with DNA replication after the lesion on DNA is skipped. I show that additional copies of DNA polymerase are recruited elsewhere on the chromosome, presumably to aid in DNA repair. This recruitment is independent of ongoing DNA replication but requires χ , a clamp loader accessory protein. This finding led me to investigate the role of χ during normal DNA replication. I show that χ increases the DNA-bound proportion and allows for more efficient recycling of the DNA polymerase and the clamp loader (together called Pol III*), most likely by reducing the time needed to search for the replication fork. My data suggests the Pol III* uses the interaction between χ and SSB to increase the binding surface during its search. This work exposes the strategies that a dynamic replisome uses to keep its integrity during DNA replication, providing clues on how all bacteria preserve their DNA's integrity during this essential cellular process.

Résumé

La réplication de l'ADN est une étape critique que toutes les cellules doivent compléter une fois par cycle cellulaire. Les conséquences des erreurs dans la réplication de l'ADN peuvent être très coûteuses pour la cellule, pouvant aller jusqu'à la mort de celle-ci. En fait, le complexe multi-protéines connu sous le nom du réplisome est responsable de compléter fidèlement la réplication de l'ADN. Des données récentes ont réfuté la croyance selon laquelle, chez *Escherichia coli* (*E. coli*), le réplisome est un assemblage stable. Au contraire, le réplisome serait plutôt très dynamique. Toutefois, il n'est pas clair dans ce nouveau modèle comment le réplisome maintient-il son intégrité lorsque certaines de ses sous-unités sont échangées après quelques secondes. Afin de répondre à cette question, j'ai utilisé la microscopie fluorescente pour évaluer directement ce qui arrive aux composantes du réplisome lorsqu'il rencontre une partie endommagée de l'ADN et pour identifier les facteurs requis pour maintenir le comportement dynamique du réplisome.

Dans ce travail, j'étudie d'abord l'effet des dommages causés à l'ADN par la lumière ultraviolette (UV) sur le réplisome. Je révèle que l'activité du réplisome se poursuit après une irradiation UV, mais à une vitesse réduite. Le Pol III HE actif peut s'arrêter au site endommagé sur l'ADN mais en raison de sa dynamique, une autre copie de Pol III* continue la réplication d'ADN après avoir passé la lésion. Je démontre aussi que des copies supplémentaires de Pol III HE sont recrutées ailleurs sur le chromosome, probablement pour aider à la réparation de l'ADN. Ce recrutement est indépendant de la réplication de l'ADN, mais nécessite la présence de χ , une protéine accessoire du chargeur de *clamp*. Cette constatation m'a amené à étudier le rôle de χ pendant la réplication normale de l'ADN. Je montre que χ augmente la proportion de Pol III* liée à l'ADN et l'efficacité du recyclage du Pol III* et ce, probablement en réduisant le temps nécessaire à la recherche de la fourche de réplication. Mes résultats suggèrent que le Pol III* utilise l'interaction entre χ et le SSB pour augmenter la surface de liaison pendant sa recherche pour la fourche. Ce travail expose les stratégies qu'un réplisome dynamique utilise pour maintenir son intégrité pendant la réplication de l'ADN, fournissant des indices sur la façon dont toutes les autres bactéries préservent leur ADN intact au cours de ce processus cellulaire essentiel.

Table of Contents

Acknowledgements	iv
Statement of Originality	vi
Contribution of Authors	vii
Abstract	viii
Résumé	ix
Chapter 1: Introduction	1
Chapter 2: Introduction to DNA Replication and Repair	4
2.1 Deoxyribonucleic Acid.....	4
2.2 Organising DNA in Bacteria.....	5
2.3 Structure of the <i>E. coli</i> replisome.....	8
2.4 Initiation of DNA replication in <i>E. coli</i>	10
2.5 Chromosome Replication.....	11
2.6 Termination of Replication.....	15
2.7 DNA Damage Repair.....	16
2.8 Fluorescence Microscopy.....	25
Chapter 3: Replisome activity slowdown after exposure to ultraviolet light in <i>Escherichia coli</i>	29
3.1 Abstract.....	30
3.2 Significance Statement.....	30
3.3 Author Contributions.....	30

3.4 Introduction.....	31
3.5 Results.....	34
3.5.1 Pol III Holoenzyme is Recruited to Multiple Sites in the Nucleoid after Exposure to UV Light.....	34
3.5.2 Slowdown in the Rate of DNA Synthesis is Only Partially Explained by Replisome Disassembly.....	36
3.5.3 Recruitment of the Pol III HE does not Require Active Replication....	38
3.5.4 Recruitment of the Pol III HE Outside the Replication Fork Depends on the χ Subunit of the Clamp Loader.....	40
3.5.5 Exposure to UV Light Changes the Binding Dynamics of the Pol III HE.....	41
3.6 Discussion.....	43
3.6.1 A Fast-Acting Rate Switch Strategy as Response to DNA Damage....	44
3.6.2 Continued DNA Replication After UV Supports a Replisome Lesion Skipping Model.....	45
3.7 Experimental Procedures.....	45
3.8 Supplemental Information.....	46
3.9 Acknowledgments.....	46
3.10 References.....	47
 Chapter 4: The χ Subunit of the Clamp Loader Promotes Fast Search Times and Increases Local Concentration of DNA Polymerase in <i>Escherichia coli</i>.....	 51

4.1 Abstract.....	52
4.2 Introduction.....	52
4.3 Results.....	54
4.3.1 The χ subunit contributes to the recruitment of the Pol III* to the replisome.....	54
4.3.2 The χ subunit contributes to the probability of recruitment and the length of Pol III* binding to the replisome.....	56
4.3.3 The χ subunit enables rapid rebinding of the Pol III* molecules to the replisome.....	58
4.4 Discussion.....	60
4.4.1 $\chi\psi$ are the hub needed to maintain a dynamic replisome.....	61
4.5 Experimental Procedures.....	63
4.5.1 Strains and growth conditions.....	63
4.5.2 Imaging.....	64
4.5.3 Spot counting analysis.....	64
4.5.4 Single molecule experiments and analysis.....	65
4.6 Acknowledgments.....	66
4.7 References.....	67
4.8 Tables.....	70
Chapter 5: Conclusions.....	71

Appendix 1: Methods	74
A1.1 Experimental Model and Subject Details.....	74
A1.2 Method Details.....	74
A1.2.1 Strains and construction.....	74
A1.2.2 EdU incorporation.....	75
A1.2.3 Dilution plating.....	75
A1.2.4 Microscopy.....	76
A1.2.5 Image analysis.....	78
A1.2.5.1 Spot counting and colocalization analysis.....	78
A1.2.5.2 Diffusion analysis.....	79
A1.2.5.3 Dwell time analysis.....	79
A1.2.5.4 Rebinding analysis.....	80
A1.2.6 Simulation of cell cycle progression.....	81
A1.3 Strain List.....	82
Appendix 2: Supplementary Information for Replisome activity slowdown after exposure to ultraviolet light in <i>Escherichia coli</i>	84
A2.1 Supplementary Experimental Procedures.....	84
A2.1.1 Strains and growth conditions.....	84
A2.1.2 EdU Incorporation.....	85

A2.1.3 Imaging.....	85
A2.1.4 Spot counting and colocalization analysis.....	86
A2.1.5 Single molecule experiments and analysis.....	86
A2.1.6 Dilution Plating.....	87
A2.1.7 Simulation of cell cycle progression.....	88
A2.2 Supplemental Figures.....	89
A2.2.1. 25 J/m ² of UV exposure mildly affects fluorescent-fusion cell viability.....	89
A2.2.2. Characterization of strains at the microscope.....	90
A2.2.3. Distribution of foci per cell.....	91
A2.2.4. Recruitment of ϵ after UV.....	92
A2.2.5. Replisome components remain in vicinity to each other after UV exposure.....	93
A2.2.6. Persistence of DNA synthesis after UV.....	94
A2.3 Supplemental Tables	95
A2.3.1. Stains used for this study.....	95
A2.3.2. Plasmids used for this study.....	97
A2.3.3. Primers used for this study.....	98
A2.3.4. Number of repeats and total cell count for each Figure.....	99
A2.4 References.....	103

Chapter 6: References..... 104

**Annex 1: Interaction with single-stranded DNA-binding protein localizes ribonuclease
HI to DNA replication forks and facilitates R-loop removal**..... 115

Chapter 1

Introduction

For cells, deoxyribonucleic acid or DNA is the molecule that stores all information needed for their survival. Changes (mutations) to that code can provide a cell with an advantage over others of its species. However, most of the time, mutations lead to problems that, in the wrong conditions, can, in turn, lead to cell death. Cells are particularly exposed to acquire mutations during DNA replication. DNA replication is a process where the parental DNA is replicated in a semi-conservative manner [1]. The result is two sets of DNA double strands, half of the strands coming from the parent and the other half newly replicated DNA. DNA replication requires unwinding the double-stranded parental copy into single-stranded DNA, which is catalyzed by the replicative helicase. Then a DNA polymerase faithfully copies the parental strand to generate a complementary strand. Other proteins are needed to ensure coordination between the helicase and DNA polymerase. These proteins assemble into a multiprotein molecular machinery called the replisome [1].

The replisome of *Escherichia coli* (*E. coli*), a gram-negative bacterium, has been the focus of intense study for at least half a century, using genetic manipulation, biochemical assays, and, more recently, single-molecule fluorescent microscopy techniques. Single-molecule fluorescent microscopy techniques like stepwise photobleaching or single-particle tracking photoactivatable localization microscopy (sptPALM) have brought new insight into the behaviour of the bacterial replisome [2-7]. A recent development has been the discovery of the dynamicity of replisome components. Multiple labs have shown *in vivo* and *in vitro* that the DNA polymerase is highly dynamic, with exchanges happening on the order of seconds amounting to anywhere between 3 – 10 kilobase pairs (kbp) of replicated DNA [2, 3]. Previous biochemical data had pointed toward a stable binding of the DNA polymerase, on the order of minutes and replicating an average of 70 kbp of DNA [8, 9]. The subunit exchange at the replisome has provided a new lens to examine old questions in the field and has opened a new set of questions on its underlying mechanisms.

Copying of the sequence of DNA during replication is done with exquisite fidelity. In bacteria, it is estimated that the mutation rate is 10⁻¹¹ per nucleotide (nt) per round of replication [10]. In great part, this is due to the low mutation rate of the catalytic subunit (α) of the Pol III

DNA polymerase. The ϵ subunit of Pol III, which is a proof-reading exonuclease, reduces the mutation rate even more. Factors contributing to the low mutation rate also include components that are not part of the core replisome [10]. For example, the Mismatch Repair (MMR) pathway removes mutations in the newly synthesized DNA [10].

However, most mutations do not arise from errors by the replication machinery. External mutagens like UV irradiation or chemical products also cause mutations to the DNA template [11]. If the DNA lesion is bulky enough to interrupt the DnaB helicase progression, a cascade of DNA repair mechanisms, like homologous recombination repair, are activated, usually through the SOS response [12]. Nevertheless, what about when the helicase can bypass the DNA lesion without destabilizing it? Two divergent models have been proposed, either the DNA polymerase is stalled by the DNA damage [13] or the DNA polymerase hops over the DNA damage and continues its replication [14]. Based on data in this work, I propose that the replisome's dynamic nature confirms both models. The DNA polymerase's dynamicity allows the original Pol III* to be stalled and a new copy of Pol III* to replace it.

Chapter 2 will provide a review on DNA replication and DNA repair during replication to give context for this thesis. This context will be in the *E. coli* organism, which was the model system used for the work presented in Chapters 3 - 4

Chapter 3 will describe what happens to the DNA replication machinery when it encounters UV damage. Unexpectedly, I found that DNA replication continues, albeit at a reduced rate. I also found that the Pol III HE is recruited elsewhere on the chromosome, that this recruitment is independent of DNA replication, and that χ , a clamp loader accessory protein, was needed for that recruitment. This work was published in *Proceedings of the National Academy of Science* (2019), where I am the first author.

Chapter 4 builds on the previous chapter by investigating the role of χ in normal DNA replication using single-molecule fluorescence microscopy techniques and degradation techniques. I found that χ is an essential piece in maintaining a dynamic replisome. It increases

the bound proportion of the DNA polymerase while also increasing the active site's competition at the replication fork. The presence of χ also increases the rate of rebinding of the Pol III*, most likely by reducing the search time. It does this through its interaction with SSB, which provides a larger binding surface.

Lastly, chapter 5 will serve as a summary and a discussion of the results presented in the thesis. Included will be an outlook into future work.

Chapter 2

Introduction to DNA Replication and Repair

This literature review will focus on *E.coli* DNA replication and repair, specifically how the replication machinery is built to adapt to any change quickly.

2.1 Deoxyribonucleic Acid

One of the essential molecules in life is deoxyribonucleic acid or DNA. All known non-viral organisms are coded in DNA, and even most viruses deal with DNA at some point of their life cycle; only viruses in classes 3-5 viruses never have a DNA intermediate [15]. For all other life forms, DNA is the code for all other biological molecules. Since 1869, in which chemist Friedrich Miescher first described “nuclein,” the scientific community has been studying DNA [16]. Tremendous progress has been made since its discovery. In the first part of the 20th century, Oswald Avery and Frederick Griffith to understand pneumococcal infections led to the surprising discovery of DNA as the hereditary material [17-20]. From then on, the work done to understand DNA has been countless. There were many open questions then, and still today, the study of DNA reveals new data.

The description of the double helix structure of DNA proposed by Watson and Crick was a ground-breaking achievement. They built off work done by Erwin Chargaff, Rosalind Franklin and Maurice Wilkins [21-23]. Their model had four major features (later scientists have made some minor changes): 1. DNA is a double-stranded helix connected by hydrogen bonds. Adenine bases pair with thymine bases, and cytosine pairs with guanine. 2. The double-stranded helices are almost always right-handed. 3. The double-strand helix is anti-parallel; the 5' end of one helix is matched with the 3' end of the other helix. 4. The nitrogen-containing outer edges of each base provide another scaffold for hydrogen bonds, providing easy access for proteins to the DNA [24]. They even hypothesized on how DNA was copied, “It has not escaped our notice that the specific pairing we have postulated immediately suggests a possible copying mechanism for the genetic material” [24]. The structure was well described with their seminal work, but it took a few years before we understood how to replicate that DNA into two strands.

From the structure, three models for replication had been stipulated. The first that replication was semi-conservative, where the parental strands would separate, and a copy of itself would be made. After replication, the daughter strands contained each an old and new strand of DNA. The second model stipulated that replication was conservative, where the parental DNA molecule would be replicated so that after replication, there would be that parental DNA molecule and a completely new DNA molecule. In the last model, the dispersive model, DNA from the parental strands is distributed randomly in both daughter strands. Matthew Meselson and Franklin Stahl decided to test these models by using isotope labels. The idea was good, as it was able to test these three models by distinguishing new and old DNA utilizing isotope labelled DNA. Using ^{15}N and ^{14}N nitrogen with *Escherichia coli* or *E. coli*, they discovered that newly synthesized DNA was semi-conservative [25, 26]. Following this discovery, many other scientists confirmed their results in many other species as well.

2.2 Organising DNA in Bacteria

Though Watson and Crick discovered the structure of DNA, information on how that DNA was organized in cells was provided much earlier. In the 19th century, Walther Flemming developed a new microscopy technique to describe the fibrous network within the nucleus, coined chromatin [27]. This discovery was in a eukaryotic cell as eukaryotic cells happen to have a striking metaphase plate. In 1910, Thomas Hunt Morgan connected heredity and the chromosome. He stipulated that “material common” to both the parent and offspring was responsible for the transmission of “characters” [28]. Prokaryotic cells being much smaller, took till the work from Avery, previously mentioned above, in the 1940s for a scientist to discover that bacteria also undergo mutation, thus had mutable genes and some form of a chromosome. This discovery was highlighted by the finding that DNA was the transmitted molecule [19]. By 1952, the nucleoid was first seen in living cells. By the early 1970s, whole compact chromosomes were being isolated for biochemical studies [29].

Bacterial chromosomes, differing from eukaryotic chromosomes, can be found in either circular or linear form. Many bacteria carry all of their genes on a single circular chromosome, like *E. coli*, while others carry their essential genes on numerous chromosomes, like *Vibrio cholerae*, which has two chromosomes. Some *Agrobacterium* species contain one circular- and

one linear-mapping chromosome [29]. While linear chromosomes and the presence of multiple chromosomes per cell have usually been associated with eukaryotes, what distinguishes bacterial and eukaryotic chromosomes is the coupling between replication and segregation; it is flexible in bacteria while tight among eukaryotes. For eukaryotes, a nuclear chromosome never contains more than one genome equivalent of DNA as it segregates to daughter cells. In bacteria, there can be one or many genome equivalents of DNA even during segregation, especially in optimal conditions.

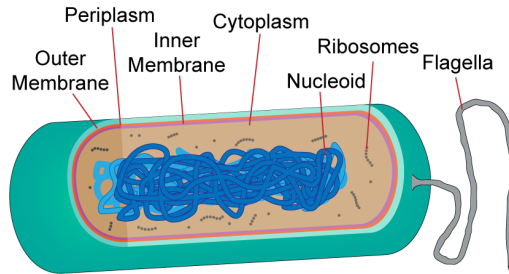


Figure 2.1: Schematic of the *E. coli* cell. Not shown are pili and capsule, as pili are only formed when the conjugation apparatus is expressed, and the capsule is not present in most lab grown strains.

E. coli, a rod-shaped, Gram-negative bacteria, has one singular circular chromosome about 4.6 million base pairs (Mbp) long (**Figure 2.1**). That is equal to a contour length of 1.6 mm in a cell of $< 6 \mu\text{m}$ long [30]. DNA is contained in the nucleoid in a negative supercoiled state [31], and can contain up to 4-fold this amount that as the cell grows [32]. More than just DNA, the nucleoid also contains all of the DNA-binding proteins. At the electron microscope, the nucleoid appears as a fine compact structure surrounded by the cytoplasm and polyribosomes [29]. This structure seems to be maintained by molecular crowding caused by polyribosomes, polyribosomes-associated proteins, RNA and other proteins [29, 33, 34].

Inside the nucleoid, the chromosome is organized by nucleoid-associated proteins (NAPs) like the structural maintenance of chromosome (SMC) complex, MukBEF, the histone-like structures (H-NS), the Histone-like protein HU, the Integration Host Factor (IHF), and the Factor for Inversion Stimulation (Fis), among others [35]. For example, MukBEF binds and bridges distant DNA segments, organizes the chromosome [36], and H-NS proteins are tasked with DNA compaction and inhibiting transcription [33].

In addition to NAPs, DNA supercoiling and molecular crowding serve to compact and organize the chromosome [37]. Understanding the organization of the chromosome in cells has been dramatically advanced by applying Hi-C, a Chromosome Conformation Capture (3C)-based method. Results in *E. coli* and *Caulobacter crescentus* help disentangle the relationship between chromosome organization, NAPs and transcription at these different scales[38].

Fluorescence microscopy has shown that, at the beginning of the cell cycle of slow-growing cells, the origin of replication *oriC* is located mid-cell [39, 40]. The chromosome then has a left arm, a right arm and the terminus of replication, *ter*, located opposite the *oriC*. The *oriC* is a central figure on the chromosome as it is the only site where replication can begin. The termination of replication does not occur at a specific spot on the chromosome but more in a general area. At the genetic level, the chromosome maintains a precise organization, where genes are oriented in a defined manner to minimize replication and transcription conflicts along with regulating expressions level [41].

The *E. coli* cell cycle is dependent on its growth conditions. In slow-growth conditions, this cycle is well defined. The first stage is the B period. This stage starts at the birth of the new cell and ends at the initiation of DNA replication. The complete process of DNA replication is done during the C period. Between the end of DNA replication and bacterial division is the D period. Slow growth is marked by the generation time being longer than the combined C-D periods [42]. The generation time is shorter in fast growth than the combined C-D periods, as multiple DNA replication events are overlapped [43-45]. In this case, there is no B period. In general, the cell cycle is defined by replication initiation and bacterial division. Both of those processes seem to be regulated by cell size. Three interrelated principles describing the cell cycle's connection to cell size and DNA replication emerged from this early work. First, the bacterial cell volume depends exponentially on the growth rate and increases exponentially as growth proceeds [43]. Second, when the generation time is shorter than the replication time, the C and D periods' combined time is constant and independent of the growth rate [44]. Third, DNA replication initiation occurs at a fixed cell volume per origin [45]. Newer methods have added to these three principles. Seemingly, DNA replication initiation is a reset point in the cell cycle regulation, as the

initiation of *E. coli* DNA replication occurs at a fixed cell volume per origin (*oriC*), independent of birth size and growth rate in individual cells [32, 46-48].

2.3 Structure of the *E. coli* replisome

For all bacterial species, the replication of their chromosome is an important event. This event will lead to the generation of daughter cells and the survival of their species. However, mistakes or some events that may occur during the replication event can threaten the survival of the individual. Thus, the cell must achieve high fidelity, processivity, and efficient repair to ensure DNA replication is a successful event. DNA replication starts at the *oriC*, from where two replication forks originate. One replication fork will travel down the chromosome's left arm, making this section of the chromosome the left replichore. The other down the right, making it the right replichore. A multi-protein complex known as the replisome is in charge of replication each of the two replichores. Each replisome has the same template, a duplex strand of DNA where the leading strand goes from the 5' to 3' orientation, while the lagging strand goes in the opposite direction, 3' to 5'.

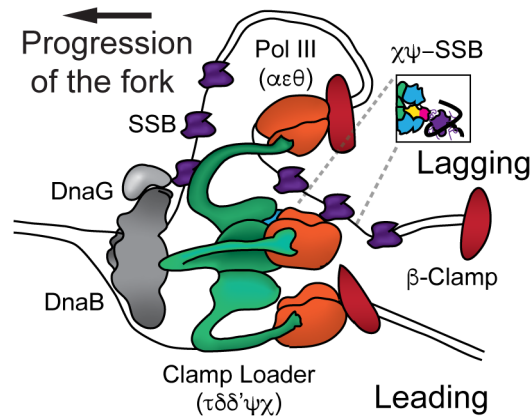


Figure 2.2: Model of the architecture of an active replisome. DNA is unwound by the DnaB helicase. DnaG primase binds to DnaB. Pol III and the clamp loader bind each other through the τ subunit of the clamp loader, which also mediates binding to the DnaB helicase. The β -clamp is left behind the fork after the completion of an Okazaki fragment at the lagging strand. SSB covers ssDNA produced during the cycle of lagging strand synthesis.

In *E. coli*, the replisome consists of six different protein complexes with various stoichiometries (Figure 2.2). The helicase, DnaB, is a homohexameric protein situated on the lagging strand. The job of the helicase is to unwind the DNA into ssDNA through a steric exclusion

model. SSB, a single-stranded binding protein, protects the DNA from degradation and serves as a recruitment hub, as it can bind many proteins and bind the available ssDNA. The helicase directly interacts with DnaG, the primase, an RNA polymerase that creates a small 12 nt RNA primer needed to initiate DNA replication. The clamp loader complex also has a direct interaction with the helicase. It is a complex built by seven subunits, $\tau_3\delta\delta'\psi\chi$. Both DnaB and Pol III α directly interact with the C-terminal domain of τ ; the clamp loader also provides an architectural function, physically coupling template unwinding with DNA synthesis. The $\psi\chi$ heterodimer directly interacts with SSB. Another function of the clamp loader complex is to load the β -clamp onto DNA. The β -clamp, which binds directly to the DNA polymerase, is required to achieve the processivity needed to synthesize a whole chromosome. The β -clamp can also bind multiple DNA polymerases, giving the replisome the flexibility needed during DNA repair [49].

Last but not least, the replisome contains a DNA polymerase. In *E. coli*, this is the DNA Pol III, a type C polymerase only found in bacteria. It consists of $\alpha\varepsilon\theta$, where α is the catalytic subunit, ε is the proofreading exonuclease and θ , a poorly understood non-essential subunit [50].

The minimal core of an active replisome is the helicase. The helicase is the most stable subunit of the replisome, bound for tens of minutes (913 ± 508 s) [2, 51]. There is one helicase per fork. The helicase has three binding sites for the DnaG primase. This does not necessarily mean that all three sites are occupied. Changing the concentrations of DnaG results in changes to Okazaki fragment length, which are in the range of 0.5-2kb [8]. There is no current published dwell time for DnaG, but it is thought to be a protein that is relatively dynamic and acts in a distributive fashion [4]. The clamp loader complex also binds to the helicase but has no physical interaction with the primase. Estimates of the stoichiometry in live cells have shown that there is one copy of δ , one copy of δ' and four copies of both $\psi\chi$ [6] in a given replisome. The τ subunit that relays the helicase to the DNA polymerase has three copies, just like three copies for the DNA Pol III [6, 52, 53]. Together the clamp loader complex and the DNA Pol III form the Pol III*, bound to DNA for approximately 10s [2]. Lastly, the β -clamp is bound to DNA for longer, ~ 50 s, as it is routinely left behind the replication fork [2]. There are more than 20 copies of this subunit near the replication

fork [54]. When β -clamp binds with the Pol III*, a new complex is formed called the Pol III holoenzyme (Pol III HE).

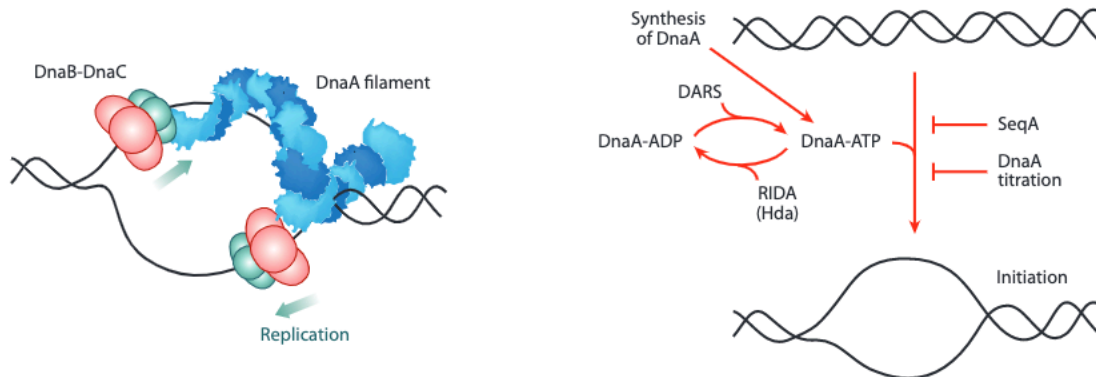


Figure 2.3: In *E. coli*, two separate helicase loadings direct bidirectional replication at *oriC* unwound by DnaA-ATP binding. The schematic on the right outlines the processes that control DnaA-ATP. Synthesis of DnaA and binding of DnaA-ADP to DnaA-reactivation sequences (DARS) promote the accumulation of DnaA-ATP, whereas Hda-mediated activation of DnaA ATPase during regulatory inactivation of DnaA (RIDA) decreases the concentration of DnaA-ATP. Figure taken with permission from [36]

2.4 Initiation of DNA replication in *E. coli*

At the *oriC* is where a replisome's journey through the bacterial chromosome begins. DnaA, a AAA+ protein, recognizes and melts the *oriC* [55]. DnaA bound to adenosine triphosphate is the only active form for DNA replication. Despite huge progress, the molecular basis of this process is not so well understood. The current model proposes that DnaA oligomerizes into a helical filament wrapping around the *oriC* [56]. This torsion destabilizes the neighbouring duplex unwinding element or DUE, leading to the DNA melting [57]. The resulting bubble of SSB-coated ssDNA is where two helicases are loaded onto DNA [58]. This activity is not, however, spontaneous; it is dependent on DnaC [1]. DnaC has been shown to interact both with DnaB and DnaA. DnaC is structurally similar to DnaA and will also form a helical filament around the ssDNA [59]. This configuration enables DnaC to break open the DnaB ring and placing DnaB around the ssDNA [60]. Once around the ssDNA and associated with the DnaG primase, the helicase is activated, allowing for the start of replisome assembly [61, 62]. The loading of DnaB onto ssDNA is done sequentially. Two replication forks will be originating from the *oriC* (**Figure 2.3**) [58]. To explain how a single DnaA filament can direct the loading of two DnaB hexamers, an asymmetric model of DnaB loading has been proposed, where DnaC-DnaB is loaded on one

strand via the interaction of DnaA with DnaC and on the other strand an interaction between DnaA and DnaB [59].

The regulation of DnaA is essential to prevent reinitiation (**Figure 2.3**). First, the rebinding of DnaA to the *oriC* is blocked by DNA adenine methylase (DAM), which methylates the A residues in GATC sequences. There are 11 such sequences in the *oriC* [63]. SeqA, a replication initiation inhibitor, binds hemimethylated DNA, blocking the docking of DnaA-ATP. The *dnaA* gene, which likewise contains multiple GATC sequences, is also bound by SeqA, resulting in inhibition of transcription of DnaA [63]. Secondly, during initiation, DnaA-ATP will also bind its own promoter, blocking its own transcription [63]. Next, the DnaA-ATP form is reduced once replication starts through the DnaA (RIDA) system's regulatory inactivation. This system relies on the β -clamp, DnaA homologue protein (Hda), and ADP. Hda has a β -clamp binding site and an AAA+ domain that interacts with DnaA. This interaction stimulates the hydrolysis of DnaA-bound ATP [63]. With less DnaA-bound ATP, there is less chance of reinitiation. Lastly, DnaA binding sites within the *datA* locus titrate away DnaA from the *oriC* [63]. This site is part of the DDAH pathway, which stimulates DNA-ATP hydrolysis independent of the RIDA system [64]. Once the cell is ready to start a new cell cycle, DnaA-reactivating sequences (DARS) reactivate DnaA for replication initiation by exchanging bound ADP with ATP. Deleting DARS sites results in impaired replication initiation; only *de novo* DnaA synthesis and possibly regeneration by alternative pathways can provide the minimum amount of ATP-DnaA required to initiate replication [65].

2.5 Chromosome Replication

The prokaryotic DNA polymerase C is unique within the family of DNA polymerases. The eukaryotic polymerase, a B family polymerase, copies DNA at a rate between 17 - 33 base pairs per second (nt s^{-1}) [66]. Most other families copy DNA near the same rate and always in the same order of magnitude. The *E. coli* DNA polymerase replicates DNA at astounding rates, ranging from 200-1800 nt s^{-1} [9, 67, 68]. Experiments *in vivo* and *in vitro* agree that prokaryotic replisomes copy DNA at a rate at least one order of magnitude faster than eukaryotes. This rate cannot be explained by any individual subunit but rather by their interaction at the replisome. This explains why in the absence of the interaction between τ with the helicase, the helicase and DNA polymerase move at a rate of only $\sim 35 \text{ nt s}^{-1}$ [69]. Uncoupling of the helicase and Pol III HE can

lead to a replication slowdown, more on that in Chapter 3 [70]. The interaction between the τ subunit of the clamp loader and the helicase seems essential for fast replication, coupling unwinding and DNA synthesis [69].

When a replisome is in action, one DNA polymerase, deemed the leading strand polymerase travels in the 5' to 3' direction with the helicase (**Figure 2.2**). The other strand is the lagging strand; the polymerase replicating this strand is playing catch up as the DNA polymerase III only replicates in the 5' to 3' direction. All of this is arranged symmetrically through their interaction with the clamp loader. The replisome has evolved to ensure that DNA unwinding and synthesis proceed uninterrupted by allowing the accumulation of ssDNA loops between Pol III and the helicase on the lagging strand. These loops are rapidly bound by SSB, which protects them from damage. The cyclical assembly, growth and disassembly of these loops, which accompanies the synthesis of each Okazaki fragment, has been compared to the slide of a trombone, hence the trombone model of DNA replication [71]. Interestingly, the presence of such trombone loops has been directly observed in simpler bacteriophage replisomes by electron microscopy and single-molecule biophysical studies [72, 73] but not yet in *E. coli* replication.

Multiple activities need to occur to synthesize the lagging-strand: first, a 12 nt RNA primer synthesis by DnaG, then loading of the clamp onto primer-template by the clamp loader, next is the loading of Pol III onto the template, and finally the release of Pol III from both the clamp and DNA upon competition of an Okazaki fragment. DnaG, however, dissociates after synthesizing an RNA primer leaving an exposed primer-template. The δ subunit of the clamp loader breaks open the β clamp ring through ATP hydrolysis, allowing the clamp to be loaded onto the primer-template [74]. The τ subunit of the clamp loader helps recruit Pol III to the β clamp at the primer-template, then DNA synthesizing begins [74, 75]. Given that the lagging-strand polymerase is recycled to the next primer-template upon completion of an Okazaki fragment, how is the polymerase removed from both DNA and β clamp? There are two common models on Pol III release, the collision-release model and the signal-release model. The first is that Pol III and the τ subunit can sense the rapidly diminishing ssDNA during synthesis, which triggers the release of Pol III, and the second states that a signal triggers the release of Pol III when a new primer is synthesized by the primase [76, 77]. It is inconclusive as to which model is correct, although the

Pol III release may result from other factors discussed below. Finally, for Okazaki fragment maturation, the RNA left from the primer is removed by Pol I, which substitutes the RNA with DNA, and the DNA ligase ligates the left-over nick [75]. This process is facilitated by the β clamp, which has been reported to bind both Pol I and ligase and is left behind on the DNA after being used by Pol III.

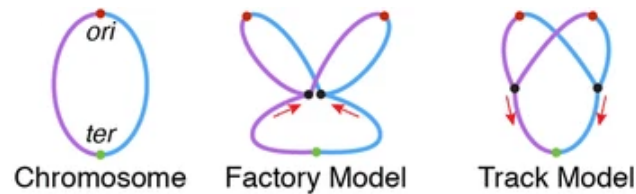


Figure 2.4: Schematic diagrams for the factory and track models. Most bacteria have a single circular chromosome (left), with a single origin (red dot), positioned roughly opposite the terminus (green dot). The left and right arms of the chromosome are colored pink and green, respectively. In the factory model (center), DNA is pulled through the replisomes (black dots) in the direction indicated by the red arrows. In the track model (right), replisomes translocate along the template DNA. Red arrows indicate the direction of replisome motion. Figure taken with permission from [70]

Currently, there are two models for the interconnectedness of replisomes after initiation (**Figure 2.4**). The first model is that DNA replication occurs in factories [78, 79]. This model stipulates that sister replisomes remain spatially co-localized as the replicating DNA is moved towards the stationary replication factory [79]. Two replication foci are only seen during termination and re-initiation of replication in sister cells [78, 79]. The second model, which is currently favoured, is that sister replisomes translocate independently along with the slowly diffusing DNA. In this model, the replisomes are completely independent [6, 39, 48, 80-82].

For a long time, the replisome was thought to be very stable; due to the replication rate and the extent of DNA replication one replication fork must complete. This was supported by in vitro data showing that a single purified replisome, once assembled on DNA, can synthesize 70 kbp of DNA without requiring replacement of the Pol III* subassembly or DnaB [8, 83]. Even greater stability has been inferred from in vivo experiments that suggest replication fork collapse is rare during chromosome replication in *E. coli* [84]. In general, chromosomal DNA presents multiple potential blocks to replisome progression. DNA lesions can result in the replisome stalling due to Pol III's inability to use damaged DNA as a template [85]. In any case, the replisome frequently encounters DNA-bound proteins, potentially resulting in pausing or fork disassembly [86, 87].

Multiple mechanisms have been proposed to safeguard replisome integrity during bypass of such obstacles [88-90] and remove bound proteins from DNA [91]. In cases where these strategies are not enough, the cell also has mechanisms to mediate the replisome's reassembly at specific DNA structures that arise following replisome collapse [92]. The mechanisms to safeguard the replisome integrity and replisome reassembly will be discussed further later in the text.

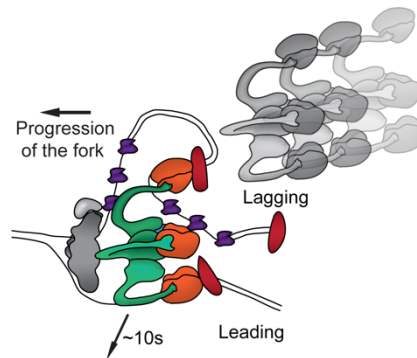


Figure 2.5: Model for the dynamic replisome. The active replisome is only bound for ~10s before it is replaced by another. Mechanism for replacement not known.

The frequency at which replisomes encounter these obstacles and the efficiency of the bypass mechanisms are still unclear. However, the realization that the replisome, specifically the Pol III*, maybe dynamic has provided an additional mechanism to bypass obstacles [2, 3, 70]. The Pol III* is surprisingly dynamic, with exchanges occurring between 4 – 10s in *in vivo* concentrations (**Figure 2.5**) [2, 3]. In contrast, the helicase is stably bound to DNA for periods of at least tens of minutes. The dynamic binding of Pol III* is concentration-dependent; at low concentrations, 0.03 nM Pol III* exchanges take ~ 40s [3]. This exchange rate is also variable depending on what condition the cells find themselves in, as exchange happens with a rate of ~16s after UV irradiation [70]. The cell can use the dynamic behaviour of the Pol III* as a switch to ensure chromosome integrity. Multiple questions remain open on the dynamic behaviour of Pol III*, including what the basis for the rapid exchange is and what are their functional advantages, if any. Given the low copy number of Pol III* in the cell, assuming three copies of Pol III per Pol III* less than 26 copies can be present in the cell [6], recruitment of a new copy of Pol III* after the active copy unbinds needs to be efficient enough as to maintain a DNA replication rate of 1kb per second. How recruitment of Pol III* occurs is the question explored in Chapter 4.

2.6 Termination of Replication

The finale to the replisome's journey is termination, a not well-understood process leading to its disassembly. The *E. coli* replisome does not encounter one hard stop but has multiple terminations sites, known as *Ter* sites. These sites are located near the midpoint of the chromosome, opposite the *oriC*. Each site has polarity in its sequence, giving them a permissive (P) and non-permissive face (NP) (**Figure 2.6.A**) [93]. Once the monomeric Tus protein binds the *Ter* site, they form a barrier to impede the replication fork if it approaches the non-permissive face. This barrier is significant enough to stall the replication fork until the other replication fork approaches from the permissive side, resulting in fork fusion and finally disassembly [94]. The polarity of the Tus-*Ter* interface is due to conformational changes from the unwinding helicase. At the NP interface, the Tus-*Ter* interface is locked, meaning the helicase cannot pass through it. From the P interface, the helicase can rapidly and easily displace Tus (**Figure 2.6.B**) [95].

Nevertheless, *in vivo*, Tus can be displaced by ~50% of replication forks at the NP interface [96, 97]. Replication speed is an essential determinant in the efficiency of the Tus-*Ter* interface. Faster replisomes can pass through the Tus-*Ter* block before adopting the “locked” conformation, while slower ones get trapped [67]. Either way, a *tus* deletion indicated that the Tus-*Ter* interface is not essential [93]. This, combined with other recent data, indicated that the Tus-*Ter* interface limits over-replication, rather than being a definitive termination site [98]

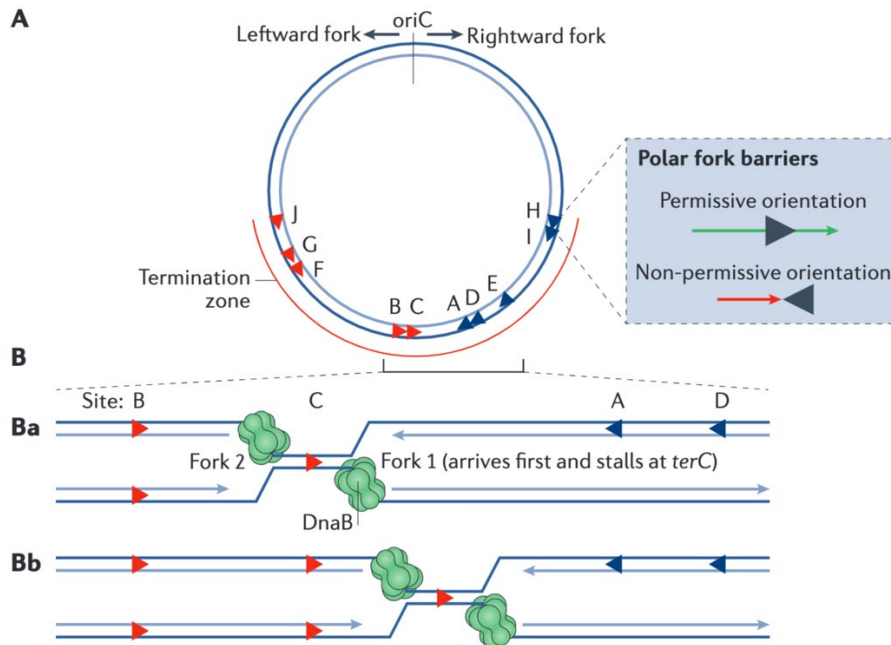


Figure 2.6: Termination of replication (A) Depiction of the *Escherichia coli* chromosome, including the origin of replication *oriC*, and the ten *ter* sites (A–J) shown as red and blue arrowheads. The termination zone is underlined in red. The *ter* sites are oriented such that the leftward fork can pass the first five *ter* sites that it encounters (red arrowheads), but stalls at the next five sites. Conversely, the rightward fork passes through the *ter* sites marked as blue arrowheads and stalls at the following sites. In the box, the green arrow represents a replication fork passing through a *ter* site in the permissive orientation, and the red arrow represents a fork stalling at a *ter* site in the non-permissive orientation. (B) Two scenarios of fork stalling in the termination zone. (Ba) The rightward fork (fork 1) arrives first and stalls at *terC*, followed by the arrival of the leftward fork (fork 2). (Bb) The two forks arrive at the termination zone simultaneously and meet between *terC* and *terA*. Part of figure taken with permission from [87]

2.7 DNA Damage Repair

As expected, the replisome has high fidelity. In general, the estimation of the mutation rate in bacteria is 10^{-9} – 10^{-11} errors per base pair per round of replication [10]. The DNA polymerase III and its exonuclease are responsible for keeping the mutation rate as low as 10^{-6} – 10^{-7} errors per base pair per round of replication, where mismatch repair (MMR) lowers the mutation rate by an additional 10^{-3} . DNA mutations are gained not only by mistakes made by the polymerase but replisome–protein collisions and external mutagens like UV irradiation. How those mutations are repaired is a well-studied field in *E. coli*. Here, I will focus solely on repair mechanisms active during replication.

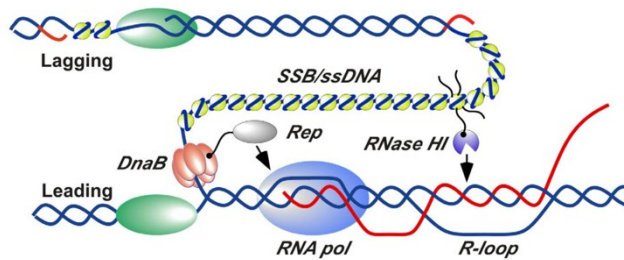


Figure 2.7: Schematic model for RNase HI and Rep helicase localization and action at sites of replication/transcription collision. RNase HI (purple) is localized to the DNA replication fork by interaction with SSB (yellow). Rep helicase (gray) is localized by interaction with DnaB (orange). SSB-Ct tails are shown explicitly for only one SSB tetramer for clarity. DNA strands are shown in blue, RNA strands are shown in red, and DNA polymerases are shown in green. Several replisome components have been omitted or separated for clarity. Figure taken with permission from [7]

One of the best ways not to accumulate DNA damage is to prevent DNA damage. In *E. coli*, cells possess a variety of mechanisms to facilitate replication through blocks on DNA. Accessory helicases like Rep, UvrD and DinG, can remove structures from DNA [99]. Rep is especially a vital candidate as it is known to interact directly with the replication fork [99]. Transcription is an excellent example of a replication block. Orientational bias plays a significant role in the outcome of transcription – replication conflicts. Co-oriented conflicts reduce the number of replisome-stalling, replisome restart and DNA break events. It is thought that this is the reason why a high number of highly transcribed and essential genes are placed in a co-oriented direction. Head-on conflict cause replisome disassembly, DNA break and local mutation rate twice as frequently as co-oriented conflicts [100]. Not only is the RNA polymerase a block to replication, but so are the R-loops formed by the transcription machinery. RNase HI, a ribonuclease that hydrolyzes RNA in RNA: DNA hybrids, is highly colocalized with the replisome (See Annex 1) [7]. In the cases of Rep, RNase HI and many proteins involved in DNA repair, SSB is crucial [7, 101]. Both Rep and RNase HI bind to SSB, and due to the nature of the replisome, constantly creating a pool of SSB, concentrations of Rep and RNase HI are kept near the replication fork.

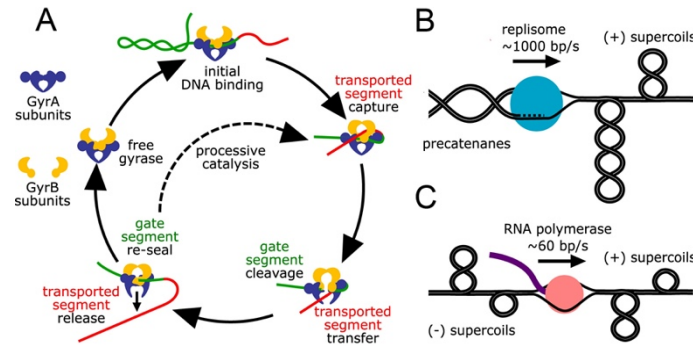


Figure 2.8: The activity of gyrase. (A) DNA gyrase catalytic cycle. (B) Replication introduces (+) supercoils ahead and precatenated DNA behind. Gyrase acts ahead of the fork while topo IV removes precatenanes behind. (C) Gyrase removes (+) supercoiling from ahead of RNAP to ensure unperturbed transcription. Figure taken with permission from [96]

DNA replication can also run into a significant block caused by the process of replication itself, supercoiling. Due to the helical structure of DNA, when the replisome is advancing, it generates massive amounts of positive supercoils ahead of the fork. In covalently closed DNA molecules, the decrease of DNA twist by the strand separation done by the helicase is compensated by increasing writhe [102]. At some point, the stress caused by the unwinding helicase will be less than the need of the DNA to release this torsional stress. At that point, the replisome will be inhibited. Two type II topoisomerases solve this topological problem: DNA gyrase and DNA topoisomerase (topo) IV. These are essential enzymes that change DNA topology by introducing transient double-stranded breaks into DNA and pass a second double-stranded DNA segment through the break before resealing it [103]. Because of the negative supercoiling state of the DNA, the positive supercoiling being added to the front of the replisome and the fact that DNA gyrase is the only topoisomerase that adds negative supercoiling, it plays a prominent role in both DNA replication and transcription (**Figure 2.8.A-C**) [104-107]. The DNA gyrase is not specific to the replisome or transcription bursts. In general, half of the DNA gyrase in a cell is bound to DNA somewhere. The DNA gyrase is also colocalized to the replisome, but that does not form a majority [103]. The gyrase functions by first binding the positive supercoiled DNA (**Figure 2.8.A**); next, it will bind the segment to be transported to release the torsional stress. The DNA is cleaved, and the other segment of DNA will be passed through the gyrase. The cleaved DNA is then resealed. Currently, it is believed the DNA gyrase near the replisome will complete multiple rounds of catalytic activity before unbinding [103]. How the DNA gyrase is recruited to the replication fork supercoils is still a mystery.

If the DNA polymerase does make a mistake in the newly synthesized DNA, DNA mismatch repair is usually used. There are varying types of mismatch repair, but the most often used methyl-directed MTHLS mismatch repair will be briefly described in this report. When the replisome makes a mismatch, the mismatch is bound by MutS and MutL, activating the MutH endonuclease, which can cleave at either side of the mismatch at a methylated site. The UvrD helicase displaces the MutH and unwinds the DNA towards the mismatch. Depending on the side, various exonucleases like RecJ, ExoI, ExoVII or ExoX will digest the single-strand end, leaving naked ssDNA to be bound by SSB and the gap is filled by the DNA Pol III HE. The repair tract for mismatch repair is up to 2kb [108].

The repair tract for base excision repair (BER) and nucleotide excision repair (NER) is much smaller, only 1-2 nt or 12-16 nt [108, 109]. While BER is mainly tasked with replacing uracil or repairing oxidative damage [110, 111], NER is a more prominent player in DNA repair. NER is tasked with removing environmentally induced DNA damage, such as the DNA lesions resulting from sunlight exposure or chemical carcinogens (**Figure 2.9**) [112]. UvrABCD, Cho and Pol I are the proteins involved. UvrA identifies the putative lesion, which recruits UvrB to confirm that the distortion is due to a damaged nucleotide. UvrB then enlists either UvrC or Cho, both endonucleases. UvrC contains two endonucleases domains which cut two nicks 12 nt apart [112]. Cho, however, will be used in conjunction with UvrC when more than 12 nt need to be excised. In that case, UvrC will make a nick, and Cho will make another nick about 16 nt apart [112, 113]. The UvrD helicase then removes the DNA between the two nicks. Lastly, Pol I fills in the empty ssDNA, and the DNA is ligated by the DNA ligase [112, 114].

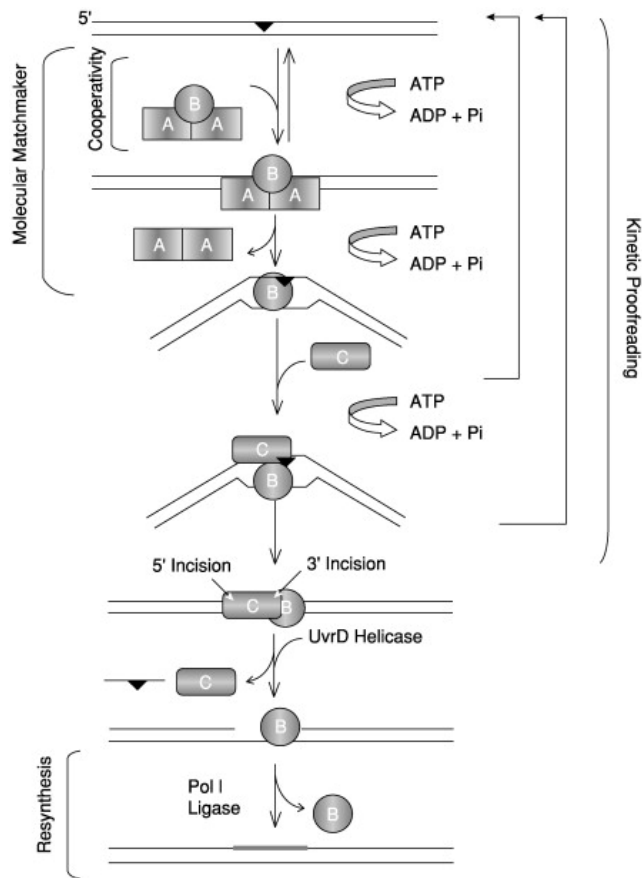


Figure 2.9: Model for excision repair in *E. coli*. UvrA dimerizes in solution and interacts with UvrB to form an A₂B₁ heterotrimer, the damage recognition subunit. UvrA delivers UvrB to the damage site (black triangles) and then dissociates (molecular matchmaker). UvrC recognizes and binds to the UvrB-DNA complex, which is bent and locally unwound. ATP hydrolysis introduces irreversible intermediates at steps along the pathway leading to dual incision and the reaction may be aborted at any step (kinetic proofreading). Dual incisions excise the damage in a 12–13 nucleotide-long oligomer. UvrD (Helicase II) displaces UvrC and the excised oligomer, and then DNA polymerase I displaces UvrB during resynthesis to fill in the gap; newly synthesized DNA (thick gray bar) is ligated to complete the repair reaction. Figure taken with permission from [107]

If there is any extensive ssDNA or replisome collapse, the next step in DNA repair is the SOS response [115]. The LexA repressor regulates the SOS response. LexA is a transcriptional repressor of multiple genes coined SOS genes. This keeps their transcriptional levels low during normal growth. After DNA damage leading to excessive ssDNA, RecA is activated to become a co-protease by forming a filament of RecA on ssDNA. This leads to the self-cleavage action of LexA. As the levels of LexA degrade and diminish, the transcription of SOS genes increases. RecA and LexA have an intertwined cycle, where LexA is heavily favoured in normal condition. However, as more and more ssDNA is made available by DNA damage or the dissociation of the Pol III HE from the helicase, RecA is activated, reducing LexA and increasing SOS genes' transcription.

However, if the amount of ssDNA is slowly reduced by DNA repair, the scales tip again, and the LexA gradually increases. These SOS genes that LexA represses are specific to DNA repair, tolerance of DNA damage and delay of the cell cycle [12, 116]. Notably, Sula is one of the early proteins produced. Its role is to inhibit cell division, providing the cell more time to repair [116]. Another notable product is the translesion polymerases (TLS), Pol II (PolB), Pol IV (DinB) and Pol V (UmuD'2C) [12, 117]. It has been shown that, though the DNA Pol III in normal conditions has a monopoly on the β -clamp and the DNA, during DNA damage conditions where the Pol III will stall, Pol IV will get access to the β -clamp. Failure of TLS will quickly allow for repriming, allowing the Pol III access to the β -clamp and the DNA, with a cost of extra ssDNA. TLS at the fork prevents the creation of ssDNA gaps by outcompeting repriming [117-119]. RecA is not only needed to activate the SOS response, but it is a crucial cog in homologous recombination repair of DNA.

In general, the response to DNA damage during DNA replication is dependent on what happens to the DnaB helicase. If the DNA damage does not inhibit the helicase, then the repair of that damage is very different from if it inhibits the helicase, causing pausing of the replication fork or, worse, replication fork collapse.

When the replisome encounters DNA damage, it results in an enzymatic train wreck referred to as either replication fork demise or inactivation [120]. The first evidence that a replication fork might be inactivated at the site of a strand break came in 1966 from work by P.C Hanawalt [11]. From there, immeasurable work has been done to understand how a cell would fix a stalled replication fork. Two pathways have emerged from that work. For either pathway, RecA is an essential step (**Figure 2.10**).

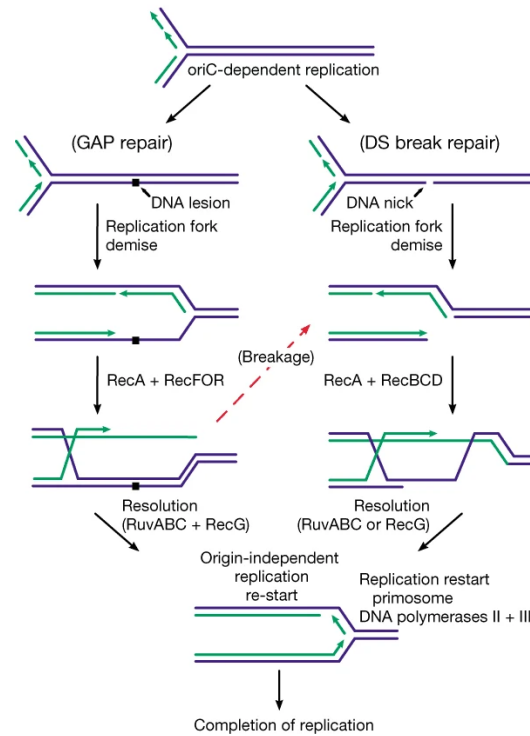


Figure 2.10: The pathways shown illustrate two of the important situations during normal cell growth that may result in replication fork demise, encounter with a DNA lesion or a DNA strand break. Reactivation involves the two main homologous genetic recombination pathways. The processes shown are broadly based on some published studies and discussions at recent national meetings; however, many of the details shown are speculative. The configurations of DNA strands shown in the intermediates are neither representative of all the proposals for fork reactivation nor intended to represent anyone's ideas of the most likely paths. Figure taken with permission from [112]

If a strand-break is what the replication fork encounters, a double-strand break will be generated. The double-strand break is repaired by the RecBCD recombination pathway (**Figure 2.10**). RecBCD first converts the blunt dsDNA end into a duplex DNA molecule possessing a 3'-terminated ssDNA tail using the Chi sequence as a marker. The RecBCD enzyme then directs the RecA protein onto this ssDNA [121]. This RecA filament promotes DNA pairing and formation of a Holliday junction. RuvO, RucB and RecG proteins bind the Holliday junction and promote branch migration [122-127]. The Holliday junction is then resolved by at least two Holliday junction resolvases, RuvC and Rus [128-131].

If an unrepaired DNA lesion is encountered, a significant DNA gap will be created by the RecQ helicase [132], followed by RecJ who will degrade the unwound DNA [133]. The role of this pathway's unique components, the RecF, RecO, and RecR proteins, is up for debate (**Figure**

2.10) [134]. It is known that the RecF protein stays relatively close to the replisome during replication at all times [135]. The RecO and RecR proteins function together and are both necessary and sufficient for the nucleation of RecA on SSB-coated ssDNA *in vitro* [136, 137]. Once RecA is loaded, strands are paired, and a Holliday junction is formed, the RecBCD and RecFOR pathways look very similar, with a few exceptions not discussed here.

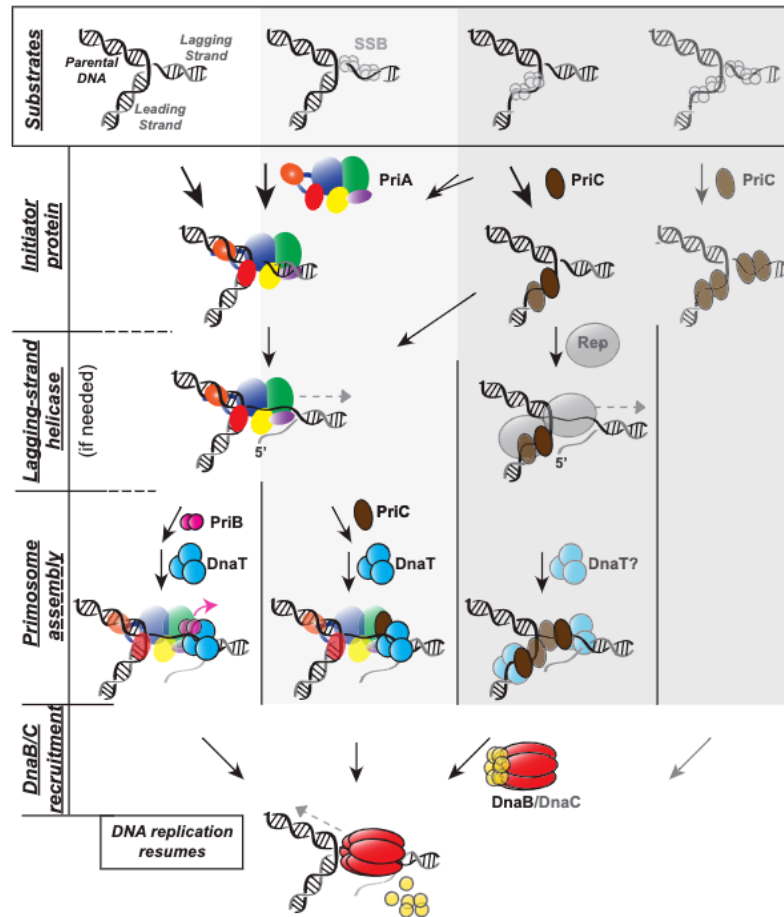


Figure 2.11: DNA replication restart pathways in *Escherichia coli*. *E. coli* and related bacteria possess three functional pathways for DNA replication restart, with the fourth column likely only occurring *in vitro*. All pathways serve to reload the replicative helicase DnaB on sites far removed from the origin of replication in a DNA structure-dependent manner. Key steps in the process are separated by row. Abandoned replication forks (various forms depicted in top row, depending on whether the strands are dsDNA or SSB-coated ssDNA gaps) are recognized by either by PriA or PriC (second row; SSB-interaction/remodeling not shown). Remodeling of the fork through helicase activity (third row) or SSB-interaction may allow for or/and proceed subsequent protein-protein interactions (fourth row). Replication restart ends with DnaB loading (bottom). Note that for simplicity PriA and PriC recognition of a select/preferred fork type is shown. PriA helicase activity is not required on many fork types and two PriA molecules could be shown on a fork. Rep helicase may function before PriC recognition on the first/left fork type. Helicase activity likely does not function exactly in this order and could occur during all steps. Taken with permission from [138]

In prokaryotes, replication can restart after it was stopped. This replication restart can happen in a few ways, through PriA or PriC (**Figure 2.11**). The dominant restart pathway is the PriA/PriB pathway, where PriA recognizes the forked DNA. This forked DNA can take many forms, with and without gaps on leading and/or lagging strands, including D-loops formed during homologous recombination or R-loops [139-141]. PriA can also remodel the fork, including SSBs arrangement on DNA, as it has been shown to interact with SSB [139, 142, 143]. The binding of PriA to ssDNA conformationally changes the PriB binding site. PriB stimulates PriA's helicase activity facilitating the formation of a ternary complex with DNA. Once DnaT has bound, PriB is released, giving space for the DnaB helicase. The PriA-DnaT ternary complex is thought to load the DnaB-DnaC complex though the mechanism remains undefined [138, 144]. PriC can also bind the lagging strand replacing PriB in that case. PriC preferentially binds ssDNA from replication forks that include more than a 7 nt gap between the leading strand and the replication fork in another pathway. Those types of substrates would be formed when the leading strand is blocked coupled with continued helicase unwinding. In this PriA independent pathway, the Rep helicase must remove nascent lagging strand DNA to enable PriC-mediated loading of DnaB. DnaT may play a role in this pathway as PriC can interact directly with DnaT [138].

A generation-old question in the field of DNA repair is what happens to the DNA polymerase when it encounters small DNA damage. At first, in 1968, when Rupp and Howard-Flanders were looking at the effects of DNA damage on the product of DNA replication, the DNA Pol III was not discovered until 1970 [14, 145]. To study this, they used the most popular and still widespread DNA damaging reagent, UV light. UV light (190 – 290 nm) is known to cause two major products on DNA, cyclobutene pyrimidine dimers (CPDs) and, to a lesser extent, 6-4 photoproducts [146]. From this seminal work, they realized that DNA replication continued after UV irradiation, even without NER. Their data has been classically interpreted as the result of Pol III hopping over CPDs [14].

Furthermore, DnaG was reported to prime both strands ahead of a lesion that would block Pol III [88, 147], providing a mechanism by which continued progression of the DnaB helicase would mediate recruitment of Pol III HE downstream of the lesions, effectively resulting in lesion hopping. However, other older works reported the replisome was stalling shortly after a lesion on

the leading strand, which does not agree with the hopping model [148-150]. Lastly, different *in vivo* studies have led to different fates for the replisome, based on either stable binding of the DnaB helicase or the complete disassembly of the replisome after UV [151, 152]. Interestingly, If UV irradiation happens during DNA replication, CPDs have been shown to inhibit Pol III activity [153] but should allow progression of the DnaB helicase as CPDs fit through its central pore [154]. Consequently, what happens to DNA Pol III when it encounters DNA damage that has passed the helicase? Does it hop over the damage, or does it stall at the damage? Chapter 3 will discuss what happens to the replisome components when they encounter DNA damage caused by UV irradiation.

2.8 Fluorescence Microscopy

Since 1994, when wtGFP was seen to function in *E. coli* and *Caenorhabditis elegans*, fluorescence microscopy has an exceptional tool for researchers to investigate gene expression and protein localization[155]. Due to the size and shape of *E. coli* cells, fluorescence microscopy has been one of the most used techniques to determine the role of individual proteins. Combining genetic tools like point mutations to genes, deletions of proteins, protein degradation or increasing the copy number of expressed proteins with fluorescence microscopy allows the direct visualization of the relationships between two proteins.

Typically, the first approach used in fluorescence microscopy is taking snapshots of proteins in cells. This allows researchers to determine the localization, stoichiometry and copy number of a protein at its interaction site. The first step is tagging the protein of interest (POI) with a fluorescent protein (FP). Commonly, tagging generates N- or C-terminal fusions of the POI with the FP. Using a microscope with an appropriate light source and filters, pictures of cells carrying these fusions are taken. For proteins that bind DNA, the resulting images may look like spots of light (foci) within a cell (**Figure 2.12.A**). For some proteins, like those in the replisome, it is customary to observe more than one focus per cell. The localization of those foci can give essential information about the protein's behaviour. For example, if fluorescence is only observed in the cell's periphery, then it most likely binds the cellular membrane. The stoichiometry and copy number can be gleaned by quantifying the intensity at those spots of light.

By analyzing the integrated intensity in single spots and displaying them in a histogram, one can determine if there is more than one copy of a protein in individual spots to give a rough estimate of the stoichiometry of that protein. To determine the exact stoichiometry of a protein within a complex, the most commonly used *in vivo* method is Stepwise Photobleaching (SPB) [6, 156]. SPB uses the decrease of fluorescence over time, resulting from photobleaching, to detect the bleaching of individual FPs. The step size represents the single-molecule intensity. The complete cellular intensity is compared to a negative control like a cell without a fluorescent protein to determine the copy number. That is then compared to the intensity of a single fluorescent protein. The result is a rough estimate of the copy number within the cell [7].

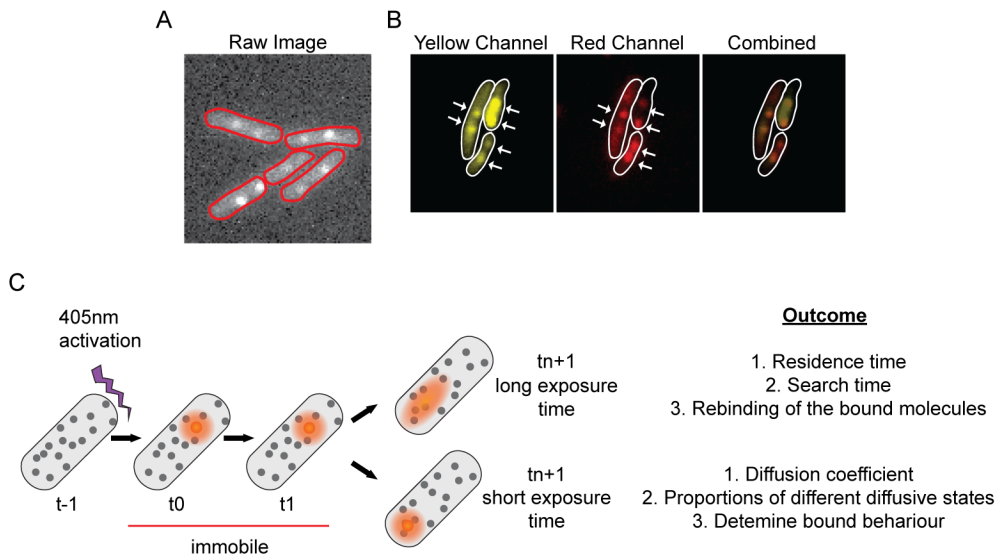


Figure 2.12: Useful fluorescent microscopy for the bacterial model. (A) Raw fluorescent microscopy snapshot image. Cells outlines are highlighted in red. (B) Two-colour snapshot experiment. (C) Diagram illustrating the sptPALM experimental design. Top displays long exposure time experiments, ~ 500 ms, and the parameters that this technique elucidates. Bottom displays short exposure time experiments, ~ 20 ms, and the parameters that this technique elucidates

Another valuable use of snapshots is to have two separate proteins tagged with two different fluorescent proteins that do not have overlapping spectrums (**Figure 2.12.B**). By measuring the distance between both protein localizations, one can determine if those proteins are colocalizing and thus most likely interacting. To measure the actual distance between two proteins, one may use fluorescence resonance energy transfer (FRET) [157]. FRET work by the energy transfer between two fluorophores (distanced by less than 8nm) with overlapping fluorescence spectra.

In the past, *in vitro* studies were used to study factors affecting the processivity and rates of individual replisomes. Fortunately, new advances in fluorescence microscopy, specifically single-particle tracking photoactivated localization microscopy (sptPALM), Fluorescence Recovery After Photobleaching (FRAP) and SPB, have been used to probe the dynamics and architecture of proteins in their native cellular context [6, 158-160]. The ability to see how proteins move in their native environments has changed long-held beliefs on the behaviour of proteins in cells [2, 6].

One of these methods, sptPALM, is a valuable tool as it has the advantage of being able to directly observe the dynamics of single copies of proteins [161]. In this technique, the POI is tagged with either a photoactivatable (PA) or photoconvertible (PC) protein. In most cases, a PC is used as it is easier to measure the protein tag's presence. An often-used PC is the mMaple protein [162, 163]. This PC is natively green, but upon excitation with low power of 405nm wavelength light, a small subpopulation of PCs will stochastically convert to a red fluorescent state (**Figure 2.12.C**). By utilizing this photoconversion, PA/PC-FPs have the advantage of allowing single molecules of high copy-number proteins to be tracked [164].

Depending on the objective of the experiment, different exposure times are used for the imaging of single molecules. Long exposure blurs diffusive molecules, allowing the user to determine residence times, search time and rebinding of the bound molecules (**Figure 2.12.C**). The residence time is measured by looking for how many frames the single-molecule is immobile. The search time and rebinding of a molecule are determined by; how many frames it takes before the single molecule is immobile again and how many immobile events there are for every molecule. Shorter exposure times allow visualization of the diffusion coefficient, proportions of different diffusive states and determine if multiple bound behaviours exist (**Figure 2.12.C**). By looking at both the fast-diffusing molecule and the slow-diffusing molecules, one can determine the apparent diffusion coefficient of each track utilizing the mean-squared displacement method. Then by analyzing the total population of apparent diffusion coefficients and displaying them in a histogram, one can determine if there are multiple diffusive states. Chapter 3, Chapter 4 and Appendix 1 will illustrate these methods in more detail.

There are still many unanswered questions on how replisomes function *in vivo*, but these recent advances in microscopy and genetic methods could provide new and exciting ways to answer them.

Chapter 3

Replisome activity slowdown after exposure to ultraviolet light in *Escherichia coli*

This chapter is based on a published manuscript: Soubry, N., Wang, A., and Reyes-Lamothe, R. Replisome activity slowdown after exposure to ultraviolet light in *Escherichia coli*. *Proceedings of the National Academy of Sciences* 2019;201819297

As highlighted in chapter 2, work in our lab has shown that the replisome is a dynamic structure. Furthermore, there were mixed opinions in the field on what happens to the replisome when it encounters DNA damage. Either the replisome skips or is stalled at DNA damage. I used fluorescent microscopy techniques previously described by the lab and new techniques I developed to measure replication speed and measure bound proportions using single-molecule microscopy to identify novel replisome behaviours. In this manuscript, I first show that after UV damage, the Pol III * is recruited to sites of the chromosome far from the replication fork in a way dependent on the χ clamp loader subunit. Secondly, I show that the replication fork slows down to one-fifth of its regular replication rate immediately after UV damage. Lastly, I propose that the apparent DNA lesion skipping done by the DNA polymerase is likely the result of independent binding events by multiple copies of Pol III *, efficiently recycled after encountering lesions on DNA.

3.1 Abstract

The replisome is a multiprotein machine that is responsible for replicating DNA. During active DNA synthesis, the replisome tightly associates with DNA. In contrast, after DNA damage the replisome may disassemble, exposing DNA to breaks and threatening cell survival. Using live cell imaging we studied the effect of ultraviolet (UV) light on the replisome of *E. coli*. Surprisingly, our results showed an increase in Pol III holoenzyme (Pol III HE) foci post-UV that do not co-localize with the DnaB helicase. Formation of these foci is independent of active replication forks and dependent on the presence of the χ subunit of the clamp loader, suggesting recruitment of Pol III HE at sites of DNA repair. Our results also showed a decrease of DnaB helicase foci per cell after UV, consistent with the disassembly of a fraction of the replisomes. By labeling newly synthesized DNA, we demonstrated that a drop in the rate of synthesis is not explained by replisome disassembly alone. Instead, we show that most replisomes continue synthesizing DNA at a slower rate after UV. We propose that the slowdown in replisome activity is a strategy to prevent clashes with engaged DNA repair proteins and preserve the integrity of the replication fork.

3.2 Significance Statement

A multi-component molecular machine, called the replisome, mediates high fidelity genome duplication, but requires error-free DNA as its template. Presence of lesions on DNA, like those generated after UV, halt replisome activity and can lead to replisome disassembly, a potentially life-threatening situation to the cell. Here we show that, in cells exposed to UV, parts of the replisome independently localize at sites far from the place of DNA synthesis. In addition, we provide evidence that the replisome responds to UV by slowing down its rate of synthesis on the damaged DNA template. Modulation of the rate of DNA replication may be a general strategy used by other organisms to minimize the impact of DNA damage on the duplicating genome.

3.3 Author Contributions

N.S. and R.R.-L. designed research; N.S. and A.W. performed research; N.S., A.W., and R.R.-L. analyzed data; and N.S. and R.R.-L. wrote the paper.

3.4 Introduction

DNA replication is carried out by a multiprotein machine called the replisome. In *E. coli*, the replisome is composed of the DnaB helicase, the DnaG primase, the DNA Pol III ($\alpha\epsilon\theta$), the processivity factor β clamp (β_2), the clamp loader ($\tau_3\delta\delta'\psi\chi$), and the single strand binding protein SSB (Figure 3.1A) (1, 2). Multiple protein-protein interactions exist among these subcomplexes. DnaB and DnaG interact with each other (3, 4). Pol III and clamp loader are physically coupled by the interaction between α and τ , forming the Pol III* subcomplex (5). Pol III* and β clamp form the Pol III HE (6). Finally, the τ subunit mediates the interaction between DnaB helicase and Pol III HE (7). Once in every cell cycle, DNA replication is initiated with the assembly of two replisome in opposite orientations at a specific locus of the chromosome, the *oriC*. Each replication fork duplicates half of the 4.6 Mbp circular chromosome at rates between 0.6-1 kbp s⁻¹ at 37 °C (8), completing replication as the two of them meet at the region opposite from *oriC*.

Successful genome duplication is dependent on undamaged template DNA. Modifications in the chemistry of DNA and the presence of strand discontinuities can inhibit the progression of the replisome or lead to its disassembly, potentially generating double strand DNA (dsDNA) breaks and life-threatening consequences to the cell (9). Specialized DNA repair systems continually act on lesions to restore DNA (10-12). Prolonged replisome stalling and replisome disassembly trigger the activation of specialized mechanisms that correct dsDNA breaks and restore the replication fork – the DNA structure on which the replisome acts – followed by mechanisms to re-assemble replisome at those sites (13-15). The frequency at which the replisome disassembles during normal growth and the timing required for replisome reassembly have not been well established.

The effect of UV-C light (190-290 nm) on DNA and DNA replication has been widely studied. UV-C generates cyclobutane pyrimidine dimers (CPDs), and to a lesser extent 6-4 pyrimidine adducts (6-4 PA), on DNA (16). CPDs have been shown to inhibit the activity of Pol III (17), but should allow progression of the DnaB helicase as they fit through its central pore (18). Shortly after UV treatment the rate of DNA replication significantly drops in *E. coli*, an effect lasting for tens of minutes (19, 20). The reduced DNA synthesis is produced in short fragments on both strands (21, 22), which was classically interpreted as the result of Pol III hopping over CPDs (21). In agreement with this model, DnaG was reported to prime both strands ahead of a lesion that

blocks Pol III (23, 24), providing a mechanism by which continued progression of the DnaB helicase would mediate recruitment of Pol III HE downstream of the lesions, effectively resulting in lesion hopping. However, previous works that reported replisome stalling shortly after a lesion on the leading strand have not yet been fully reconciled with this data (25-27). In addition, different live cell studies have led to opposing conclusions on the fate of the replisome, suggesting either stable binding of the DnaB helicase or the complete disassembly of the replisome after UV (28, 29).

We used fluorescence microscopy to directly test the effect of UV on the replisome and DNA synthesis at a single-cell level. We used slow-growth conditions, with generation times above 100 minutes, to minimize convolution of our data by new rounds of DNA replication, as reported previously (29). Our results lead us to conclude that most replisomes remain active, although progressing at a diminished rate, after exposing cells to UV at doses where CPDs decorate DNA at every few kilobases. Our data is consistent with the capacity of the replisome to skip over lesions on DNA. In addition, we show that the Pol III HE can act independently of the DnaB helicase and the replication fork after being recruited to other sites of the chromosome in a manner dependent of the χ subunit. Pol III HE activity outside the fork may contribute to filling DNA gaps, and in conjunction with its β -clamp loading activity, may influence other processes like translesion DNA synthesis

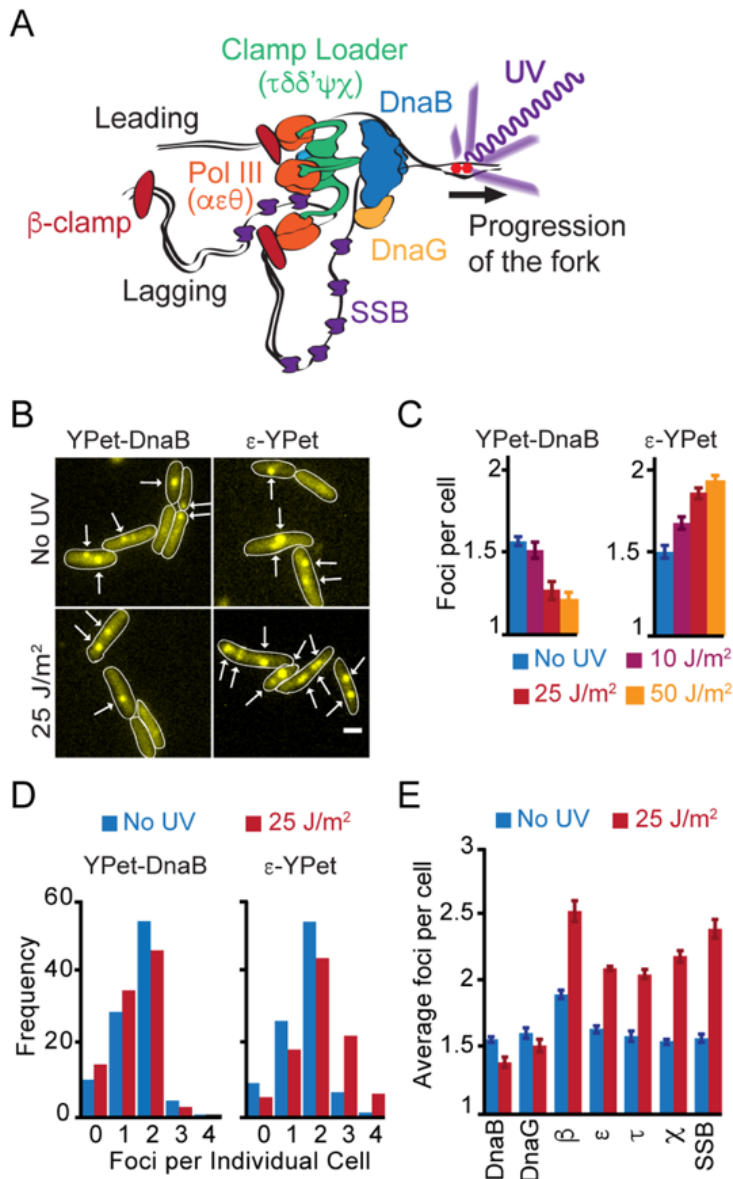


Figure 3.1. Unbinding of replisome subunits at an UV lesion. (A) Model of the architecture of an active replisome. DNA is unwound by the DnaB helicase. DnaG primase binds to DnaB. Pol III and the clamp loader bind each other through the τ subunit of the clamp loader, which also mediates binding to the DnaB helicase. The β -clamp is left behind the fork after the completion of an Okazaki fragment at the lagging strand. SSB covers ssDNA produced during the cycle of lagging strand synthesis. (B) Representative images of cells carrying YPet-DnaB or ϵ -YPet before and 5 minutes after exposure to 25 J/m² UV dose. White arrows mark the location of foci. Scale bar 1 μ m. (C) Average number of the foci per cell of YPet-DnaB or ϵ -YPet 5 minutes after exposure to different UV doses. (D) Distribution of the number of foci per cell in cells carrying YPet-DnaB or ϵ -YPet 5 minutes after exposure to UV. (E) Average number of foci for all the replisome subunits tested: YPet-DnaB, YPet-DnaG, YPet- β , ϵ -YPet, τ -YPet, χ -YPet and SSB-YPet. Pictures were taken 5 minutes after exposure. Error bars represent SE.

3.5 Results

3.5.1 Pol III Holoenzyme is Recruited to Multiple Sites in the Nucleoid after Exposure to UV Light.

To test directly for replisome subunit stability after UV treatment, we used fluorescence microscopy in live cells. We studied the replisome by using previously characterized *E. coli* strains carrying derivatives of replisome components fused to the yellow fluorescent protein YPet (30, 31). We grew cells in conditions where they undergo a single replication event, and have at most 2 replication forks, which translate into cells with 0, 1 or 2 fluorescent spots for DnaB and the proof-reading exonuclease subunit of Pol III, ϵ (Figure 3.1 B) (30). 5 minutes after exposing cells to UV at a dose of 25 J/m^2 , we observed a small decrease in the average number of YPet-DnaB foci, going from 1.57 ± 0.02 (SE) before to 1.39 ± 0.03 spots per cell after treatment (Figure 3.1B & 2D). Disappearance of DnaB spots supports the idea that the replisome has disassembled in those cells. In unexpected contrast, ϵ -YPet showed an increase in the number of spots per cell, going from 1.64 ± 0.03 before to 2.10 ± 0.03 spots per cell after treatment. Notably, this included a significant increase in the percentage of cells with 3 and 4 spots, from 8.4% to 29.5% (Figure 3.1D). The effects of UV on the distribution of DnaB and ϵ spots correlated with the UV dose used (Figure 3.1C).

Further characterization of replisome subunits corroborated the existence of two different behaviors in the subcomplexes of the replisome. YPet-DnaG showed a slight reduction in the number of fluorescent spots per cell, similar to DnaB but to a lower extent, going from 1.61 ± 0.04 to 1.52 ± 0.05 before and after treatment, respectively. Whereas reminiscent of the results for ϵ , the number of fluorescent spots increased after UV for β -clamp from 1.9 ± 0.03 to 2.53 ± 0.08 ; for τ from 1.59 ± 0.04 to 2.06 ± 0.03 ; for χ from 1.55 ± 0.02 to 2.19 ± 0.04 ; and for SSB from 1.57 ± 0.03 to 2.40 ± 0.07 (Figure 3.1E, Figure A2.2.3.A). These results match the architecture of the replisome, as DnaG needs to interact with DnaB for recruitment to the replication fork, and β -clamp, clamp loader and Pol III form the Pol III HE (Figure 3.1A). In addition, our data agrees with studies on the replisome dynamics, where we and others showed that Pol III and the clamp loader frequently unbind from the replication fork, while the DnaB helicase is stably bound (32, 33).

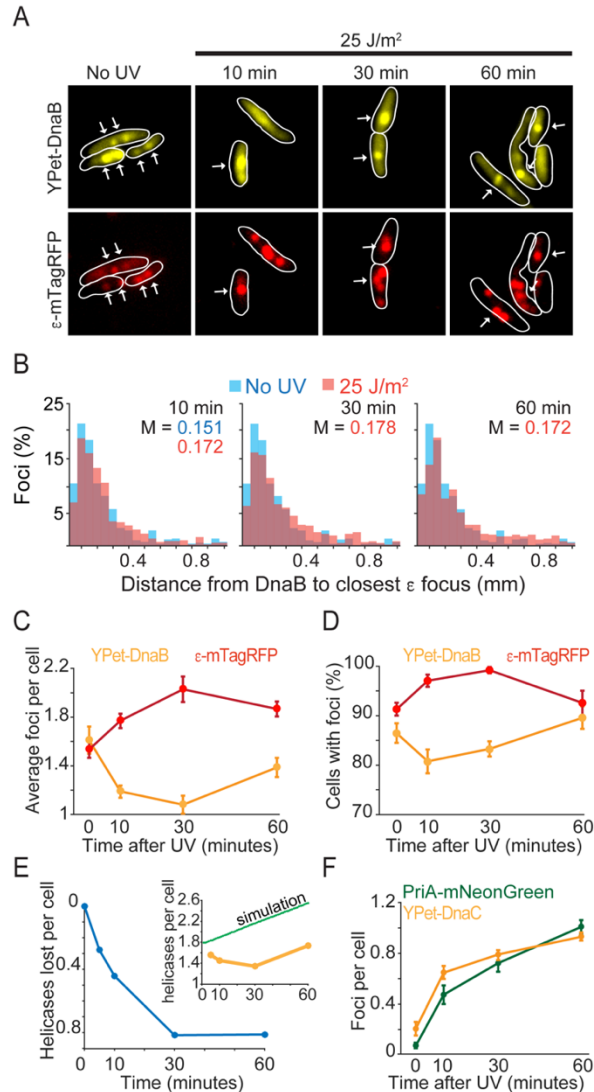


Figure 3.2. DnaB remains in proximity to Pol III after UV. (A) Representative images of a strain carrying YPet-DnaB and ϵ -mTagRFP, before and at various times after UV treatment. White arrows mark co-localization of foci in the two channels. Scale bar 1 μ m. (B) Distribution of apparent distances between a YPet-DnaB focus and the closest ϵ -mTagRFP focus in a cell. The untreated sample is compared with the results at 10, 30 and 60 minutes after UV. The median (M) of each population is shown. (C) Average number of foci per cell for YPet-DnaB and ϵ -mTagRFP before (0 minutes) and at various times after treatment. (D) Number of cells with at least one fluorescent focus for YPet-DnaB or ϵ -mTagRFP at various times after treatment. (E) Estimation of helicase disassembly at various times after UV treatment. Numbers are based on the difference between a simulated growth of foci, assuming no disassembly, and the data of YPet-DnaB from Figure 3.1C and Figure 3.2C (Inset). (F) Number of PriA-mNeonGreen (green) and YPet-DnaC (yellow) foci per cell before (0 minutes) and at various times after exposure to UV. Error bars represent SE.

To characterize the two binding regimes in the replisome, we imaged cells carrying both YPet-DnaB and ϵ -mTagRFP (Figure 3.2). In untreated cells we expected to observe co-localizing foci for both subunits as the replisome should contain both of them. Our results confirm this

expectation, the median distance between DnaB and the closest ϵ spot was $0.151\mu\text{m}$ (Figure 3.2A & 2F). In agreement with the results described above, the number of DnaB spots decreased and the number of ϵ spots increased after UV (Figure 3.2C-D, Figure A2.2.3.B). The greatest contrast in the spot distribution of these two subunits was reached 30 minutes after UV exposure, after which we observed a trend of recovery towards the pretreated state (Figure 3.2C-D). Despite the difference in abundance, the distance between DnaB and the closest ϵ spot did not dramatically change, having a median of $0.178\mu\text{m}$ after 30 minutes. Therefore, our results suggest that all replisome subunits remain in the proximity of the replication fork after UV treatment, although they may not be active – as they might be binding to gaps behind the replication fork. They also suggest the recruitment of additional copies of the Pol III HE and SSB at other sites on the chromosome, perhaps participating in DNA repair or as a result of DNA processing caused by UV lesions.

3.5.2 Slowdown in the Rate of DNA Synthesis is Only Partially Explained by Replisome Disassembly.

Our initial estimates of replisome disassembly, as measured by the disappearance of YPet-DnaB foci, did not account for the elongation of cells after UV. In UV treated cells, cell division is inhibited but initiation of DNA replication continues (29). To obtain an accurate assessment of the frequency of replisome disassembly, we simulated the expected number of replisomes per cell in a scenario where no disassembly occurs, making the assumption that UV inhibits cell division but that the rate initiation of DNA replication remains unchanged (29), resulting in an increase in the number of replisomes per cell over time (Figure 3.2E). Comparing our results to the simulated data showed that replisome disassembly continued for about 30 minutes, plateauing at an average of 0.8 replisomes lost per cell, when >30% of the replisomes are lost (Figure 3.2E). Recovery of replisomes is not observed even after 60 minutes.

To complement these observations, we monitored DnaB re-loading using a mNeonGreen fusion to the reloading protein PriA (Figure 3.2F, Figure A2.2.3.B). PriA is a crucial component of the protein complex that loads the helicase-loader DnaC-DnaB helicase in an *oriC*-independent manner (34). The fraction of cells with PriA spots increased after UV treatment from $7 \pm 0.2\%$ (SE), and an average of 0.067 ± 0.021 spots per cell, in untreated cells, to $78.9 \pm 0.5\%$, and an

average of 1 ± 0.05 spots per cell, 60 minutes after UV treatment (Figure 3.2F), closely matching the estimated replisome loss. We observed a similar trend for cells carrying a YPet derivative of the helicase loader DnaC, where the frequency of cells with spots increased after UV treatment from $14.20 \pm 3.1\%$ (SE), and an average of 0.19 ± 0.05 spots per cell, in untreated cells, to $61.61 \pm 5\%$, and an average of 0.92 ± 0.03 spots per cell, 60 minutes after UV treatment (Figure 3.2F, Figure A2.2.3.B). However, these results reported a lower frequency of cells with DnaC foci compared to PriA, despite the role of DnaC in both *oriC*-dependent and -independent initiation. This may suggest a significant time delay between PriA binding and DnaC recruitment during reloading of the replisome.

We then estimated the rate of DNA synthesis at a single cell level by fluorescently labeling newly replicated DNA through a 2-minute pulse of ethyl deoxyuridine (EdU) and azide-coupled Fluor 545 (35). The number of cells with EdU fluorescent foci dropped slightly, from 93.8 ± 0.05 (SE) before UV to 82.5 ± 8.4 after 30 minutes (Figure 3.3A-B), indicating that DNA synthesis continued in most cells after UV treatment. We estimated the rate of new DNA incorporation based on the integrated intensity of detected spots in a given cell. DNA synthesis sharply decreased after 5 minutes of UV treatment, resulting in only $16.2 \pm 5.8\%$ (SE) of the incorporation in untreated cells, and progressively increasing reaching $81.9 \pm 13.8\%$ of the original incorporation after 60 minutes (Figure 3.3C, ‘observed’). This decrease in DNA synthesis could be due to the fewer number of replisomes in cells following UV-induced replisome disassembly. To test this hypothesis, we calculated the predicted rate of synthesis based on our estimates of replisome loss, assuming unimpeded DNA synthesis with the same constant rate as before treatment (Figure 3.3C, ‘Expected’). Interestingly, replisome loss could only account for a small part of the observed decrease in DNA synthesis, raising the possibility that the remaining replisomes act more slowly after UV. We used this ‘expected’ rate to normalize the observed EdU incorporation, so we could assess the relative synthesis rate per replisome (Figure 3.3D). The corrected rates of synthesis showed that replisomes progress at 18.7% and 84.7% of their unperturbed rate 5 and 60 minutes after UV, respectively. Since replicating the entire chromosomes takes 65 minutes at 37°C (30), we estimate that the rate of replication goes from $\sim 600 \text{ bp s}^{-1}$ before to $\sim 114 \text{ bp s}^{-1}$ 5 minutes after UV. These results show that a considerable proportion of replication forks progress at a diminished average rate after UV treatment.

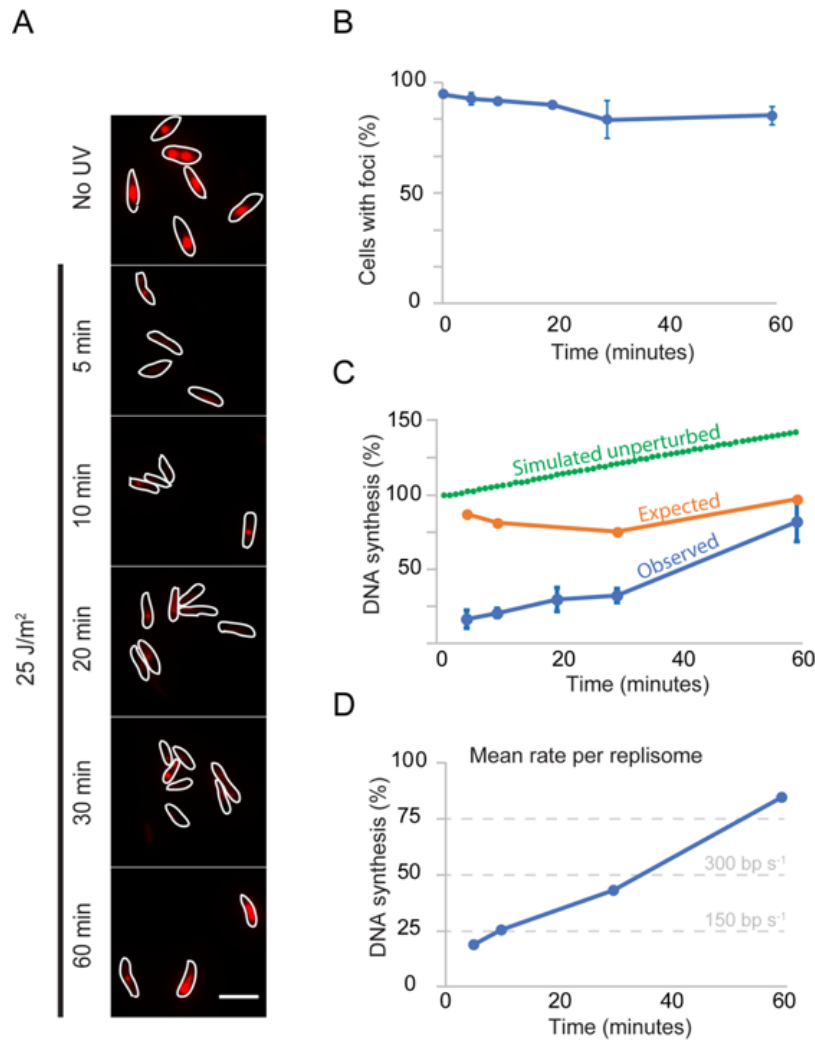


Figure 3.3. Persistence of DNA synthesis after UV. (A) Representative images of a strain carrying $\Delta yjjG \Delta deoB$ after EdU labeling. A 2-minute pulse of EdU, followed by fixation and coupling of fluorescence through click chemistry. Cells were sampled at various times after UV. Scale bar 5 μ m. Contrast and brightness have been normalized. (B) Percentage of cells with at least one focus for EdU before (0 minutes) and at various times after UV. Error bars represent SE. (C) Estimated normalized DNA synthesis at various times after UV (Observed), as measured by the integrated intensity of all spots in a cell. Compared to the expected synthesis if all remaining DnaB foci in Figs. 1 and 2 were fully functional replisomes (Expected), and to the expected synthesis in cells with fully functional replisomes and no replisome disassembly (Simulated unperturbed). Error bars represent SE. (D) Mean rate per replisome obtained by re-normalizing the ‘Observed’ data using the ‘Expected’ data in C. The estimated

3.5.3 Recruitment of the Pol III HE does not Require Active Replication.

Copies of Pol III HE subunits at sites outside of the replication fork may mark points of DNA repair. Alternatively, they may represent new DNA replication events from *oriC* or mark sites behind the replication fork. To test these later models, we targeted an inactive copy of Cas9

(dCas9) to *oriC*, which has previously shown to inhibit initiation of DNA replication (36) (Figure A2.2.1.B). We then waited for a period of 2 hours to allow completion of ongoing DNA replication events. In these conditions, we observed a relatively high background of DnaB spots. We speculate that this is because the inhibition of initiation by dCas9 may still permit binding, but not activation, of DnaB at the *oriC*. But consistent with the results above, the number of spots in arrested cells did not change substantially after UV, going from 0.64 ± 0.05 to 0.58 ± 0.07 (Figure 3.4A-B). In contrast, the number of ϵ -YPet foci went from 0.29 ± 0.02 to 1.25 ± 0.08 after UV in the induced cells (Figure 3.4A-B). As an independent confirmation of these results, we used previously characterized strains carrying a *dnaC2* temperature sensitive allele to block initiation of DNA replication (30). As before, we allowed completion of ongoing replication events by incubating cells at the restrictive temperature (37°C) for 2 hours. Similar to the results above, we observed a relatively high background of DnaB spots, but consistent with previous experiments the number of spots in arrested cells changed only slightly after UV, from 0.87 ± 0.08 to 0.98 ± 0.05 (Figure 3.4C-D). In contrast, the number of ϵ -YPet foci went from 0.10 ± 0.02 to 0.80 ± 0.04 after UV when cells were incubated at the restrictive temperature (Figure 3.4C-D). Thus, we determined that the additional Pol III HE foci are not due to new initiation events. In addition, our results also demonstrate that additional Pol III HE foci can form even in conditions where there are no replication forks. Hence, even if some of these foci may be produced by Pol III HE binding behind the replication fork during active synthesis, a fraction of them are likely to bind elsewhere in the chromosome.

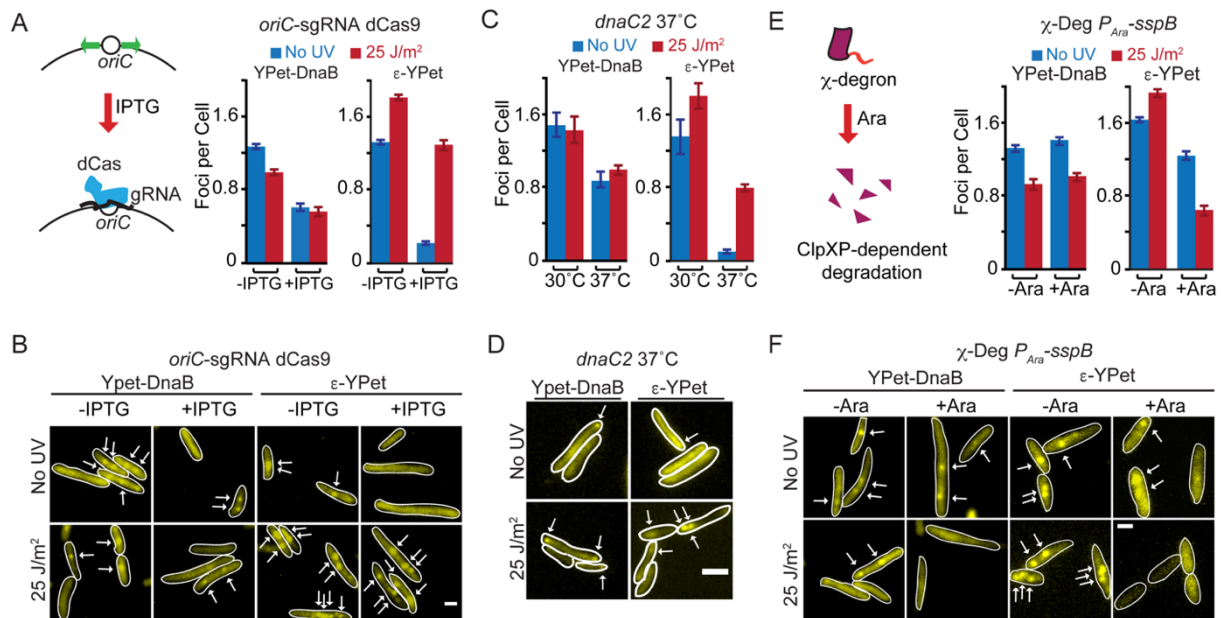


Figure 3.4. Pol III HE recruitment is independent of ongoing replication and dependent on the χ subunit. (A) (Left) Description of the system to stop initiation of DNA replication. IPTG-inducible CRISPR-dCas targets the *oriC* to prevent new replication round. (Right) Cells were induced for 3 hours. Average number of foci per cell of YPet-DnaB and ϵ -YPet before and after treatment with UV 5 minutes after exposure in conditions where initiation proceeds unimpeded (-IPTG) or when it is blocked (+IPTG). (B) Representative images of cells carrying YPet-DnaB or ϵ -YPet and the *oriC* blocking CRISPR-dCas system. Arrows marks position of fluorescent foci. Scale bar 1 μ m. (C) Cells were incubated at the restrictive temperature for 3 hours. Average number of foci per cell of YPet-DnaB and ϵ -YPet in a *dnaC2* temperature sensitive background at permissive and non-permissive temperature. (D) Representative images of cells carrying YPet-DnaB or ϵ -YPet in a *dnaC2* temperature sensitive background at non-permissive temperature. Scale bar 2 μ m. (E) (Left) Description of the degron system used in this work. (Right) Average number of foci per cell of YPet-DnaB and ϵ -YPet before and after treatment with UV 5 minutes after exposure in conditions where χ is present (-Ara) or after χ has been degraded (+Ara). (F) Representative images of cells carrying YPet-DnaB or ϵ -YPet and a degradable copy of the χ subunit. Scale bar 1 μ m.

3.5.4 Recruitment of the Pol III HE Outside the Replication Fork Depends on the χ Subunit of the Clamp Loader.

Pol III HE interacts with the DnaB helicase at the replication fork, but our data suggested that it can also be at other sites independently of DnaB. To explain this observation, we hypothesized that SSB serves as an anchor for the Pol III HE at these extra sites, as this protein binds to ssDNA, and SSB interacts with the χ subunit of the clamp loader (37). We tested this idea by inducing rapid depletion of the χ subunit in a strain carrying a degron-tagged version of this protein (Figure 3.4E-F) (31, 38). Imaging was done 45 minutes after arabinose induction. We observed a sharp

decrease in the number of ϵ -YPet spots after UV, going from 1.22 ± 0.04 before to 0.63 ± 0.05 spots per cell after UV (Figure 3.4E-F). Depletion of χ had a smaller effect on YPet-DnaB after UV, where the number of foci decreased from 1.39 ± 0.04 to 1 ± 0.04 , showing a similar trend as in conditions where χ is present (Figure 3.4E-F). These results are consistent with the idea that χ helps to recruit Pol III HE at other sites of the chromosome. Nonetheless, the χ subunit has also been reported to have a role in replisome stability (39). Consequently, an alternative interpretation of these results is that UV further destabilizes the weakened χ -depleted replisome. Indeed, we observed a drop in ϵ -YPet foci in χ -depleted conditions before UV, compared to control cells (Figure 3.4E-F), which agrees with a role for χ in retaining Pol III HE at the fork. Consequently, at present we cannot rule out a contribution of the stabilizing role of χ in our results.

3.5.5 Exposure to UV Light Changes the Binding Dynamics of the Pol III HE.

To further characterize the role of the additional Pol III HE spots in the cell, we studied the binding kinetics of the DNA Pol III using single-molecule experiments. We used a fusion of ϵ with the photoconvertible fluorescent protein mMaple (32, 40), and the technique of single-particle tracking Photoactivated Localization Microscopy (sptPALM) to determine the average residence time (bound-time) of this subunit as previously described (Figure 3.5A) (32). Between 15 and 30 minutes after UV, we observed an increase in the bound-time going from $10.80\text{s} \pm 0.94$ before treatment, consistent with previous results (32), to $16.18\text{s} \pm 2.11$ after treatment (Figure 3.5B). These results are reminiscent of the increased bound-time observed for Pol III* after treatment with the DNA polymerase inhibitor hydroxyurea (32).

We also determined the proportion of ϵ bound to DNA before and after UV by sptPALM. Capturing pictures at 20 ms rates under low-intensity continuous 405 nm-laser activation, resulted on average in a single fluorescent spot per cell per frame. We characterized the behavior of DNA-bound molecules by studying a strain carrying LacI-mMaple and a *lacO* array, where most of the molecules are bound to the chromosome (Figure 3.5C) (32). The distribution of apparent diffusion coefficients for ϵ -mMaple before treatment showed at least two fractions, one of which represented the DNA-bound molecules – overlapping with the LacI data –, and a second showing the diffusive fraction (Figure 3.5C). Using a Gaussian mixture model to estimate the fraction of DNA-bound molecules in the population, we estimated that the proportion increased from 16.4% before

treatment, to 35.5% between 15-30 minutes after UV treatment (Figure 3.5C). This data supports the idea that the Pol III HE bound to DNA is not always active after UV. It also shows that exposure to UV increases the length and the frequency of the binding events of Pol III* to DNA.

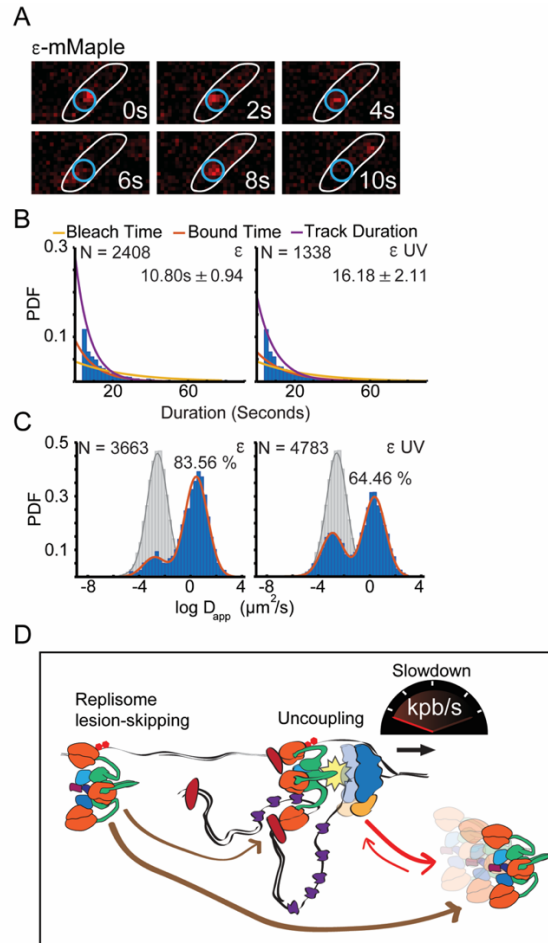


Figure 3.5. UV irradiation affects the dynamics of the replisome. (A) Representative images of ϵ -mMaple in an sptPALM experiment to characterize its binding kinetics. (B) Representative examples of the distribution of fluorescent foci life-spans (blue bars) for Pol III ϵ subunit, before and after UV, showing fitting of a single-exponential decay model (purple line), the estimated bleaching rate in the same conditions (yellow line) and the corrected estimated bound-time (red line). PDF stands for probability density function. Numbers indicate bound time in seconds with the SE in parenthesis. (Left) Pol III ϵ subunit before UV. (Right) Pol III ϵ subunit after UV (C) The distribution of the logarithm of the apparent diffusion coefficient (blue bars) for Pol III ϵ subunit and LacI bound control (grey bars), before and after UV, showing the fitting of a gaussian mixture model (red and grey line). Percentage indicates the proportion of diffusing molecules. (Left) Pol III ϵ subunit before UV. (Right) Pol III ϵ subunit after UV. Y-axis represents probability density function. (D) Model for the replisome slowdown. After encountering an UV lesion on the leading strand, the helicase continues unwinding through this site, but the Pol III is stalled, leading to the uncoupling between the Pol III HE and the helicase. This in turn results in a decrease translocation rate of the helicase. Priming by DnaG downstream of the lesion on the leading strand leads to the recruitment of a new copy or the same copy of Pol III to resume DNA synthesis causing replisome lesion-skipping.

3.6 Discussion

We have investigated the fate of the replisome after encountering a DNA lesion capable of inhibiting Pol III activity, but that in principle does not threaten DnaB helicase integrity. A large body of literature that studied the effect of UV on DNA replication, spanning the last 50 years, precedes our work. However, this is the first report that focuses on the effect of UV on the replisome subunits, resulting in unique insight into response of the replisome to DNA damage, and the dynamics of DNA synthesis on a damaged DNA template. We expect that our conclusions will be also valid to other non-bulky DNA modifications that do not hinder helicase translocation.

Contrary to the long-held belief that the replisome subunits remain bound during long periods of the replication cycle, recent data from our group and other groups have demonstrated much more frequent turnover in this complex. Single-molecule *in vivo* data from the *Bacillus subtilis* and *E. coli* have shown that the active replicative DNA polymerase is replaced every few seconds (32, 41). Similar observations were made in an independent study using a reconstituted *E. coli* replisome *in vitro* (33). Replisome disassembly exposes DNA structures sensitive to breakage, which can occur independently of external aggressions such as UV. It is therefore unclear why a stable replisome complex was not favored in evolution.

Our work unveils potential advantages of a dynamic replisome. The data is consistent with the recruitment Pol III HE to sites other than the replication fork in a DnaB-independent manner. This is a striking result, as these two subcomplexes were assumed to be found only at the replisome. We favor the model that Pol III HE is recruited at ssDNA gaps, given the presence of SSB. Polymerization activity at these sites is also likely and agrees with reports that established Pol III activity at ssDNA gaps (42, 43). Pol III HE might also contribute to loading of β -clamp at these sites which could then serve for the recruitment of Pol V translesion polymerase. Some of these sites are likely to be found behind the replication fork, resulting from the replisome skipping over UV lesions. But since Pol III HE foci formed after UV even when cells are not replicating (Figure 3.4A-D), our data suggests that there are other recruitment sites in the chromosome which are independent of the replication fork. Loading of β -clamp away from the DNA replication fork, and subsequent unbinding of the clamp loader, would agree with a lack of overlap in the localization of the clamp loader and the translesion polymerases Pol IV and Pol V during DNA

repair (44-46). Though we note that the presence of the Pol III HE at those sites may facilitate resuming DNA synthesis after bypass by Pol V.

3.6.1 A Fast-Acting Rate Switch Strategy as Response to DNA Damage.

A much clearer advantage of a dynamic Pol III* binding is an almost immediate slowdown of the rate of DNA replication in response to DNA damage. Such strategy would reduce the probability of encounters between the DnaB helicase and the engaged NER system, which may lead to helicase disassembly. It is unlikely that the rate change is due to competition of Pol III with the translesion polymerases, as this effect should increase with the induction of the SOS response, and should be minimal at 5 minutes after UV. Instead, we propose that Pol III disengages from DnaB after encountering a CPD, triggering a change in DnaB translocation rate (Figure 3.5D). Previous reports show slower DnaB helicase translocation in the absence of Pol III* (47, 48). Our results show that shortly after treatment with UV the replisome proceeds at about 114 bp s^{-1} (30) (Fig 3D). This is just slightly higher than the $\sim 80 \text{ bp s}^{-1}$ single-molecule estimates of the DnaB helicase activity when it uncouples from DNA synthesis (49, 50). Thousands of CPDs are generated in the chromosome after a 25 J/m^2 UV dose –we estimate one every $\sim 9 \text{ kbp}$ on the leading strand based on Courcelle *et al.* (51). The rate of DNA synthesis progressively increased, reaching $>80\%$ of the original rate 60 minutes after UV, in agreement with the proposed dynamics of CPD removal after exposure to UV (52). The DNA replication averages described above using 2-minute pulses of EdU labeling would then be the result of multiple cycles of engagement and disengagement, each lasting few seconds. As such, the rate of replisome progression reflects the density of lesions on DNA.

A much greater number of replisomes simultaneously acting on the genome in eukaryotic cells, although progressing at slower rates, should increase the rate of clashes with the DNA repair systems. As in bacteria, a mechanism to rapidly modulate the rate of replisome progression has been proposed. Binding of the Mrc1-Tof1-Csm3 (MTC) complex in budding yeast has been shown to be needed for a maximal rate of DNA synthesis (53-55). In addition, the interaction between the replisome and MTC is highly dynamic, making it a good candidate to mediate a fast response to DNA damage (56). As such, fast modulation of DNA synthesis by the replisome seems to be a common strategy evolved in both eukaryotes and prokaryotes. It is tempting to speculate that

replisome slowdown in eukaryotes precedes the global DNA damage response (DDR), mediated by protein kinases, which should take more time to be established (57).

3.6.2 Continued DNA Replication After UV Supports a Replisome Lesion Skipping Model.

A classical model suggests that after UV, DNA Pol III can hop on DNA to avoid prolonged stalling at lesions (21). A mechanistic explanation was provided by data showing that helicase progression provides a platform for priming on both strands, mediating polymerase lesion skipping after UV treatment (23, 24). We note that the original envisioning of this model, where the same copy of the DNA polymerase resumes synthesis after skipping a DNA lesion, is unlikely to occur in cells given that Pol III* is frequently exchanged (see above). Hence, it is more probable that the resumption of DNA synthesis occurs after a different copy of Pol III* is recruited from the diffusing pool. However, consistent with the idea of lesion skipping by the replisome, our data provides yet another set of evidence by showing that even though the rate of DNA synthesis drops after UV exposure, DNA synthesis continues (Figure 3.5D). Previous reports were not able to distinguish between replisome slowdown, disassembly and cell heterogeneity as they were based on population averages. Furthermore, we show that β -clamp continues to accumulate at sites containing DnaB helicase (Figure A2.2.3.), and that the DnaB helicase remains in proximity of ϵ at all times after UV (Figure 3.2), further supporting the idea that the activities of priming and DNA elongation continue after UV.

3.7 Experimental Procedures

Detailed description of the experimental procedures used are available in SI Materials and Methods. In brief, strain construction was done using P1 transduction or lambda red recombination in an AB1157 background (58). Cells were routinely grown in LB or in M9 glycerol. For microscopy, cells were grown overnight in M9 glycerol, then diluted in the same medium and grown to an OD₆₀₀ between 0.1-0.2. For degron experiments cells were induced with 0.5% arabinose at an OD₆₀₀ of 0.1 after the dilution in M9 and grown for 45-60 minutes before imaging. For degron CRISPR experiments cells were induced with 0.5mM IPTG 45 minutes after the dilution in M9 and grown for 2 hours before imaging. DnaC2 strains were incubated at 37°C for 2 hours before UV treatment. Cells were spotted on a 1% agarose pad in M9-Glycerol. UV irradiation was performed in a UV Stratalinker 2400 (Stratagene) at the dose specified in the text

before placing the coverslip. Images were taken exactly at minutes 5 to 10 after irradiation unless stated otherwise. For single molecule experiments, collection of images started at 15 minutes and ended at 30 minutes post-irradiation. Imaging was performed at room temperature on an inverted Olympus IX83 microscope from a single-line cellTIRF illuminator (Olympus). For EdU incorporation, all cells were grown overnight in M9 glycerol at 37°C, then diluted in the same medium and grown to an OD₆₀₀ between 0.1-0.2. A sample of cells was put aside as an untreated control while the rest of the liquid culture was put in a sterile petri dish and then UV irradiated. EdU to a concentration of 20 µg/mL was added for 2 minutes before fixation at specified times after UV exposure. Fixing and labelling was done using a modified protocol described by (59). All analysis was done using custom Matlab scrips and TrackMate software in ImageJ. A custom Matlab script was used to simulate the increase in the number of copies of replisome per cell when cell division is inhibited and replication proceeds at a slower rate. Number of repeats, sample size, and statistical tests for pairwise comparisons for all microscopy analysis presented in the figures can be found in Table A2.4.

3.8 Supplemental Information

Supplemental Information (Appendix 2) includes the SI Materials & Methods, six figures and four tables.

3.9 Acknowledgments

We thank Anjana Badrinarayanan, Gregory Marczyński, Christian Rudolph, Steph Weber and members of the Reyes lab for helpful discussions. Some of the experiments were done using equipment from the Integrated Quantitative Bioscience Initiative (IQBI), funded by CFI 9. This work was funded by the Natural Sciences and Engineering Research Council of Canada (NSERC# 435521-2013), the Fonds de Recherche du Quebec –Nature et technologies (FRQNT #2017-NC-198919), the Canadian Institutes for Health Research (CIHR MOP# 142473), the Canada Foundation for Innovation (CFI# 228994), and the Canada Research Chairs program.

3.10 References

1. Beattie TR & Reyes-Lamothe R (2015) A Replisome's journey through the bacterial chromosome. *Front Microbiol* 6:562.
2. Lewis JS, Jergic S, & Dixon NE (2016) The E. coli DNA Replication Fork. *Enzymes* 39:31-88.
3. Tougu K & Marians KJ (1996) The interaction between helicase and primase sets the replication fork clock. *J Biol Chem* 271(35):21398-21405.
4. Tougu K & Marians KJ (1996) The extreme C terminus of primase is required for interaction with DnaB at the replication fork. *J Biol Chem* 271(35):21391-21397.
5. Gao D & McHenry CS (2001) tau binds and organizes Escherichia coli replication through distinct domains. Partial proteolysis of terminally tagged tau to determine candidate domains and to assign domain V as the alpha binding domain. *J Biol Chem* 276(6):4433-4440.
6. Stukenberg PT, Studwell-Vaughan PS, & O'Donnell M (1991) Mechanism of the sliding beta-clamp of DNA polymerase III holoenzyme. *J Biol Chem* 266(17):11328-11334.
7. Gao D & McHenry CS (2001) tau binds and organizes Escherichia coli replication proteins through distinct domains. Domain IV, located within the unique C terminus of tau, binds the replication fork, helicase, DnaB. *J Biol Chem* 276(6):4441-4446.
8. Pham TM, *et al.* (2013) A single-molecule approach to DNA replication in Escherichia coli cells demonstrated that DNA polymerase III is a major determinant of fork speed. *Mol Microbiol* 90(3):584-596.
9. Kuzminov A (1999) Recombinational repair of DNA damage in Escherichia coli and bacteriophage lambda. *Microbiol Mol Biol Rev* 63(4):751-813, table of contents.
10. Krwawicz J, Arczewska KD, Speina E, Maciejewska A, & Grzesiuk E (2007) Bacterial DNA repair genes and their eukaryotic homologues: 1. Mutations in genes involved in base excision repair (BER) and DNA-end processors and their implication in mutagenesis and human disease. *Acta Biochim Pol* 54(3):413-434.
11. Iyer RR, Pluciennik A, Burdett V, & Modrich PL (2006) DNA mismatch repair: functions and mechanisms. *Chem Rev* 106(2):302-323.
12. Truglio JJ, Croteau DL, Van Houten B, & Kisker C (2006) Prokaryotic nucleotide excision repair: the UvrABC system. *Chem Rev* 106(2):233-252.
13. Marians KJ (2018) Lesion Bypass and the Reactivation of Stalled Replication Forks. *Annu Rev Biochem*.
14. Michel B, Boubakri H, Baharoglu Z, LeMasson M, & Lestini R (2007) Recombination proteins and rescue of arrested replication forks. *DNA Repair (Amst)* 6(7):967-980.
15. Michel B & Sandler SJ (2017) Replication Restart in Bacteria. *J Bacteriol* 199(13).
16. Sinha RP & Hader DP (2002) UV-induced DNA damage and repair: a review. *Photochem Photobiol Sci* 1(4):225-236.
17. Echols H & Goodman MF (1990) Mutation induced by DNA damage: a many protein affair. *Mutat Res* 236(2-3):301-311.
18. Belle JJ, Casey A, Courcelle CT, & Courcelle J (2007) Inactivation of the DnaB helicase leads to the collapse and degradation of the replication fork: a comparison to UV-induced arrest. *J Bacteriol* 189(15):5452-5462.
19. Setlow RB, Swenson PA, & Carrier WL (1963) Thymine Dimers and Inhibition of DNA Synthesis by Ultraviolet Irradiation of Cells. *Science* 142(3598):1464-1466.

20. Boyce RP & Howard-Flanders P (1964) Release of Ultraviolet Light-Induced Thymine Dimers from DNA in *E. Coli* K-12. *Proc Natl Acad Sci U S A* 51:293-300.
21. Rupp WD & Howard-Flanders P (1968) Discontinuities in the DNA synthesized in an excision-defective strain of *Escherichia coli* following ultraviolet irradiation. *J Mol Biol* 31(2):291-304.
22. Courcelle CT, Belle JJ, & Courcelle J (2005) Nucleotide excision repair or polymerase V-mediated lesion bypass can act to restore UV-arrested replication forks in *Escherichia coli*. *J Bacteriol* 187(20):6953-6961.
23. Yeeles JT & Marians KJ (2011) The *Escherichia coli* replisome is inherently DNA damage tolerant. *Science* 334(6053):235-238.
24. Yeeles JT & Marians KJ (2013) Dynamics of leading-strand lesion skipping by the replisome. *Mol Cell* 52(6):855-865.
25. McInerney P & O'Donnell M (2007) Replisome fate upon encountering a leading strand block and clearance from DNA by recombination proteins. *J Biol Chem* 282(35):25903-25916.
26. Pages V & Fuchs RP (2003) Uncoupling of leading- and lagging-strand DNA replication during lesion bypass in vivo. *Science* 300(5623):1300-1303.
27. Higuchi K, *et al.* (2003) Fate of DNA replication fork encountering a single DNA lesion during *oriC* plasmid DNA replication in vitro. *Genes Cells* 8(5):437-449.
28. Jeiranian HA, Schalow BJ, Courcelle CT, & Courcelle J (2013) Fate of the replisome following arrest by UV-induced DNA damage in *Escherichia coli*. *Proc Natl Acad Sci U S A* 110(28):11421-11426.
29. Rudolph CJ, Upton AL, & Lloyd RG (2007) Replication fork stalling and cell cycle arrest in UV-irradiated *Escherichia coli*. *Genes Dev* 21(6):668-681.
30. Reyes-Lamothe R, Possoz C, Danilova O, & Sherratt DJ (2008) Independent positioning and action of *Escherichia coli* replisomes in live cells. *Cell* 133(1):90-102.
31. Reyes-Lamothe R, Sherratt DJ, & Leake MC (2010) Stoichiometry and architecture of active DNA replication machinery in *Escherichia coli*. *Science* 328(5977):498-501.
32. Beattie TR, *et al.* (2017) Frequent exchange of the DNA polymerase during bacterial chromosome replication. *Elife* 6.
33. Lewis JS, *et al.* (2017) Single-molecule visualization of fast polymerase turnover in the bacterial replisome. *Elife* 6.
34. Heller RC & Marians KJ (2006) Replisome assembly and the direct restart of stalled replication forks. *Nat Rev Mol Cell Biol* 7(12):932-943.
35. Salic A & Mitchison TJ (2008) A chemical method for fast and sensitive detection of DNA synthesis in vivo. *Proc Natl Acad Sci U S A* 105(7):2415-2420.
36. Wiktor J, Lesterlin C, Sherratt DJ, & Dekker C (2016) CRISPR-mediated control of the bacterial initiation of replication. *Nucleic Acids Res* 44(8):3801-3810.
37. Kelman Z, Yuzhakov A, Andjelkovic J, & O'Donnell M (1998) Devoted to the lagging strand-the subunit of DNA polymerase III holoenzyme contacts SSB to promote processive elongation and sliding clamp assembly. *EMBO J* 17(8):2436-2449.
38. McGinness KE, Baker TA, & Sauer RT (2006) Engineering controllable protein degradation. *Mol Cell* 22(5):701-707.
39. Marceau AH, *et al.* (2011) Structure of the SSB-DNA polymerase III interface and its role in DNA replication. *EMBO J* 30(20):4236-4247.

40. McEvoy AL, *et al.* (2012) mMaple: a photoconvertible fluorescent protein for use in multiple imaging modalities. *PLoS One* 7(12):e51314.
41. Liao Y, Li Y, Schroeder JW, Simmons LA, & Biteen JS (2016) Single-Molecule DNA Polymerase Dynamics at a Bacterial Replisome in Live Cells. *Biophys J* 111(12):2562-2569.
42. Sedgwick SG & Bridges BA (1974) Requirement for either DNA polymerase I or DNA polymerase 3 in post-replication repair in excision-proficient *Escherichia coli*. *Nature* 249(455):348-349.
43. Johnson RC (1978) Reduction of postreplication DNA repair in two *Escherichia coli* mutants with temperature-sensitive polymerase III activity: implications for the postreplication repair pathway. *J Bacteriol* 136(1):125-130.
44. Robinson A, *et al.* (2015) Regulation of Mutagenic DNA Polymerase V Activation in Space and Time. *PLoS Genet* 11(8):e1005482.
45. Henrikus SS, *et al.* (2018) DNA polymerase IV primarily operates outside of DNA replication forks in *Escherichia coli*. *PLoS Genet* 14(1):e1007161.
46. Thrall ES, Kath JE, Chang S, & Loparo JJ (2017) Single-molecule imaging reveals multiple pathways for the recruitment of translesion polymerases after DNA damage. *Nat Commun* 8(1):2170.
47. Kim S, Dallmann HG, McHenry CS, & Marians KJ (1996) Coupling of a replicative polymerase and helicase: a tau-DnaB interaction mediates rapid replication fork movement. *Cell* 84(4):643-650.
48. Dallmann HG, Kim S, Pritchard AE, Marians KJ, & McHenry CS (2000) Characterization of the unique C terminus of the *Escherichia coli* tau DnaX protein. Monomeric C-tau binds alpha AND DnaB and can partially replace tau in reconstituted replication forks. *J Biol Chem* 275(20):15512-15519.
49. Ribeck N, Kaplan DL, Bruck I, & Saleh OA (2010) DnaB helicase activity is modulated by DNA geometry and force. *Biophys J* 99(7):2170-2179.
50. Graham JE, Marians KJ, & Kowalczykowski SC (2017) Independent and Stochastic Action of DNA Polymerases in the Replisome. *Cell* 169(7):1201-1213 e1217.
51. Courcelle CT, Chow KH, Casey A, & Courcelle J (2006) Nascent DNA processing by RecJ favors lesion repair over translesion synthesis at arrested replication forks in *Escherichia coli*. *Proc Natl Acad Sci U S A* 103(24):9154-9159.
52. Koehler DR, Courcelle J, & Hanawalt PC (1996) Kinetics of pyrimidine(6-4)pyrimidone photoproduct repair in *Escherichia coli*. *J Bacteriol* 178(5):1347-1350.
53. Tourriere H, Versini G, Cordon-Preciado V, Alabert C, & Pasero P (2005) Mrc1 and Tof1 promote replication fork progression and recovery independently of Rad53. *Mol Cell* 19(5):699-706.
54. Szyjka SJ, Viggiani CJ, & Aparicio OM (2005) Mrc1 is required for normal progression of replication forks throughout chromatin in *S. cerevisiae*. *Mol Cell* 19(5):691-697.
55. Yeeles JTP, Janska A, Early A, & Diffley JFX (2017) How the Eukaryotic Replisome Achieves Rapid and Efficient DNA Replication. *Mol Cell* 65(1):105-116.
56. Lewis JS, *et al.* (2017) Single-molecule visualization of *Saccharomyces cerevisiae* leading-strand synthesis reveals dynamic interaction between MTC and the replisome. *Proc Natl Acad Sci U S A* 114(40):10630-10635.
57. Iyer DR & Rhind N (2017) The Intra-S Checkpoint Responses to DNA Damage. *Genes (Basel)* 8(2).

58. Datsenko KA & Wanner BL (2000) One-step inactivation of chromosomal genes in *Escherichia coli* K-12 using PCR products. *Proc Natl Acad Sci U S A* 97(12):6640-6645.
59. Wang X, Lesterlin C, Reyes-Lamothe R, Ball G, & Sherratt DJ (2011) Replication and segregation of an *Escherichia coli* chromosome with two replication origins. *Proc Natl Acad Sci U S A* 108(26):E243-250.

Chapter 4

The χ Subunit of the Clamp Loader Promotes Fast Search Times and Increases Local Concentration of DNA Polymerase in *Escherichia coli*

This chapter is based on a manuscript in preparation: Soubry, N., Lopez Jauregui, C. V., Rascon Perez, J.P., and Reyes-Lamothe, R. The χ Subunit of the Clamp Loader Promotes Fast Search Times and Increases Local Concentration of DNA Polymerase in *Escherichia coli*

With the surprising finding that χ , a clamp loader subunit, mediates the Pol III HE recruitment independently of the replication fork, I decided to test the hypothesis that χ has a role in maintaining the dynamic replisome. I used fluorescence microscopy techniques to determine the effect of χ on the dwell time, the DNA-bound proportion, and the DNA polymerase Pol III's search time. I found that depletion of χ resulted in less Pol III* bound to DNA as reported by the number of spots per cell, the fluorescence intensity of spots, and the frequency of immobile single-molecules in the cell. I also found that χ increased the frequency of observed consecutive unbinding and binding (rebinding) events by single copies of Pol III*. However, my results showed only minor differences in the dwell times of Pol III* and time between rebinding events (effectively Pol III* search time) in the absence of χ , suggesting incomplete χ depletion or the presence of additional factors. I propose that the association of χ with SSB bound to ssDNA is used to modulate the rate at which Pol III* is recruited to the replication fork. The initial capture of Pol III* by SSB would be followed by the interaction with other replisome subunits and the growing DNA chains. I also suggest that extended periods without Pol III* at the replication fork, observed in χ -depleted cells, results in replisome disassembly and fork collapse. Hence explaining previous observations of χ in the stability of the replication fork.

4.1 Abstract

The replisome is a dynamic multiprotein machine that is responsible for replicating DNA. During active DNA synthesis, The Pol III* is constantly exchanging. This exchange is beneficial for the cell as it can respond quickly to its surrounding environment by either slowing down its rate or exchanging for translesion polymerases. Previous work has shown that the χ subunit of the clamp loader can recruit the Pol III holoenzyme independent of active replication forks. The χ subunit has been shown to tether the clamp loader to SSB. Using a degradation technique, we removed χ and investigated how that affected the Pol III*. Our results show that χ is crucial to replisome stability. Degradation of χ results in 50% less Pol III DNA-bound in the cell, affecting half of the replisomes. Our results also show that χ helps reduce the search time of Pol III*, increasing the probability a single molecule of Pol III* will bind more than once. We propose that χ provides stability to the replisome by reducing the search time and increasing the local concentration of Pol III* near the replication fork.

4.2 Introduction

DNA replication is an important activity carried out by every cell type. In *Escherichia coli*, this process is carried out by the replisome, a multifunctional machine composed of more than twelve proteins (Figure 4.4.1. A). The DNA polymerase, Pol III, which performs the DNA synthesis, comprises three subunits [1-3], $\alpha\epsilon\theta$. Three DNA Pol III copies are incorporated into the polymerase through an interaction with the τ subunit of the clamp loader complex ($\tau_3\delta\delta'\psi\chi$) to make the Pol III* ($(\alpha\epsilon\theta)_3 \tau_3\delta\delta'\psi\chi$). The clamp loader is also responsible for loading the β -clamp dimer onto DNA, which is required for processive synthesis by Pol III. The addition of β -clamp to Pol III* forms the Pol III holoenzyme (Pol III HE). At the center of the replisome is the replicative helicase, DnaB, which unwinds the parental DNA. Located on the lagging strand, the DnaB helicase recruits the primase, DnaG, which synthesizes the RNA primers needed by the DNA Pol III. The DnaB complex is tied to the Pol III HE via its interaction with τ of the clamp loader complex. Once in every cell cycle, DNA replication is initiated with the assembly of two replisomes in opposite orientations at a specific locus of the chromosome, the *oriC* [4]. Each replication fork duplicates half of the 4.6-Mbp circular chromosome at rates between 0.6 and 1

kbp·s⁻¹ at 37 °C [5], completing replication as the two of them meet at the region opposite from *oriC*.

Each replisome is committed to replicating half of the 4Mbp chromosome. Hence in the past, it was assumed that the replisome needed to be a stable entity. This was supported by previous *in vitro* data where a single purified replisome assembled on DNA synthesized on average 70 kbp of DNA without requiring any additional or replacement DNA Pol III [6, 7]. This, combined with data showing that replisomes undergo one disassembly event every five replication cycles, indicates that replisomes are very stable and processive [8]. However, when individual Pol III* dwell times* were investigated *in vivo*, the Pol III* was shown to exchange every 10s, a stark difference from the previously estimated average [9]. This finding was confirmed independently *in vitro* in conditions where Pol III* was in excess, suggesting competition between active and diffusive subunits [10].

It is still unclear how does the replisome maintains rates of 1kb per second under fast Pol III* turnover. However, recent work in our lab hinted at the role of the χ subunit in this process. In the study in question, an interaction between the χ and SSB resulted in Pol III HE's recruitment to DNA away from the replication fork after UV exposure [11]. Also, removing χ in these experiments resulted in a decrease in the number of Pol III molecules bound to DNA in cells not exposed to UV.

The $\psi\chi$ complex forms a bridge between the $\tau_3\delta\delta'$ pentamer and SSB (Figure 4.4.1.A) [12-18]. ψ interacts with τ/γ and χ , and χ interacts with SSB. Furthermore, the ψ - τ interaction favours the assembly of the $\tau_3\delta\delta'$ pentamer in conditions limiting $\delta\delta'$ concentrations [19, 20]. It stabilizes an ATP-activated DNA-high affinity conformation of the clamp loader and facilitates the clamp loading reaction *in vitro* [21, 22]. The absence of χ severely impairs growth, particularly at high temperatures. Cells are also usually elongated due to the activation of the SOS response. A duplication of the *ssb* gene partly restores the viability of the χ and ψ when either is depleted [23]. SOS is constitutively expressed in the ψ (*hold*) mutant due to the accumulation of single-stranded DNA gaps in lagging strands [24].

We used fluorescence microscopy to test the effect of depleting χ on the binding replisome components. Our results lead us to conclude that χ increases the recruitment of Pol III to the fork. In our model, the function of the $\psi\chi$ complex is to reduce the search time and maintain a higher concentration of the Pol III* near the replication fork. The higher concentration of the Pol III* near the replication fork creates a competition for the elongating 3' end DNA chain. This ensures that if there is any stalling of the active Pol III* or damage to the active replisome, a new Pol III* or a translesion polymerase can easily be incorporated. Our data provides a mechanistic explanation of the previously described role of χ as a stabilizing factor of the replication fork.

4.3 Results

4.3.1 The χ subunit contributes to the recruitment of the Pol III* to the replisome

To determine the χ subunit's role in DNA replication, we used fluorescence microscopy to visually determine how the removal of χ alters replisome subunit stability during replication. First, we tried to produce a strain carrying $\Delta holC$ (coding for χ); however, these cells had a complicated elongated morphology under the microscope, removing the possibility of fluorescence microscopy (data not shown). We then used a previously described χ degradation system to remove χ during growth [11]. This system was added to strains carrying derivatives of replisome components fused to the yellow fluorescent protein YPet [2, 25]. We used slow-growth conditions, with generation times above 100 min, to minimize convolution of our data by new rounds of DNA replication, as reported previously. In these conditions, cells undergo a single replication event and have at most two replication forks, translating into cells with zero, one, or two spots for fluorescently tagged replisome subunits. We tagged the proof-reading exonuclease subunit of Pol III, ϵ . When imaging, we used exposure times of 5 seconds to determine the average behaviour of each component. After 1 hour of χ degradation, we saw a decrease in the average number of ϵ -YPet foci per cell from 1.34 before treatment to 0.48 after treatment (Figure 4.1. C, Figure S4.1). This decrease in foci number suggests that there are replisomes without DNA Pol III for periods of few seconds or a decline in the number of replisomes in the cell. Alternatively, these results could also suggest a spatial rearrangement of the pair of replisomes in the cell without decreasing their number.

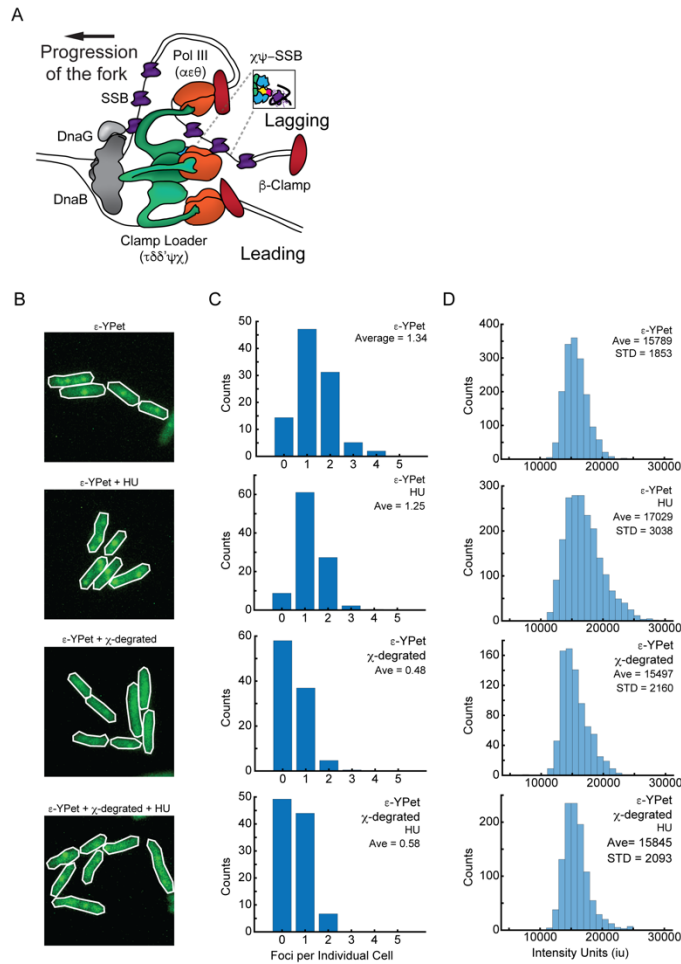


Figure 4.1 (A) Model of the architecture of an active replisome. The DnaB helicase unwinds DNA. DnaG primase binds to DnaB. Pol III and the clamp loader bind each other through the clamp loader's τ subunit, which also mediates binding to the DnaB helicase. The β -clamp is left behind the fork after the completion of an Okazaki fragment at the lagging strand. SSB covers ssDNA produced during the cycle of lagging strand synthesis. (B) Sample images of cells carrying ϵ -YPet with the addition of HU and/or 0.5% Arabinose. (C) Distribution of the number of foci per cell in cells carrying ϵ -YPet with the addition of HU and/or 0.5% Arabinose. (D) Distribution of individual spot intensity in cells carrying ϵ -YPet with the addition of HU and/or 0.5% Arabinose.

To test if we were observing a decrease in the number of active replisomes, we then looked at the intensity of individual spots. We reasoned that a higher intensity would mean a higher stoichiometry of ϵ at the replication fork. Surprisingly the degradation of χ did not affect the intensity of single foci. The average intensity of foci went from 15895 ± 1853 iu (intensity units) before treatment to 15497 ± 2160 iu after treatment (Figure 4.1. D). Thus, it seemed as if χ was

leading to replisome instability, but individual replisomes did not display a change in stoichiometry.

Our results suggested that χ and SSB may help recruit Pol III* to the replisome. Hence, we wondered if increasing the amount of ssDNA at the replication fork could increase the number of Pol III* copies observed. To test this, we looked at the intensity of these spots after the addition of hydroxyurea (HU). HU inhibits the ribonucleotide reductase, leading to a depletion of the deoxyribonucleoside triphosphate pools [26]. This, therefore, stalls the DNA polymerase but leaves the helicase unaffected, creating long ssDNA stretches where SSB binds. Adding HU did cause an increase in the intensity of the ϵ -YPet foci. As before, χ degradation resulted in a decrease in foci' average intensity, going from 17029 ± 3039 iu and after χ degradation, 15845 ± 2093 iu (Figure 4.1. D). The average number of foci for the post-HU cells was similar to the pre-HU cells. Though using a rough estimate, this data indicates that during normal replication, the stoichiometry of ϵ -YPet at the foci is similar, regardless of χ . However, this imprecise measurement of stoichiometry hints that stalled replication forks, χ can recruit more Pol III*. The data above supports the role of χ as a recruiter of the DNA polymerase to SSB at the replication fork.

4.3.2 The χ subunit contributes to the probability of recruitment and the length of Pol III* binding to the replisome

To further characterize the role of χ in the replisome, we studied the binding kinetics of the DNA Pol III with or without the presence of χ using single-particle tracking Photoactivatable Localization Microscopy (sptPALM) [11]. We first tested for a decrease in the number of copies of Pol III* bound to the replisome when χ is not present. We used a previously characterized fusion of ϵ with the photoconvertible fluorescent protein mMaple [27]. We used exposure times of 20-ms and continuous low-intensity activation with the 405-nm laser. This resulted in low rates of stochastic photoconversion and about one fluorescent molecule per cell at any given time point during a 5000-frame movie. Single molecules were tracked and classified as either bound or diffusing inside cells based on their diffusion coefficients. In conditions where χ was present, the DNA-bound proportion of ϵ -mMaple was 20.12 ± 0.08 % (Figure 4.2. A). After treatment, the DNA-bound proportion dropped to 12.51 ± 0.18 % (Figure 4.2. A). Thus, this data supports the

conclusion of a more significant number of copies of ϵ at replication forks when χ is present and with the loss of about half of the active replisomes.

We then applied sptPALM using different imaging parameters to determine how the removal of χ would affect the residence time of ϵ . In this technique, we used longer exposure times (500ms) to blur diffusing molecules. Then we measured the lifetime of single particles after a single activation. To get an accurate assessment of the dwell time, we then compared the track duration to a photobleaching control, LacI-mMaple bound to a *lacO* array [9]. With χ present, the dwell time of ϵ -mMaple was 5.85 s (Figure 4.2. B). This dwell time is significantly shorter than a previously counted number. We determined this shorter dwell time due to improvements to the filtering process that now uses machine learning to sort out noise [28]. When χ was degraded, the dwell time was slightly longer, 8.19 s (Figure 4.2. B). Combined, these results indicate that χ increases the amount of DNA polymerase bound to DNA and slightly reduces the dwell time of bound DNA polymerase molecules.

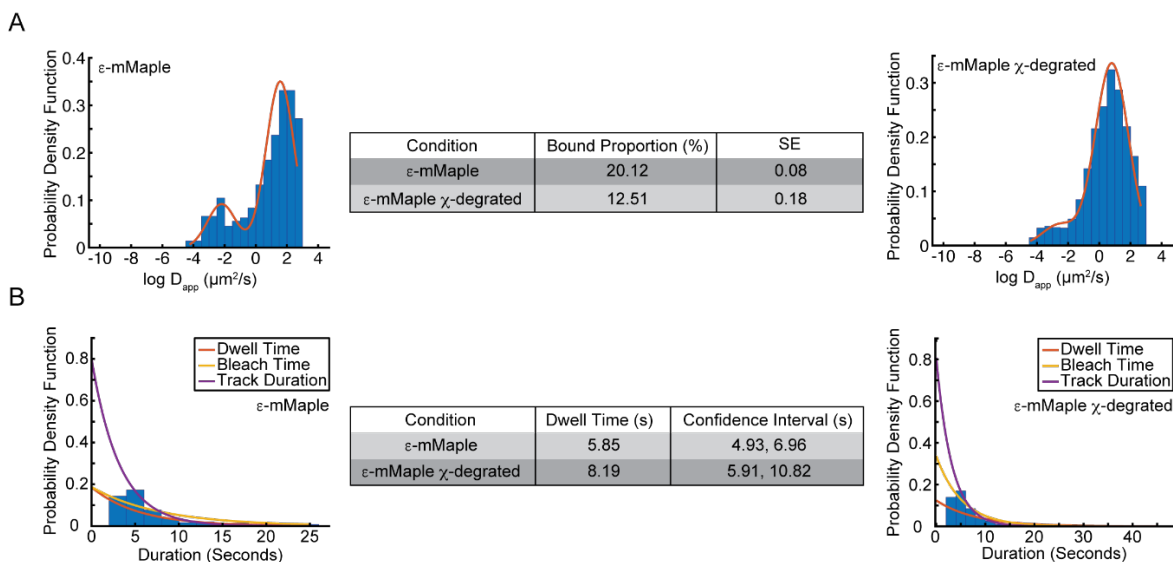


Figure 4.2 (A) The distribution of the logarithm of the apparent diffusion coefficient (blue bars) for Pol III ϵ , before and after χ degradation, showing the fitting of a gaussian mixture model (red and grey line). Percentage indicates the proportion of diffusing molecules. (Left) Pol III ϵ subunit. $n = 235$ cells (Center) Table with results shown in both table for both conditions (Right) Pol III ϵ subunit after χ degradation. $n = 357$ cells (B) Representative examples of the distribution of fluorescent foci life-spans (blue bars) for Pol III ϵ subunit, before and after χ degradation, showing the fitting of a single-exponential decay model (purple line), the estimated bleaching rate in the same conditions (yellow line) and the corrected estimated dwell-time (red line). (Left) Pol III ϵ subunit. $n = 512$ cells (Center) Table with results shown in both table for both conditions (Right) Pol III ϵ subunit after χ degradation. $n = 337$ cells

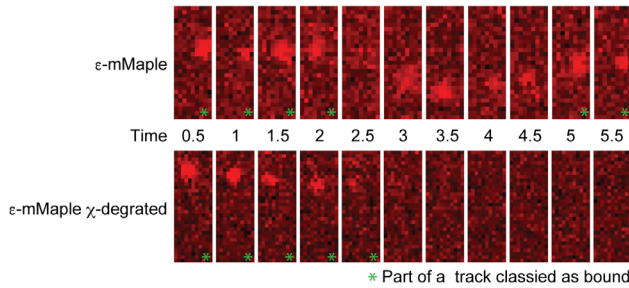
4.3.3 The χ subunit enables rapid rebinding of Pol III* molecules to the replisome.

When examining long capture videos to determine the dwell times, it was frequently observed that individual copies of Pol III* undergo multiple binding events. However, after the depletion of χ , these events became less frequent. We attempted to quantify the number of rebinding events to replication fork sites that would provide us with the frequency, length, and time between these events. Rebinding events were classified as multiple bound events for a single molecule (Figure 4.3. A). It is worth noting that the time between consecutive rebinding events of single copies of ϵ -mMaple is a direct measurement of the Pol III* search time for the replication fork. However, to detect these rebinding events, often separated by only a few frames, we did two changes in our tracking analysis: first, we removed the memory parameter that allows for the disappearance of the spot for a single frame and still be joined as a track; second, we shortened the required number of localizations for a track from 4 to 3. These changes, although required for the detection of rebinding events, also generated false positives. To quantify our measurements' basal error, we used DnaB-mMaple, which has dwell times of several minutes and should not rebind in our experiments. Using this strain, we estimated that the rebinding error in our analysis occurred 15.21 ± 7.01 % of the time (Figure 4.3. B). When χ was present, there was a rebinding event, 40.19 ± 2.26 % of the time, compared to 28.94 ± 5.48 % when χ was degraded, confirming our hypothesis (Figure 4.3. B). The higher incidence of rebinding when χ was present demonstrated the ability of χ to reduce the search time of the Pol III*. We emphasize, however, that these numbers likely underestimate the frequency of rebinding in the presence of χ .

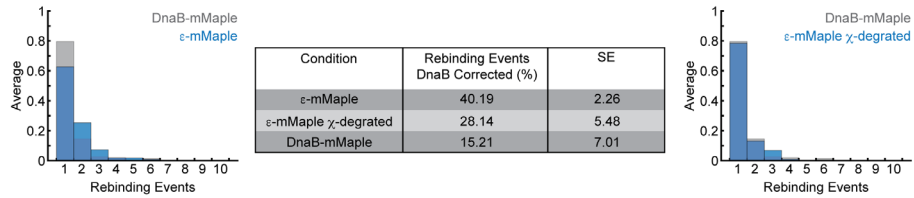
The results above showed that the presence of χ has a significant impact on the time between consecutive ϵ -mMaple binding events. In χ -depleted cells, this time was sufficiently long to miss the detection of many of them in our experiments. To better quantify the difference in the search time of ϵ -mMaple, we then looked to measure the interval time between consecutive binding events in the presence or absence of χ . In normal conditions, the search time of ϵ -mMaple was 9.22 s (Figure 4.3. C), whereas, without χ , the search time was only slightly longer, 11.71 s (data not shown). The single exponential fit for the χ -degraded cell was not ideal, so a two-exponential model was tested for all three conditions. The two-exponential fit for the DnaB control and ϵ -mMaple with χ had a low goodness-of-fit (data not shown). However, for our χ -degraded

condition, the goodness-of-fit was better with the two-exponential fit. This fit indicated two behaviours, with one with a track interval of 2.38 s and the other with a track interval of 14.45 (Figure 4.3. C). For both of these results, the search time was longer than in our control, DnaB, which was dominated by track fragmentation caused by fluctuations in the intensity of spots. However, the difference between the wt and the χ -depleted cells is smaller than what we expected from our rebinding frequency results. In our search time estimate in χ -depleted conditions, the caveat is that we may be measuring cells where degradation did not occur or was incomplete. Overall, our results support that χ has an active role in recruiting the Pol III* by reducing the search time. Still, currently, we cannot confidently quantify the reduction in the search time mediated by χ .

A



B



C

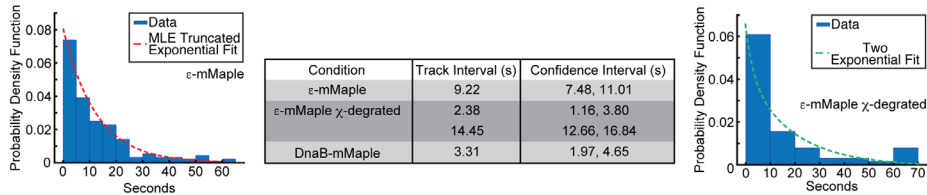


Figure 4.3 (A) Representative examples of videos for both ϵ -mMaple and ϵ -mMaple with the addition of 0.5% arabinose. Green asterisks represent spots part of a track classified as bound. (B) Representative examples of the distribution of fluorescent foci rebinding events (blue bars) for Pol III ϵ subunit and DnaB bound control (grey bars), before and after χ degradation. (Left) Pol III ϵ subunit. n = 317 cells (Center) Table with results shown in both table for both conditions (Right) Pol III ϵ subunit after χ degradation. n = 309 cells (C) Representative examples of the distribution of fluorescent foci time interval between foci tracks (blue bars) for Pol III ϵ subunit, before and after χ degradation, showing the fitting of a single-exponential decay model (red line) or a two-exponential decay (green line). (Left) Pol III ϵ subunit. n = 317 cells (Center) Table with results shown in both table for both conditions (Right) Pol III ϵ subunit after χ degradation. n = 309 cells

4.4 Discussion

Recent work from our group and other groups has dramatically changed our understanding of what is happening to the replisome components during DNA replication. The replisome for an extended time was thought to be a stable and progressive entity. With the emerging use of single-molecule fluorescence microscopy techniques *in vivo* and *in vitro*, multiple groups have described a greater exchange rate of replisome subunits. This report focuses on how the replisome can keep its integrity while being dynamic (Figure 4.4). By keeping a higher local concentration, this dynamic molecular machine can maintain a copy of Pol III* at the replisome most of the time.

A dynamic replisome may be more adaptive to its surrounding environment. For example, when encountering DNA damage, using its dynamic behaviour and low copy number, the replisome can slow down its replication rate to give the repair mechanisms time to fix the DNA damage before the replisome encounters or bypasses many lesions. In wild-type situations, a dynamic replisome would also allow for the bypass of DNA-interacting proteins. However, when the SOS response is activated, and the translesion polymerases' concentration increases dramatically, the translesion polymerases can take over. Seemingly, the cell uses a concentration-based approach to give itself flexibility and speed in its response to outside influences.

Multiple groups have suggested a link between the $\chi\psi$ subunits and the stability of the replication fork. However, the mechanism by which they acted was unclear. Here we define that the cy subunits' interaction with SSB allows SSB to serve as a recruiting platform for Pol III* (Figure 4.4). This interaction provides the replisome with a tunable approach to recruit the Pol III*. It is interesting to highlight that without a copy of Pol III* at the replisome, the helicase would

continue unwinding DNA and contribute to the accumulation of bound SSB. This, in turn, should increase the likelihood that a Pol III* would be recruited to continue replication. We hypothesize that DnaB may be less stable without Pol III*, leading to the eventual disassembly from DNA. An additional contributing factor to fork instability is the potential runout of available SSB to cover ssDNA in cases of prolonged uncoupling between helicase and polymerase. Our work suggests that, despite the poor evolutionary conservation of $\chi\psi$, equivalent strategies should be found in all bacteria.

4.4.1 $\chi\psi$ are the hub needed to maintain a dynamic replisome

SSB is known as a master recruiter, recruiting multiple different proteins to aid in cell survival. Its interaction with χ provides it with another role as an essential cog in maintaining a healthy replisome. Recent data from our group demonstrated that the χ could recruit the Pol III* to other sites on the chromosome immediately after DNA damage. The Pol III* bound to additional sites was entirely dependent on the presence of χ . When we degraded χ in wild-type conditions, our results show us that, like previous reports, the stability of the replisome was significantly reduced (Figure 4.1. C). Furthermore, fewer Pol III* were bound to DNA. Those bound, presumed active, maybe bound longer, but this difference was not statically significant (Figure 4.2). *In vitro* data where the replisome works in conditions without excess subunits replicated 85 kb of DNA fragments, equivalent to a dwell time of 185s in our conditions [5, 6]. Our results are much shorter than that number, possibly meaning there are still other elements causing shorter dwell times we see *in vivo*. This may indicate that competition between multiple Pol III* is only one of the factors that determine its dissociation rate in the cell. Competition for binding with other partners of β clamp and DNA supercoiling are additional factors that may influence Pol III* binding kinetics.

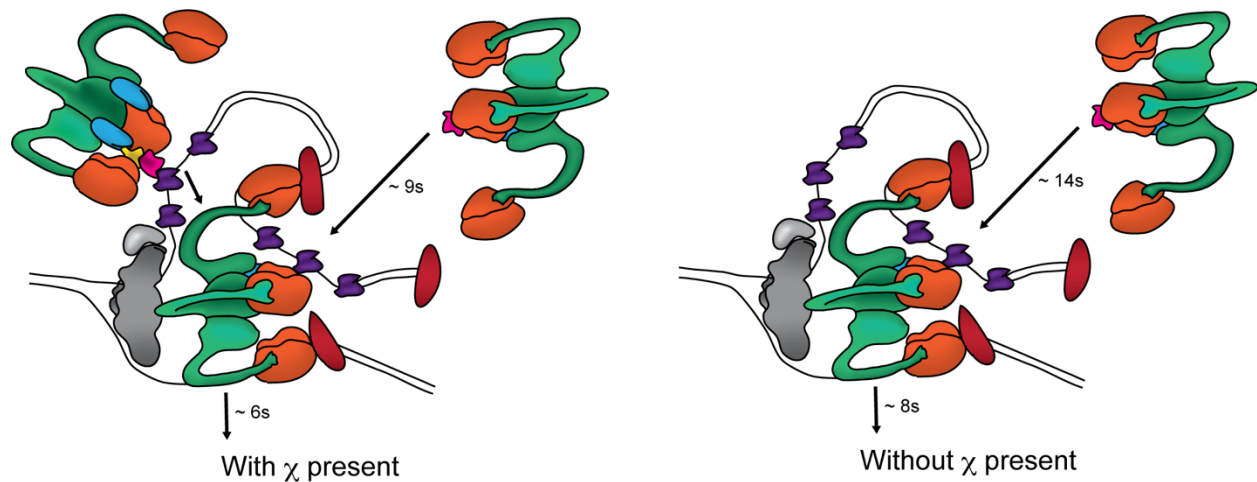


Figure 4.4. Model for the role of χ in the replisome. (Left) When χ is present, the active replisome is bound for approximately 6 seconds, there is more Pol III* bound to the fork, and the search time for Pol III* is around 9 seconds. (Right) When χ is not present, the active replisome is bound for a longer time, approximately 8 seconds, there is less Pol III* bound to the fork, and the search time for Pol III* is more prolonged around 12 seconds.

However, we found conflicting results when investigating the role of χ in reducing the Pol III* search time (Figure 4.4.3. B). When removing χ , the bound proportion of the Pol III* was significantly lower, indicating that χ was responsible for keeping a certain fraction of Pol III* at the replication fork (Figure 4.2.A). This result is substantiated by the HU experiments, which show a larger pool of Pol III* bound in the presence of χ (Figure 4.1.C). Lastly and most importantly, the frequency of rebinding events was higher with χ present, meaning it facilitates recycling of Pol III* (Figure 4.3.B). These results indicate that χ is reducing the search time of Pol III*; however, in our data, the increase of time seen in our track interval data (Figure 4.3.C) is confusing with two modes, one acting almost like track fragmentation seen with DnaB and the other significantly longer than when χ is present, but not as long as we had anticipated. We believe that this is presumably due to background χ caused by its incomplete degradation.

The survival of *holC* or *hold* mutant strains is dependent on various suppressor mutations. Our results can explain those results. The first of those mutations is a suppressor mutation inactivating the SOS response [24]. The SOS response is activated in response to DNA damage. The SOS response activates many repair genes, especially three different translesion polymerases; Pol II, Pol IV and Pol V [20, 29]. The SOS response is activated in a *hold* mutant as there is an accumulation of ssDNA. Pol II and Pol IV contribute to the mutant's low viability by outcompeting

the native Pol III* at the replication fork [24, 30]. By removing $\chi\psi$, the Pol III* recruitment takes longer, thus allowing the wrong polymerases to continue replication, increasing the mutation rate. Another mutation is the duplication of *ssb*. The authors proposed that the amount of SSB protein favours a replicative mode of SSB binding to DNA, which stabilizes ψ -less Pol III HE [23]. We suggest that with a duplication of SSB, there will be more SSB to protect ssDNA accumulated by the inefficient exchange of the Pol III*. Mutations affecting potassium import (*trkA*, *trkE*, *sapC*, *rfaP*) also restored viability as an increase of intracellular potassium strengthens the electrostatic interaction between replisome proteins and between the replisome and DNA [12, 31]. With the recruitment of the Pol III* affected in these mutants, stabilizing the replisome to DNA ensures DNA replication will continue. This would be less of a burden on SSB to cover ssDNA caused by the inefficient exchange of the Pol III*. Cells with χ can also overcome or avoid conflicts between the replisome and transcription machinery [32]. Generally, when the cell cannot efficiently recruit Pol III*, the cells generate other mutations to ensure that no conflict would lead to an increase in ssDNA.

Further work needs to be done to confirm these results in conditions where χ is wholly removed. We suspect that some molecules of χ have not yet been degraded in our assays, leading to ambiguity in the track interval analysis (Figure 4.3.C). Despite this limitation, we demonstrate that χ is an essential factor in the dynamics in the replisome. Our data favours a model where χ serves as a recruiter to increase the recycling of the Pol III* and increase the local concentration of the Pol III* near the replication fork. Our work hints at the use of fast search times and high local concentrations as general strategies to maintain dynamic molecular machines in the broader scope.

4.5 Experimental Procedures

4.5.1 Strains and growth conditions

All strains used are derivatives of AB1157. Cells were routinely grown in LB or M9 minimal media. M9 was supplemented with glycerol (final concentration 0.2%); 100 $\mu\text{g/ml}$ of amino acids threonine, leucine, proline, histidine and arginine; and thiamine (0.5 $\mu\text{g/ml}$). When required, antibiotics were added at the following concentrations: ampicillin (100 $\mu\text{g/ml}$), kanamycin (30

$\mu\text{g/ml}$), and chloramphenicol (25 $\mu\text{g/ml}$). Chromosomal replacement of replisome genes by fluorescent derivatives, degron-tagged alleles or deletions was done by P1 transduction. These include; WM32. Strain list is available in Table 4.1.

Before imaging, cells were grown in LB for at least 5 hours then transferred to M9 media via a 1:1000 dilution. After being grown overnight, cells were diluted again in M9 and grown to an OD_{600} between 0.1- 0.2 before being used for imaging. For degron experiments, cells were induced to a concentration of 0.5% arabinose at an OD_{600} of 0.1 after the second dilution in M9 and grown for 45 minutes to an hour before imaging. For hydroxyurea experiments, treatment with 100mM hydroxyurea was done on the agarose pad by mixing HU with media and agarose.

4.5.2 Imaging

Imaging was performed at room temperature on an inverted Olympus IX83 microscope using a 60x oil objective lens (Olympus Plan Apo 60X NA 1.42 oil) or 100x oil objective lens (Olympus Plan Apo 100X NA 1.40 oil). Images were captured using an Andor Zyla 4.2 sCMOS camera. Z-stacks were done using a NanoScanZ piezo by Prior Scientific. Excitation was done from an iChrome Multi-Laser Engine from Toptica Photonics and a 405/488/561/640nm laser set (Chroma) or X-Cite 120LED lamp using the ET – ECFP/EYFP/mCherry filter set (Chroma). Laser triggering was done through a real-time controller U-RTCE (Olympus). Experiments were done from a single-line cellTIRF illuminator (Olympus). Olympus CellSens 2.1 imaging software was used to control the microscope and lasers.

For microscopy, cells were spotted on a 1% agarose pad in M9-Glycerol. A 32-frame Z-stack of brightfield images was taken for each fluorescent image.

4.5.3 Spot counting analysis

All analysis was done using custom scripts written in MATLAB (Mathworks). A 32-frame bright field Z-stacks was compressed to create a black and white phase-contrast image for cell segmentation [33]. Spots were counted using a modified version of a previously developed tracking software [34]. Spots were determined using an intensity threshold then further processed using a 2D-elliptical Gaussian fit. The extracted fitted parameters were: x-position, y-position, x-

standard deviation, y-standard deviation, intensity and background. For cells with only one spot, the intensity of the spot minus the background was recorded. For cells with multiple spots, the intensity of each spot minus the background was added together to get the integrated intensity of all spots within a cell.

4.5.4 Single-molecule experiments and analysis

We determined the dwell times using a modified protocol described in our lab [28]. Briefly, cells were harvested from early log-phase cultures in M9-Glycerol (OD_{600} 0.1-0.2), concentrated and spotted onto a pad of 1% agarose in M9-Glycerol, contained in a gene frame. Coverslips cleaned with versa-clean, acetone and methanol were used to minimize fluorescent background. A single 405nm wavelength activation event, typically lasting less than 20ms, was followed by multiple 561nm wavelength excitation events with camera captures of 500ms spaced by 1s intervals. Analysis of this data was done as previously described [28]. To characterize the rate of bleaching of mMaple, we analyzed the lifetime of LacI-mMaple foci, which on average should bleach before unbinding.

Rebinding was determined using a similar protocol as the dwell time protocol. A single 405nm wavelength activation event, typically lasting less than 20ms, was followed by multiple 561nm wavelength excitation events with camera captures of 500ms with no interval. We used the same analysis pipeline mentioned above [28]. However, instead of measuring the track length and comparing it to a bleaching control, we looked at the number of "bound" tracks per activation and the amount of time between each "bound" track. Since we are looking at single molecules, this time becomes analogous to the search time.

Bound proportions were determined using a similar protocol as described in our lab [11]. Briefly, we took 5000 frames of continuous illumination of 561 nm wavelength at capture rates of 20ms with an interval time of as fast as possible under continuous 405-nm activation. For analysis, images were first segmented to remove out-of-cell noise coming from contaminants on the coverslip. Binary masks were created using MATLAB from the green fluorescent channel of mMaple. PALM tracking was performed using the TrackMate software in ImageJ [35]. Tracks were then filtered using the binary masks. We quantified the diffusion of each track using a

previously described method [34]. We then used the Gaussian mixture modelling function found in Matlab to determine bound and diffusing proportions.

4.6 Acknowledgments

We thank Anjana Badrinarayanan, Steph Weber and members of the Reyes lab for helpful discussions. Some of the experiments were done using equipment from the Integrated Quantitative Bioscience Initiative (IQBI), funded by CFI 9. This work was funded by the Natural Sciences and Engineering Research Council of Canada (NSERC# 435521-2013), the Fonds de Recherche du Quebec –Nature et technologies (FRQNT #2017-NC-198919), the Canadian Institutes for Health Research (CIHR MOP# 142473), the Canada Foundation for Innovation (CFI# 228994), and the Canada Research Chairs program.

4.7 References

1. Beattie, T.R. and R. Reyes-Lamothe, *A Replisome's journey through the bacterial chromosome*. 2015. **6**.
2. Reyes-Lamothe, R., D.J. Sherratt, and M.C. Leake, *Stoichiometry and architecture of active DNA replication machinery in Escherichia coli*. 2010. **328**(5977).
3. Kurth, I. and M. O'Donnell, *New insights into replisome fluidity during chromosome replication*. Trends Biochem Sci, 2013. **38**(4): p. 195-203.
4. Costa, A., I.V. Hood, and J.M. Berger, *Mechanisms for initiating cellular DNA replication*. Annu Rev Biochem, 2013. **82**: p. 25-54.
5. Pham, T.M., et al., *A single-molecule approach to DNA replication in Escherichia coli cells demonstrated that DNA polymerase III is a major determinant of fork speed*. Molecular microbiology, 2013. **90**(3): p. 584-96.
6. Tanner, N.A., et al., *E. coli DNA replication in the absence of free β clamps*. The EMBO Journal, 2011. **30**(9): p. 1830-1840.
7. Yao, N.Y., et al., *Single-molecule analysis reveals that the lagging strand increases replisome processivity but slows replication fork progression*. Proceedings of the National Academy of Sciences of the United States of America, 2009. **106**(32): p. 13236-41.
8. Maisnier-Patin, S., K. Nordström, and S. Dasgupta, *Replication arrests during a single round of replication of the Escherichia coli chromosome in the absence of DnaC activity*. Molecular Microbiology, 2001. **42**(5): p. 1371-1382.
9. Beattie, T.R., et al., *Frequent exchange of the DNA polymerase during bacterial chromosome replication*. eLife, 2017. **6**.
10. Duderstadt, K.E., et al., *Simultaneous Real-Time Imaging of Leading and Lagging Strand Synthesis Reveals the Coordination Dynamics of Single Replisomes*. Molecular cell, 2016. **64**(6): p. 1035-1047.
11. Soubry, N., A. Wang, and R. Reyes-Lamothe, *Replisome activity slowdown after exposure to ultraviolet light in Escherichia coli*. Proceedings of the National Academy of Sciences, 2019: p. 201819297.
12. Michel, B. and A. Sinha, *The inactivation of rfaP, rarA or sspA gene improves the viability of the Escherichia coli DNA polymerase III holdD mutant*. Molecular Microbiology, 2017. **104**(6): p. 1008-1026.
13. Marceau, A.H., et al., *Structure of the SSB–DNA polymerase III interface and its role in DNA replication*. The EMBO Journal, 2011. **30**(20): p. 4236-4247.
14. Yuan, Q. and C.S. McHenry, *Strand displacement by DNA polymerase III occurs through a tau-psi-chi link to single-stranded DNA-binding protein coating the lagging strand template*. J Biol Chem, 2009. **284**(46): p. 31672-9.
15. Tondnevis, F., et al., *Solution study of the Escherichia coli DNA polymerase III clamp loader reveals the location of the dynamic psichi heterodimer*. Struct Dyn, 2015. **2**(5): p. 054701.
16. Glover, B.P. and C.S. McHenry, *The $\chi\psi$ Subunits of DNA Polymerase III Holoenzyme Bind to Single-stranded DNA-binding Protein (SSB) and Facilitate Replication of an SSB-coated Template*. Journal of Biological Chemistry, 1998. **273**(36): p. 23476-23484.

17. Gulbis, J.M., et al., *Crystal structure of the chi:psi subassembly of the Escherichia coli DNA polymerase clamp-loader complex*. European Journal of Biochemistry, 2004. **271**(2): p. 439-449.
18. Kelman, Z., et al., *Devoted to the lagging strand—the χ subunit of DNA polymerase III holoenzyme contacts SSB to promote processive elongation and sliding clamp assembly*. The EMBO Journal, 1998. **17**(8): p. 2436-2449.
19. Olson, M.W., H.G. Dallmann, and C.S. McHenry, *DnaX complex of Escherichia coli DNA polymerase III holoenzyme. The chi psi complex functions by increasing the affinity of tau and gamma for delta.delta' to a physiologically relevant range*. The Journal of biological chemistry, 1995. **270**(49): p. 29570-7.
20. Anderson, S.G., et al., *A Function for the ψ Subunit in Loading the Escherichia coli DNA Polymerase Sliding Clamp*. Journal of Biological Chemistry, 2007. **282**(10): p. 7035-7045.
21. Simonetta, K.R., et al., *The mechanism of ATP-dependent primer-template recognition by a clamp loader complex*. Cell, 2009. **137**(4): p. 659-71.
22. Gao, D. and C.S. McHenry, *Tau binds and organizes Escherichia coli replication proteins through distinct domains. Domain III, shared by gamma and tau, binds delta delta ' and chi psi*. The Journal of biological chemistry, 2000. **276**(6): p. 4447-53.
23. Duigou, S., et al., *ssb Gene Duplication Restores the Viability of Δ holC and Δ hold Escherichia coli Mutants*. PLoS Genetics, 2014. **10**(10): p. e1004719.
24. Viguera, E., et al., *Lethality of bypass polymerases in Escherichia coli cells with a defective clamp loader complex of DNA polymerase III*. Molecular Microbiology, 2003. **50**(1): p. 193-204.
25. Reyes-Lamothe, R., E. Nicolas, and D.J. Sherratt, *Chromosome replication and segregation in bacteria*. 2012. **46**.
26. Sinha, N.K. and D.P. Snustad, *Mechanism of inhibition of deoxyribonucleic acid synthesis in Escherichia coli by hydroxyurea*. J Bacteriol, 1972. **112**(3): p. 1321-4.
27. McEvoy, A.L., et al., *mMaple: a photoconvertible fluorescent protein for use in multiple imaging modalities*. PLoS One, 2012. **7**(12): p. e51314.
28. Kapadia, N., Z.W. El-Hajj, and R. Reyes-Lamothe, *Bound2Learn: A Machine Learning Approach for Classification of DNA-Bound Proteins from Single-Molecule Tracking Experiments*. bioRxiv, 2020.
29. Walsh, J.M., *Escherichia coli Y family DNA polymerases*. Frontiers in Bioscience, 2011. **16**(1).
30. Heltzel, J.M., et al., *Escherichia coli DNA polymerase IV (Pol IV), but not Pol II, dynamically switches with a stalled Pol III* replicase*. J Bacteriol, 2012. **194**(14): p. 3589-600.
31. Durand, A., et al., *Mutations Affecting Potassium Import Restore the Viability of the Escherichia coli DNA Polymerase III hold Mutant*. PLoS genetics, 2016. **12**(6): p. e1006114.
32. Cooper, D.L., et al., *The role of replication clamp-loader protein HolC of Escherichia coli in overcoming replication / transcription conflicts*. bioRxiv, 2020.
33. Julou, T., et al., *Cell-cell contacts confine public goods diffusion inside Pseudomonas aeruginosa clonal microcolonies*. Proceedings of the National Academy of Sciences, 2013. **110**(31): p. 12577-12582.
34. Uphoff, S., et al., *Single-molecule DNA repair in live bacteria*. Proc Natl Acad Sci U S A, 2013. **110**(20): p. 8063-8.

35. Schindelin, J., et al., *Fiji: an open-source platform for biological-image analysis*. Nat Methods, 2012. **9**(7): p. 676-82.

4.8 Tables

Table 4.1. Strains used for this study.

Strain	Relevant genotype	Source
AB1157	<i>thr-1, araC14, leuB6(Am), DE(gpt-proA)62, lacY1, tsx-33, qsr'-0, glnV44(AS), galK2(Oc), LAM-, Rac-0, hisG4(Oc), rfbC1, mgl-51, rpoS396(Am), rpsL31(strR), kdgK51, xylA5, mtl-1, argE3(Oc), thi-1</i>	<i>Dewitt and Adelberg, 1962</i>
TB80	<i>ΔsspB::frt, nocus-PBAD-sspB frt, dnaQ-ypet frt, holC-degrom kan</i>	<i>Soubry et al. (2019)</i>
WM7	<i>frt mMaple-DnaB</i>	<i>Beattie et al. (2017)</i>
WM32	<i>ΔsspB::frt, nocus-PBAD-sspB frt, dnaQ-mMaple frt, holC-degrom kan, Δarabad CM</i>	<i>This study</i>

Chapter 5

Conclusions

Preserving the integrity of the replisome is a crucial task for life. Fortunately, the replisome has been modified over generations upon generations to become an efficient and reliable machine. The bacterial replisome is a highly dynamic machine capable self-regulating its function to ensure cell survival [2]. This work exposes the strategies that the dynamic replisome in bacteria uses to keep its integrity through the cell cycle and when DNA is damaged.

We investigated the fate of the replisome after encountering a DNA lesion capable of inhibiting Pol III activity, but that in principle does not threaten DnaB helicase integrity (Chapter 3). Being the first to focus on the effect of UV on the replisome subunits, resulted in unique insight into the response of the replisome to DNA damage, and the dynamics of DNA synthesis on a damaged DNA template. This work unveils potential advantages of a dynamic replisome, as there is an almost immediate slowdown of the rate of DNA replication in response to DNA damage. This slowdown enables the replisome to continue to function even when there is DNA damage. Such strategy would reduce the probability of encounters between the DnaB helicase and the engaged NER system, which may lead to helicase disassembly. Further work needs to be done to test if this is a general strategy for all DNA damage able to bypass the helicase.

When the DNA Pol III does encounter DNA damage, our data suggests that it may stall. However due to the dynamic nature of the replisome, a new Pol III HE will engage and continue replication. This finding resolves a long debate between two models. The first model stipulated that the DNA polymerase hops over DNA damage and continues synthesis [14]. The second dictates that the DNA polymerase stalls [13]. Our data would propose a model where both findings make sense.

We also identified the recruitment of Pol III HE to sites other than the replication fork in a DnaB-independent manner. Previously, these subcomplexes were assumed to be found only at the replisome. We support a model where the Pol III HE is recruited at ssDNA gaps, given the presence of SSB. This recruitment is dependent on χ a subunit of the clamp loader. It is still unknown if the DNA Pol III at these sites is involved in filling in the ssDNA or if the recruitment of the Pol III

HE at these sites is for the loading of the β -clamp away from the DNA replication fork and subsequent unbinding of the clamp loader. This last possibility would agree with a lack of overlap in the localization of the clamp loader and the translesion polymerases Pol IV and Pol V during DNA repair [118, 165, 166]. The cause of these ssDNA gaps away from the replication fork is still a mystery. Unpublished data has shown that by removing components in either NER or MMR removes part of the Pol III HE recruitment away from the replication fork. More work is needed to understand this Pol III HE recruitment. Specifically, if NER sites may be recruiting the Pol III HE, how is SSB, which bind a minimum 35 nt of ssDNA [167], binding to the maximum 16 nt site created during NER [112, 113]? Also, why is MMR being recruited during UV damage repair? Is it just an all hands-on deck stochastic process, where all repair mechanisms are recruited? If so, is the recruitment of MMR possibly causing helicase disassembly?

The role of χ in recruiting the Pol III HE to SSB sites during DNA damage, led us to question its role during normal DNA replication. The role of χ as a stability factor for the replisome [168-171] seemed to contend with recent data that the replisome was dynamic [2, 3]. So how was χ stabilizing the dynamic replisome? Here we define that the interaction of the $\chi\psi$ subunits with SSB, allows SSB to serve as a recruiting platform for Pol III* (Chapter 4). When we removed χ , like previous reports, we noticed a loss of replication forks indicating a loss of replisome stability. Consequentially, fewer Pol III* were bound to DNA and those bound, presumed active, were bound for slightly longer. This may indicate that in the cell, competition between multiple Pol III* is only one of the factors that determine its dissociation rate. Competition for binding with other partner of β clamp and DNA supercoiling are additional factors that may influence Pol III* binding kinetics. Furthermore, the use of a degron tag may not provide us with consistent removal of χ , muddying our interpretation. Further work using one of the previously characterized χ mutants or a catalytically inactive CRISPR-dCas9 targeting *holC* may provide more discernable results.

We suggest that an essential role of χ is reducing the Pol III* search time through its use of SSB as a recruiting platform. This interaction provides the replisome a tunable approach to recruit the Pol III*. It is interesting to highlight that without a copy of Pol III* at the replisome, the helicase would continue unwinding DNA and hence contribute to the accumulation of bound SSB. This in turn, should increase the likelihood that a Pol III* would be recruited to continue

replication. We hypothesize that DnaB may be less stable without Pol III*, leading to the eventual disassembly from DNA. An additional contributing factor to fork instability is the potential runout of available SSB to cover ssDNA in cases of prolonged uncoupling between helicase and polymerase. In our data we clearly observed a higher frequency of rebinding events and higher stoichiometry in cells with χ . The search time of cells with and without χ was different, cells without χ seem to have a longer binding time but also have two behaviors. More work needs to be done to clearly understand SSBs role as a recruiter. Recent data has shown that SSB may phase separate [172]. It may be possible that replisome recruitment is due to the association of the clamp loader with a SSB phase separated condensate.

In conclusion, the work presented in this thesis offers a new understanding of how a highly dynamic replisome can keep its integrity during ongoing DNA replication or through DNA damage. It provides insight into what happens to the replication machinery when faced with DNA damage too small to block the helicase. The dynamic features of the replisome allow it to quickly adapt to its environment and provide it with an extra layer of protection to properly complete the replication cycle. An exciting prospect in the future is the substantiation of SSB phase separation *in vivo* and how that would corroborate with our dynamic replisome model.

Appendix 1

Methods

A1.1 Experimental Model and Subject Details

Bacterial strains were made in the AB1157 background. Details on their genotype can be found in Table A1. Strains were grown at 37 °C. Exceptions were made for temperature-sensitive mutants such as RRL93 and RRL497 that were grown at 30 °C. Microscopy was done at room temperature, i.e., 23 °C.

A1.2 Method Details

A1.2.1 Strains and construction

The strains used in this thesis are all from an AB1157 background and are shown in Table A1. Chromosomal replacement of replisome genes by fluorescent derivatives was done by lambda red or transduction [81, 173].

For lambda red, plasmids carrying a copy of YPet [81, 174], mCherry [175], mNeonGreen [176] and mMaple [162] followed or preceded by a kanamycin resistance cassette flanked by *frt* sites were used as PCR templates. Flexible peptides with sequences SAGSAAGSGEF (YPet, mNeonGreen and mTagRFP C-ter fusions) or SAGSAAGSGSA (mCherry and YPet N-ter fusions) were used as a linker between the fluorescent protein (FP) and the protein targeted. Primers carrying 40-50 nt tails with identical sequences to the chromosomal locus for insertion were used to amplify the *linker-FP-kanR* from template plasmids. The resulting PCR product was transformed by electroporation into a strain carrying the lambda red-expressing plasmid pKD46. Colonies were selected by kanamycin resistance and ampicillin sensitivity, screened by PCR using primers annealing to regions flanking the insertion and sequencing. In the N-terminal fusion RRL388 and RRL396, to minimize the effect of the insertion on the gene expression levels, the kanamycin cassette was removed by expressing the Flp recombinase from the plasmid pCP20 [173]. Gene fusions did not have any apparent detrimental effect on cell growth.

The dCas9 under the PLlac promoter with constitutive LacI expression was inserted into the *attB* site using the pTB35 plasmid expressing the lambda integrase. The sgRNA pROD166 was inserted into the *argE* site by lambda red recombination. pROD166 plasmid contains sgRNA that binds to oriC (AGCTTATACGGTCCAGGATC).

Other strains were created using P1 transduction [177]. A phage is grown in a strain containing a resistant marker flanking a deletion, degron-tagged or fluorescent protein to be moved in this strategy. The resulting phage lysate is used to infect the recipient strain. This lysate contains both the phage and bacterial DNA. The recipient strain incorporates the bacterial DNA into its chromosome through genetic recombination and selection pressure due to an antibiotic.

A1.2.2 EdU Incorporation

For EdU incorporation, both VC1 (Figure 3.3 & Figure A2.2.5) and NPS30 were used (Figure A2.2.5). For both strains, an overnight culture in M9-Glycerol was diluted in the same medium. All cells were grown to an OD₆₀₀ in a 37°C incubator between 0.1- 0.2 before EdU was added. Once EdU was added, the cells were placed in a 37°C incubator for a specified amount of time. When testing for linear incorporation, EdU was added to a concentration of 10, 20, 40 and 160 µg/mL. Cells were then fixed after varying times (2m, 4m, 6m, 8m, 10m, 20m, 40m, 60m). For incorporation after UV, cells were UV irradiated with 25 J/m² once the OD₆₀₀ of 0.1 was reached. Then at different times after UV (5m, 10m, 20m, 30m, 60m), EdU was added to a concentration of 20 µg/mL for 4 minutes of incorporation at 37°C for VC1 cells and 20 µg/mL for 2 minutes of incorporation at 37°C for NPS30 cells. Lastly, cells were fixed. Fixing and labelling were done using a modified protocol described by (3). TBS was used instead of PBS. The Click-iT reaction mixture was contained 100mM tris, 1mM CuSO₄, 100mM ascorbic acid and 25 mM Azide-Fluor 545 (Sigma). Cells were then washed in a 0.5% Triton X-100 in TBS.

A1.2.3 Dilution Plating

Dilution plating was done by growing cells in LB overnight. Then a log-dilution of the overnight cultures was done seven times. 5 µL of the overnight and its subsequent seven dilutions were plated twice. The first plate was placed in a 37°C incubator, while the second plate was placed in the Stratagene UV Stratalinker then UV irradiated at 25 J/m².

A1.2.4 Microscopy

Before imaging, cells were grown in LB for at least 5 hours then transferred to M9 media via a 1:1000 dilution. After being grown overnight, cells were diluted again in M9 and grown to an OD₆₀₀ between 0.1- 0.2. For degron experiments, cells were induced to a concentration of 0.5% arabinose at an OD₆₀₀ of 0.1 after the second dilution in M9 and grown 45 minutes to an hour before imaging. For degron CRISPR experiments, cells were induced to a concentration of 0.5mM IPTG 45min after the second dilution in M9 and grown for 2 hours before imaging. Cells were spotted on a 1% agarose pad in M9-Glycerol within a Gene Frame (Thermo Scientific). The pad was made by mixing 100 µl of 5x M9-Glycerol with 400 µl of boiling 2% agarose. 113 µl of this mixture was pipetted in the gene frame. Quickly a clean coverslip was placed on top and flattened by pressing on all four corners. Once dry, the coverslip was removed, and the cells were placed on this pad, and a new clean coverslip was placed on top. If cells were exposed to either arabinose or IPTG, the 1% agarose pad contained the concentration mentioned above for each chemical. Coverslips were cleaned with the following steps: 1) Place coverslips in 2% Versa Clean detergent solution overnight. 2) Wash with MilliQ water 3x. 3) Sonicate in acetone for 30 minutes. 4) Wash with MilliQ water 3x. 5) Place coverslips in methanol and flame coverslips using Bunsen burner. 6) Place coverslips in Plasma Etch plasma oven for 10 minutes

For UV irradiated experiments, cells were irradiated in the UV Stratalinker 2400 (254-nm UV light bulbs, 15 watts each) (Stratagene) at the dose specified in the text before placing the coverslip. Images were taken precisely at minutes 5 to 10 after irradiation. For time-course experiments, images were taken at indicated times.

Imaging was performed at room temperature on an inverted Olympus IX83 microscope using a 60x oil objective lens (Olympus Plan Apo 60X NA 1.42 oil) or 100x oil objective lens (Olympus Plan Apo 100X NA 1.40 oil). Images were captured using a Hamamatsu Orca-Flash 4.0 or Andor Zyla 4.2 sCMOS camera. Z-stacks were done using a NanoScanZ piezo by Prior Scientific. Excitation was done from an iChrome Multi-Laser Engine from Toptica Photonics and a 405/488/561/640nm filter set (Chroma) or X-Cite 120LED lamp using the ET – ECFP/EYFP/mCherry filter set (Chroma). Laser triggering was done through a real-time controller

U-RTCE (Olympus). Experiments were done from a single-line cellTIRF illuminator (Olympus). Olympus CellSens 2.1 imaging software was used to control the microscope and lasers.

For snapshots, if the image was taken with the laser, the laser power was set to 15% for an exposure of 1s. If the snapshot was taken with the lamp, the lamp power was set to 100% for an exposure of 5s. In both cases, a 32-frame Z-stack of brightfield images was taken after the exposure. For each experiment, 5 to 10 images were taken for each condition.

In the fast capture sptPALM experiments, 5000 frames were taken in the 561nm channel with a 20ms exposure. The 561nm laser was set to 9% for the entirety of the video. The 405nm laser was set to 15% in the Olympus software. However, in the Toptica Photonics software, the 405nm laser strength was set to 1% at the start of acquisition. If no photoconversion was seen in the live video, the Toptica Photonics software 405nm laser strength was increased by 1% till activation was seen. After each video, a 32-frame Z-stack of brightfield images was taken after the exposure. For non-UV experiments, 5 to 10 images were taken for each condition. For UV experiments, videos were taken for 15 minutes, if the 5-video minimum was not reached in that time, then a new slide with fresh cells would be made, and the slide would UV irradiated.

In long capture sptPALM experiments, 450 frames were taken in the 561nm channel with a 500ms exposure. The 561nm laser was set to 12% for the entirety of the video. Before frames 1, 150 and 300, the 405 nm laser would be activated for two pulses of 5-10 ms at 15-20% power to photoconvert the mMaple protein. A 150-frame interval between reactivation was used as it was determined that all mMaple photoconverted proteins were photobleached after 150 consecutive frames of illumination. Three more pictures were taken after each video: first, the 405nm laser was activated for 100ms at 20% to photoconvert many molecules. Second, a picture was captured in the native 488nm channel where the non-converted molecules are. Lastly, a 32-frame Z-stack of brightfield images was taken after the exposure. If using long-capture videos to evaluate the rebinding of the test protein, no interval was used. For dwell time experiments, an interval of 1 second or 2 seconds was used. The interval includes the previous exposure.

For the experiments done using a quartz coverslip, cells were grown in the same manner described previously. Then cells were spotted on a 1% agarose pad in M9-Glycerol, and the quartz coverslip was placed. Cells were imaged for the untreated control. The slide with the quartz coverslip was placed in the Stratagene UV Stratalinker then UV irradiated at 25 J/m². The images were taken at indicated times. A 32-frame Z-stack of brightfield images was taken after the exposure.

A1.2.5 Image analysis

All analysis except for tracking was done using custom scripts written in MATLAB (Mathworks). Tracking was done in Fiji using Trackmate [178].

A1.2.5.1 Spot counting and colocalization analysis

The 32-frame bright field Z-stacks were compressed to create a black and white phase-contrast image for cell segmentation [179]. Cells were then segmented using SuperSegger [180]. Spots were counted using a modified version of a previously developed tracking software [109]. Spots were determined using an intensity threshold then further processed using a 2D-elliptical Gaussian fit. The extracted fitted parameters were: x-position, y-position, x-standard deviation, y-standard deviation, intensity and background. For cells with only one spot, the intensity of the spot minus the background was recorded. For cells with multiple spots, the intensity of each spot minus the background was added together to get the integrated intensity of all spots within a cell.

Colocalization analysis was done by measuring the distance between the positions of the least abundant protein to a second protein in two-colour experiments. If cells had multiple foci of the same protein, then the shortest distance was recorded, and the two spots measured were removed so their positions would not be used again in further calculations. For the EdU experiments, spots were determined using the same method described above. For cells with only one spot, the intensity of the spot minus the background was recorded. For cells with multiple spots, the intensity of each spot minus the background was added together to get the integrated intensity of all spots within a cell.

A1.2.5.2 Diffusion analysis

The 32-frame bright field Z-stacks were processed in the same way as above [180][180][179][180][179][178][177][176][176][175][175][179][179][178][177][176][176][175][174][173][172][171][188][187][186]. The fast capture videos were imported into MATLAB and segmented cell by cell. When segmenting the cells, a rectangular video was made from a cylindrical cell. To remove the chance that nearby cells would not affect our tracking, every pixel outside of the cell was simulated using a range of intensities between the 20th dimmest pixel within a cell to the 80th brightest pixel within the cell. A Gaussian filter was applied to remove bright pixels. These videos were then imported into Fiji. Tracking was done using Trackmate. Spots were localized using the differences of the gaussian (DoG) method with a spot diameter of 4. The intensity threshold was set a bit lower to prevent track fragmentation due to intensity fluctuations. For each video, an individual quality factor was used to remove spots that were most like due to bright pixels remaining from the simulated outside of cells. The linear assignment problem (LAP) algorithm was used to form tracks from spots. Spots formed tracks if they were located within 15 pixels from one frame to the next. A gap frame of 1 was allowed for the temporary disappearance of the molecule due to blinking. Tracks needed to be longer than five spots long to be recorded. Track data was then transferred to MATLAB for further analysis. The apparent diffusion coefficients (D^*) were estimated from individual tracks by calculating the mean squared displacement (MSD). The equation used was modified from [109]:

$$D^* = \frac{\text{MSD}}{4 \Delta t} - \sigma_{loc}^2 / \Delta t$$

To classify tracks using their D^* estimates, GMM fitting was performed on the distribution of D^* , with two components, and clustered tracks according to their D^* to assign them as a bound or diffusive state. The bound proportion was measured from the percentage of total tracks that were bound.

A1.2.5.3 Dwell time analysis

The dwell time analysis was done using similar methods described in [181]. Modification to the published methods is described below. The 32-frame bright field Z-stacks, segmentation of single cells from long capture videos and the simulation of the background in segmented cells were

processed in the same way as above. These videos were imported into Fiji. Tracking was done using Trackmate.

Spots were localized using the differences of the gaussian (DoG) method with a spot diameter of 4. The intensity threshold was set a bit lower to prevent track fragmentation due to intensity fluctuations. For each video, an individual quality factor was used to remove spots that were most like due to bright pixels remaining from the simulated outside of cells. The linear assignment problem (LAP) algorithm was used to form tracks from spots. Spots formed tracks if they were located within 3 pixels from one frame to the next. A gap frame of 2 was set to allow for the molecule's temporary disappearance due to blinking. Tracks needed to be longer than three spots long to be recorded. A cost on quality ranging from 0.3 to 1 was used to split up tracks where the size and intensity of spots differed. Track data was then transferred to MATLAB for further analysis. A machine-learning algorithm was incorporated to filter our remaining tracks to remove tracks that either did not behave like a bound molecule or the brightness of the spot within the track indicated multiple molecules within a spot in the track. This machine-learning algorithm was trained on both LacI and DnaB bound molecules. After this final classification, the remaining tracks were analyzed to determine the dwell times. The track duration of the resulting tracks was fit with a truncated exponential model to compensate for discarding short duration tracks, using Maximum Likelihood Estimation (MLE) through Matlab's "mle" function, to calculate the mean track duration. Dwell times were calculated using the following equation after combining data from multiple experiments collected with the same time interval.

$$T_{bound} = T_{track} * T_{bleach} / (T_{track} - T_{bleach})$$

Lastly, to calculate the errors on the estimate, bootstrap sampling was performed on the track duration. A 10% variation for the T_{bleach} estimate was allowed to ensure our results incorporated biologically relevant error.

A1.2.5.4 Rebinding analysis

The rebinding analysis was done almost exactly like the dwell time analysis described above. Here tracks with only three spots were allowed. After the data was filtered using the machine learning

algorithm, the number of classified bound tracks per photoconversion was measured. To ensure that only binding events at the replication fork were being analyzed, the spot counting analysis described above was used on the overactivated 561nm channel image, the 488nm channel image, and a standard deviation z-projection of the complete long capture video. Then all the spots found for each channel in one cell were combined into one MATLAB variable. The maximum number of spots observed after a combination of these three channels was three spots. For most cells, using this method, one spot was detected. After having combined spot variables, how many tracks from the video fall within a 3-pixel radius from all spots found within that combined spot variable. If there were two tracks, then that would count as one rebinding event, and the time between binding events is then the track interval or search time. If there were more than two tracks, then the number of tracks minus 1 is the number of rebinding events. The track interval is calculated chronologically so that the end of one track is only compared to the next track's start. A single exponential and a two-exponential decay fit were used to determine the average track duration. To determine which exponential was used, the sum of squares due to error and the degree-of-freedom adjusted coefficient of determination (adjusted R-squared) was used. The fit which had better values in these goodness-of-fit statistics was used.

A1.2.6 Simulation of cell cycle progression

A custom MATLAB script was used to simulate the increase in the number of copies of replisome per cell when cell division is inhibited, and replication proceeds at a slower rate. We first generated a population of cells with ages from 1 to 190 minutes exponentially distributed following the equation:

$$f(a) = 2ae^{-\alpha a}$$

described by Koch and Schechter [182] where $f(a)$ is the frequency distribution of cell ages, α is the $\log(2)/\tau$, and τ is the generation time (190 minutes at room temperature). The starting population contained 0 or 2 replisomes, depending on their age. We assumed that cells initiate DNA replication at minute 1 and that the C-period lasts for 160 minutes at full replication rate [2]. Based on the results using EdU, we estimated the relation between the rate of DNA replication and time after treatment with UV, which we incorporated in the model. Conversion number of replisomes to observed foci was done using a probability of 35% that two replisomes are observed as one focus, obtained from our experiments

A1.3 Strain List

Table A1 Strains used for this study.

Strain	Relevant genotype	Source
AB1157	<i>thr-1, araC14, leuB6(Am), DE(gpt-proA)62, lacY1, tsx-33, qsr'-0, glnV44(AS), galK2(Oc), LAM-, Rac-0, hisG4(Oc), rfbC1, mgl-51, rpoS396(Am), rpsL31(strR), kdgK51, xylA5, mtl-1, argE3(Oc), thi-1</i>	<i>Dewitt and Adelberg, 1962</i>
AW1	<i>dnaQ-mtagRFP kan frt-ypet-dnaB</i>	This thesis
AW13	<i>dnaQ-ypet frt, ΔrecF::kan</i>	This thesis
NPS25	<i>Placq-lacI PLLac-s-dCas9 cat::ΔattB, oriC13 sgRNA cm, ypet-dnaB kan</i>	This thesis
NPS26	<i>ΔsspB::frt, nocus-PBAD-sspB frt, holC-degron kan</i>	This thesis
NPS28	<i>Placq-lacI PLLac-s-dCas9 cat::ΔattB, oriC13 sgRNA cm, dnaQ-ypet kan</i>	This thesis
NPS30	<i>ΔdeoB ΔyjjG</i>	This thesis
NPS31	<i>ΔsspB::frt, nocus-PBAD-sspB frt, ypet-dnaB frt, holC- degron kan</i>	This thesis
RRL27	<i>holC-ypet kan</i>	<i>Reyes-Lamothe et al. (2008)</i>
RRL32	<i>ssb-ypet kan</i>	<i>Reyes-Lamothe et al. (2008)</i>
RRL93	<i>dnaC2, thr::tn10 dnaQ-ypet kan</i>	<i>Reyes-Lamothe et al. (2008)</i>
RRL183	<i>frt pBAD-sspB</i>	<i>Reyes-Lamothe et al. (2010)</i>
RRL187	<i>frt dnaQ-ypet</i>	<i>Reyes-Lamothe et al. (2008)</i>
RRL196	<i>frt ypet-dnaN</i>	<i>Reyes-Lamothe et al. (2010)</i>
RRL203	<i>frt dnaG-ypet</i>	<i>Reyes-Lamothe et al. (2010)</i>
RRL280	<i>dnaX(τ)-ypet kan</i>	<i>Reyes-Lamothe et al. (2010)</i>
RRL368	<i>frt ypet-dnaB</i>	<i>Reyes-Lamothe et al. (2010)</i>
RRL369	<i>frt ypet-dnaC</i>	This thesis
RRL388	<i>frt mCherry-dnaN</i>	This thesis
RRL396	<i>mCherry-dnaN kan frt ypet- dnaB</i>	This thesis
RRL497	<i>dnaC2, thr::tn10 ypet-dnaB</i>	<i>Reyes-Lamothe et al. (2008)</i>
RRL551	<i>priA-mNeonGreen kan</i>	This thesis

TB80	<i>ΔsspB::frt, nocus-PBAD-sspB frt, dnaQ-ypet frt, holC- degron kan</i>	This thesis
VV13	<i>kan dnaQ-mNeonGreen frt mCherry-dnaN</i>	This thesis
WM6	<i>frt dnaQ-mMaple</i>	<i>Beattie et al. (2017)</i>
WM7	<i>frt mMaple-DnaB</i>	<i>Beattie et al. (2017)</i>
WM32	<i>ΔsspB::frt, nocus-PBAD-sspB frt, dnaQ-mMaple frt, holC- degron kan, Δarabad CM</i>	This thesis

Appendix 2

Supplementary Information for Replisome activity slowdown after exposure to ultraviolet light in *Escherichia coli*

A2.1 Supplementary Experimental Procedures

A2.1.1 Strains and growth conditions

All strains used are derivatives of AB1157. Cells were routinely grown in LB or in M9 minimal media. M9 was supplemented with glycerol (final concentration 0.2%); 100 µg/ml of amino acids threonine, leucine, proline, histidine and arginine; and thiamine (0.5 µg/ml). When required, antibiotics were added at the following concentrations: ampicillin (100 µg/ml), kanamycin (30 µg/ml), and chloramphenicol (25 µg/ml). Chromosomal replacement of replisome genes by fluorescent derivatives, degron-tagged alleles or deletions was done by P1 transduction. These include; AW1, AW13, NPS25, NPS26, NPS28, NPS30, NPS31, RRL396, TB80 and VV13.

Strains used for CRISPR experiment were constructed via lambda red integration (1, 2). RRL 369 strain was constructed using lambda red recombination with the pROD44 plasmid containing N-terminal YPet. RRL388 strain was constructed using lambda red recombination with the pROD84 plasmid containing a copy of *mCherry* to generate N-terminal fusions. RRL 551 strain was constructed using lambda red recombination with the pVV04 plasmid containing a copy of *mNeonGreen* to generate C-terminal fusions. The dCas9 under the PLlac promoter with constitutive LacI expression was inserted into the *attB* site using the pTB35 plasmid expressing the lambda integrase. The sgRNA pROD166 was inserted into the *argE* site by lambda red recombination. pROD166 plasmid contains sgRNA that binds to oriC, (AGCTTATACGGTCCAGGATC). Strain list (Table S1), plasmid list (Table S2) and primer list (Table S3) are available in the supplemental information.

Before imaging cells were grown in LB for at least 5 hours then transferred to M9 media via a 1:1000 dilution. After being grown overnight cells were diluted again in M9 and grown to an OD₆₀₀ between 0.1- 0.2. For degron experiments cells were induced to a concentration of 0.5% arabinose at an OD₆₀₀ of 0.1 after the second dilution in M9 and grown for 45 minutes to an hour

before imaging. For degron CRISPR experiments cells were induced to a concentration of 0.5mM IPTG 45min after the second dilution in M9 and grown for 2 hours before imaging.

A2.1.2 EdU Incorporation

For EdU incorporation we used both VC1 (Figure 3.3 & Figure A2.2.5) and NPS30 (Figure A2.2.5). For both strains, an overnight culture in M9-Glycerol was diluted in same medium. All cells were grown to an OD₆₀₀ in a 37°C incubator between 0.1- 0.2 before EdU was added. Once EdU was added, the cells were placed again in a 37°C incubator for a specified amount of time. When testing for linear incorporation, EdU was added to a concentration of 10, 20, 40 and 160 µg/mL. Cells were then fixed after varying times (2m, 4m, 6m, 8m, 10m, 20m, 40m, 60m). For incorporation after UV, cells were UV irradiated with 25 J/m² once the OD₆₀₀ of 0.1 was reached. Then at different times after UV (5m, 10m, 20m, 30m, 60m) EdU was added to a concentration of 20 µg/mL for 4 minutes of incorporation at 37°C for VC1 cells and 20 µg/mL for 2 minutes of incorporation at 37°C for NPS30 cells. Lastly cells were fixed. Fixing and labelling was done using a modified protocol described by (3). TBS was used instead of PBS. The Click-iT reaction mixture was contained 100mM tris, 1mM CuSO₄, 100mM ascorbic acid and 25 mM Azide-Fluor 545 (Sigma). Cells were then washed in a 0.5% Triton X-100 in TBS.

A2.1.3 Imaging

Imaging was performed at room temperature on an inverted Olympus IX83 microscope using a 60x oil objective lens (Olympus Plan Apo 60X NA 1.42 oil) or 100x oil objective lens (Olympus Plan Apo 100X NA 1.40 oil). Images were captured using a Hamamatsu Orca-Flash 4.0 sCMOS camera. Z-stacks were done using a NanoScanZ piezo by Prior Scientific. Excitation was done from an iChrome Multi-Laser Engine from Toptica Photonics and a 405/488/561/640nm filter set (Chroma) or X-Cite 120LED lamp using the ET – ECFP/EYFP/mCherry filter set (Chroma). Laser triggering was done through a real-time controller U-RTCE (Olympus). Experiments were done from a single-line cellTIRF illuminator (Olympus). Olympus CellSens 2.1 imaging software was used to control the microscope and lasers.

For microscopy, cells were spotted on a 1% agarose pad in M9-Glycerol. UV irradiated in the UV Stratalinker 2400 (254-nm UV light bulbs, 15 watts each) (Stratagene) at the dose specified

in the text before placing the coverslip. Images were taken exactly at minutes 5 to 10 after irradiation. For time course experiments, images were taken at indicated times. A 32-frame Z-stack of brightfield images was taken for each fluorescent image.

For the experiments done using a quartz coverslip (Figure A2.2.4.A), cells were grown in the same manor described previously. Then cells were spotted on a 1% agarose pad in M9-Glycerol and the quartz coverslip was placed. Cells were imaged for the untreated control. Then the slide with the quartz coverslip still on was placed in the Stratagene UV Stratalinker then UV irradiated at 25 J/m². Then images were taken at indicated times. A 32-frame Z-stack of bright field was taken for each fluorescent image.

A2.1.4 Spot counting and colocalization analysis

All analysis was done using custom scripts written in MATLAB (Mathworks). A 32-frame bright field Z-stacks was compressed to create a black and white phase contrast image for cell segmentation (4). Spots were counted using a modified version of a previously developed tracking software (5). Spots were determined using an intensity threshold then further processed using a 2D-elliptical Gaussian fit. The extracted fitted parameters were: x-position, y-position, x-standard deviation, y-standard deviation, intensity and background. Co-localization analysis was done by measuring the distance between the positions of the least abundant protein to a second protein in two-colour experiments. If cells had multiple foci of the same protein, then the shortest distance was recorded, and the 2 spots measured were removed so their positions would not be used again in further calculations. Sample size and number of repeats for the data presented in here can be found in Table S4 in the supplemental information. For the EdU experiments, spots were determined using the same method described above. For cells with only one spot, the intensity of the spot minus the background was recorded. For cells with multiple spots, the intensity of each spot minus the background was added together to get the integrated intensity of all spots within a cell.

A2.1.5 Single molecule experiments and analysis

We determined the bound times using a modified protocol described in our lab (6). Briefly, Cells were harvested from early log-phase cultures in M9-Glycerol (OD₆₀₀ 0.1-0.2), concentrated and

spotted onto a pad of 1% agarose in M9-Glycerol, contained in a gene frame. For UV treated cells, they were imaged starting at 15 minutes after irradiation with the last timelapse finishing before the 30-minute mark. Coverslips cleaned with versa-clean, acetone and methanol were used to minimize fluorescent background. Imaging was performed at room temperature on an inverted Olympus IX83 microscope using a 100x oil objective lens (Olympus Plan Apo 100X NA 1.40 oil). Images were captured using a Hamamatsu Orca-Flash 4.0 sCMOS camera. Excitation was done from an iChrome Multi-Laser Engine from Toptica Photonics. Laser triggering was done through a real-time controller U-RTCE (Olympus). Experiments were done using HiLo illumination setup (7) from a single-line cell[^]TIRF illuminator (Olympus). Olympus CellSens 2.1 imaging software was used to control the microscope and lasers. A single 405nm wavelength activation event, typically lasting less than 20ms, was followed by multiple 561nm wavelength excitation events with camera captures of 500ms spaced by 2s intervals. Analysis of this data was done as previously described (6). To characterize the rate of bleaching of mMaple, we analyzed the lifetime of LacI-mMaple foci, which on average should bleach before unbinding.

Bound proportions were determined using a similar protocol as described above. However, we took 5000 frames of continuous illumination of 561 nm wavelength at capture rates of 20ms with an interval time of as fast as possible under continuous 405-nm activation. For analysis, images were first segmented in order to remove out-of-cell noise coming from contaminants on the coverslip. Binary masks were created using Matlab, from the green fluorescent channel of mMaple. PALM tracking was performed using the TrackMate software in ImageJ (8). Tracks were then filtered using the binary masks. We quantified the diffusion of each track using a previously described method (5). We then used Gaussian mixture modelling function found in Matlab to determine bound and diffusing proportions.

A2.1.6 Dilution Plating

Dilution plating was done by growing cells in LB overnight. Then a log-dilution of the overnight cultures was done 7 times. 5 μ L of the overnight and its subsequent 7 dilutions were plated twice. The first plate was placed in a 37°C incubator while the second plate was placed in the Stratagene UV Stratalinker then UV irradiated at 25 J/m².

A2.1.7 Simulation of cell cycle progression

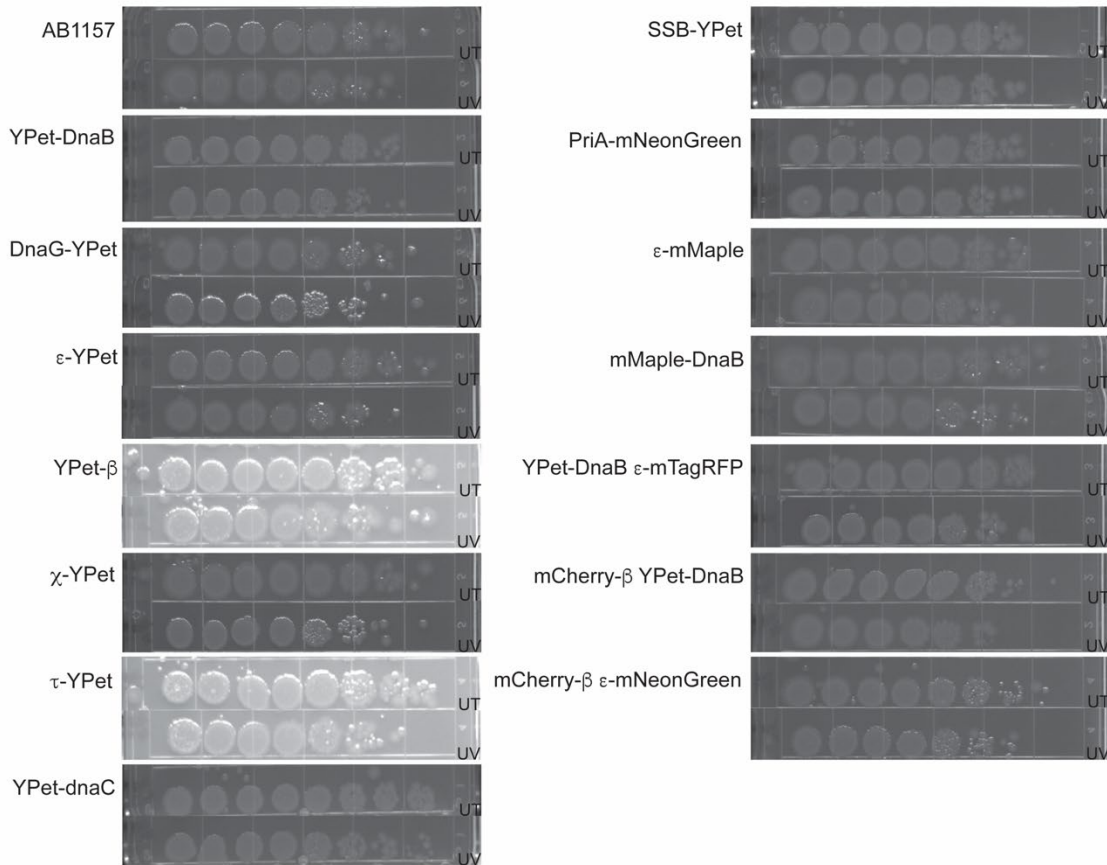
A custom Matlab script was used to simulate the increase in the number of copies of replisome per cell when cell division is inhibited and replication proceeds at a slower rate. We first generated a population of cells with ages from 1 to 190 minutes exponentially distributed following the equation:

$$f(a)=2ae^{-\alpha a}$$

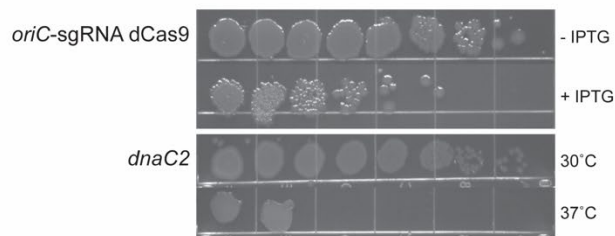
described by Koch and Schechter (9) where $f(a)$ is the frequency distribution of cell ages, α is the $\log(2)/\tau$, and τ is the generation time (190 minutes at room temperature). The starting population contained 0 or 2 replisomes, depending on their age. We assumed that cells initiate DNA replication at minute 1 and that the C-period last for 160 minutes at full replication rate (6). Based on the results using EdU, we estimated the relation between rate of DNA replication and time after treatment with UV which we incorporated in the model. Conversion number of replisomes to observed foci was done using a probability of 35% that two replisomes are observed as one focus, obtained from our experiments.

A2.2 Supplemental Figures

A

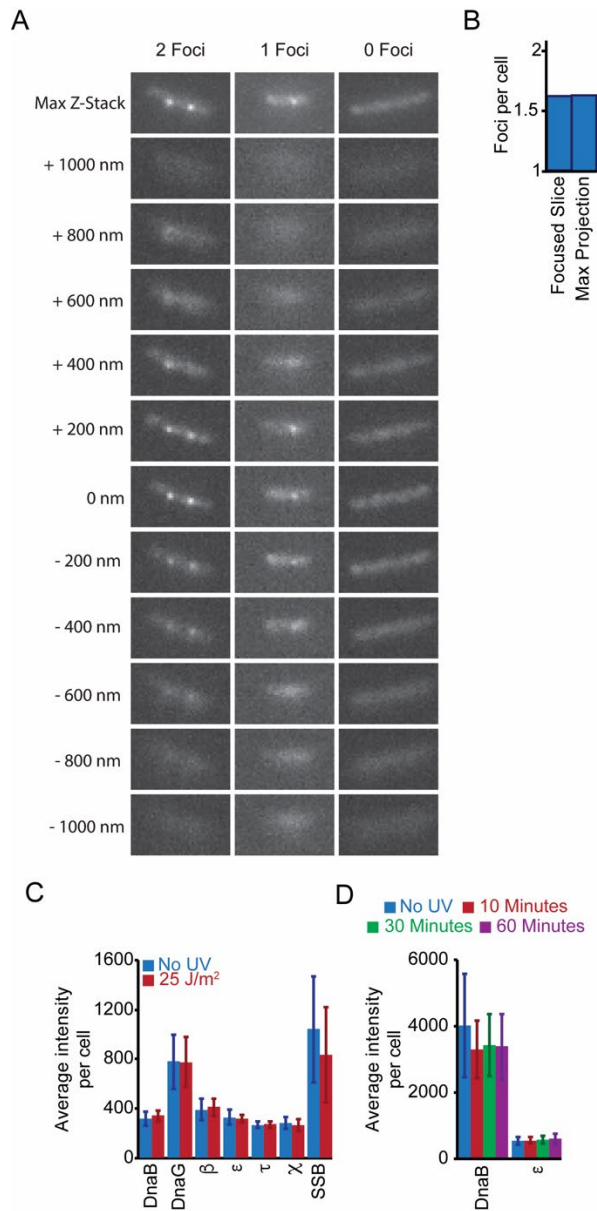


B



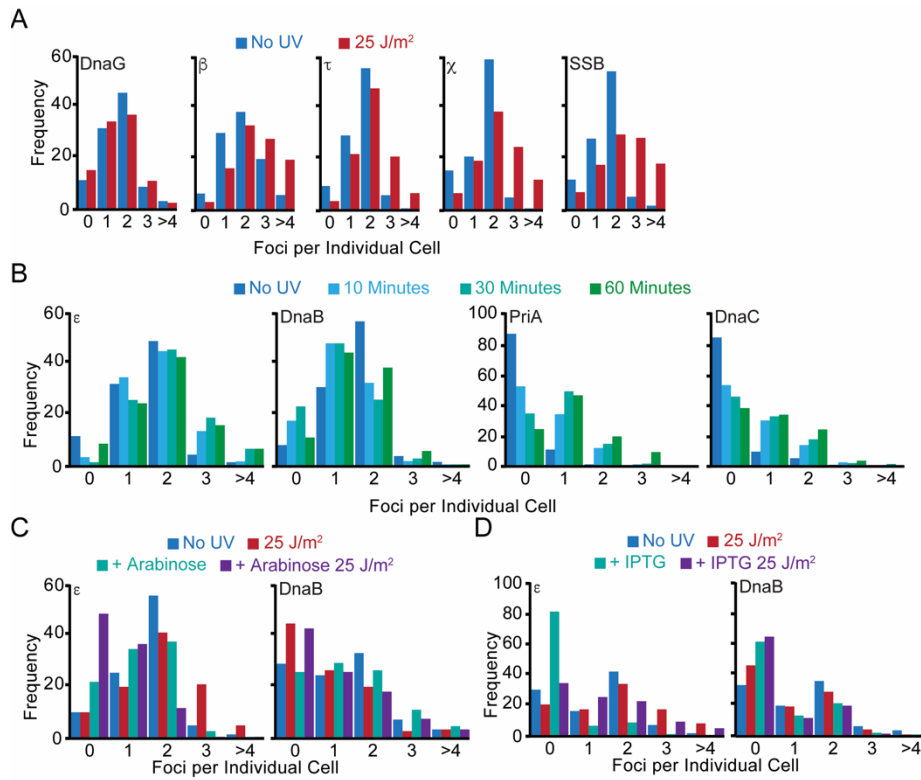
Supplementary Figure 1

Supplementary Figure A2.2.1. 25 J/m² of UV exposure mildly affects fluorescent-fusion cell viability. (A) Serial 10-fold dilutions of liquid bacterial cultures with fluorescent protein fusions plated on LB. Plates were exposed with 25 J/m² of UV exposure. (B) Serial 10-fold dilutions of liquid bacterial cultures with the *oriC* blocking CRISPR-dCas system and the *dnaC2* temperature sensitive background plated on LB.



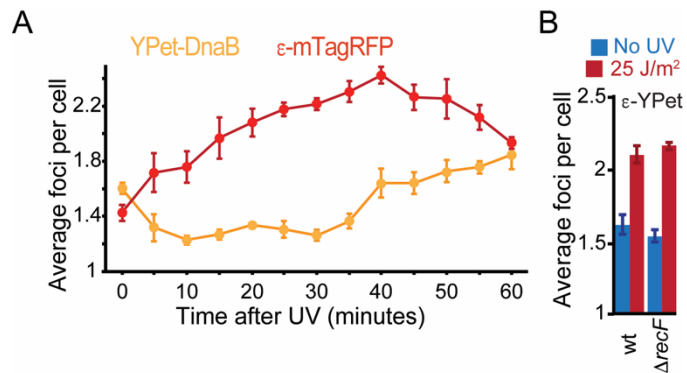
Supplementary Figure 2

Supplementary Figure A2.2.2. Characterization of strains at the microscope. (A) Representative Z-stack images and a max projection of 2, 1, 0 foci cells of an SSB- YPet strain. Focused slice taken at 0 nm. (B) Average number of the foci per cell of an SSB- YPet strain when the focused slice is taken compared to the max projection. (C) Average cell intensity before and after exposure to UV for all the replisome subunits tested: YPet-DnaB, YPet-DnaG, YPet-β, ε-YPet, τ-YPet, χ-YPet and SSB-YPet. Note that since microscope acquisition settings varied across experiments with different strains, these results do not represent relative copy numbers among subunits. (D) Average cell intensity for YPet-DnaB and ε-mTagRFP before (0 minutes) and at various times after treatment.



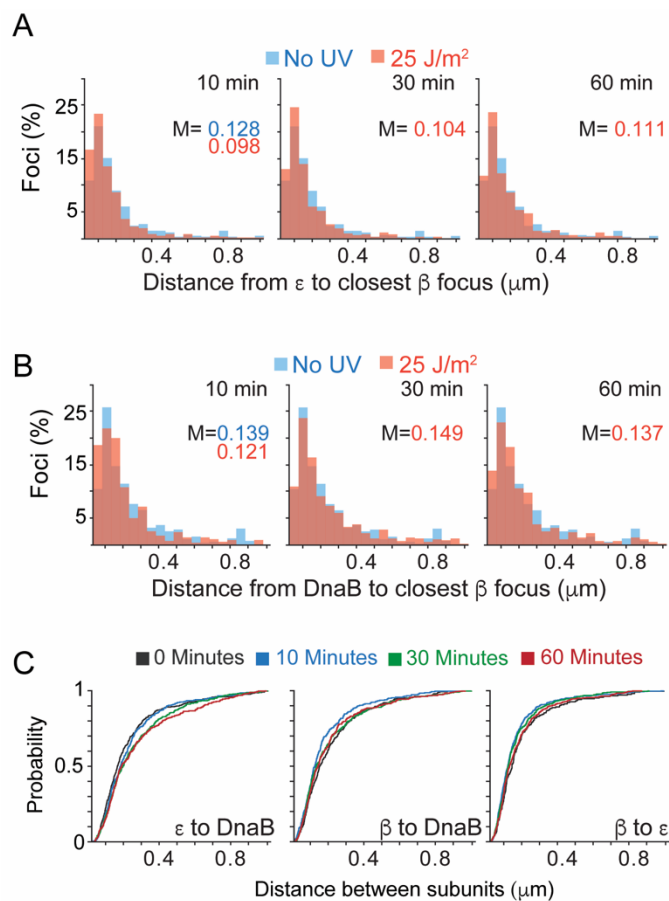
Supplementary Figure 3

Supplementary Figure A2.2.3. Distribution of foci per cell. (A) Distribution of the number of foci per cell for Fig. 1D, 5 minutes after exposure to UV. (B) Distribution of the number of foci per cell for Fig. 2C. and Fig. 2F. (C) Distribution of the number of foci per cell for Fig. 4A. and Fig 4E.



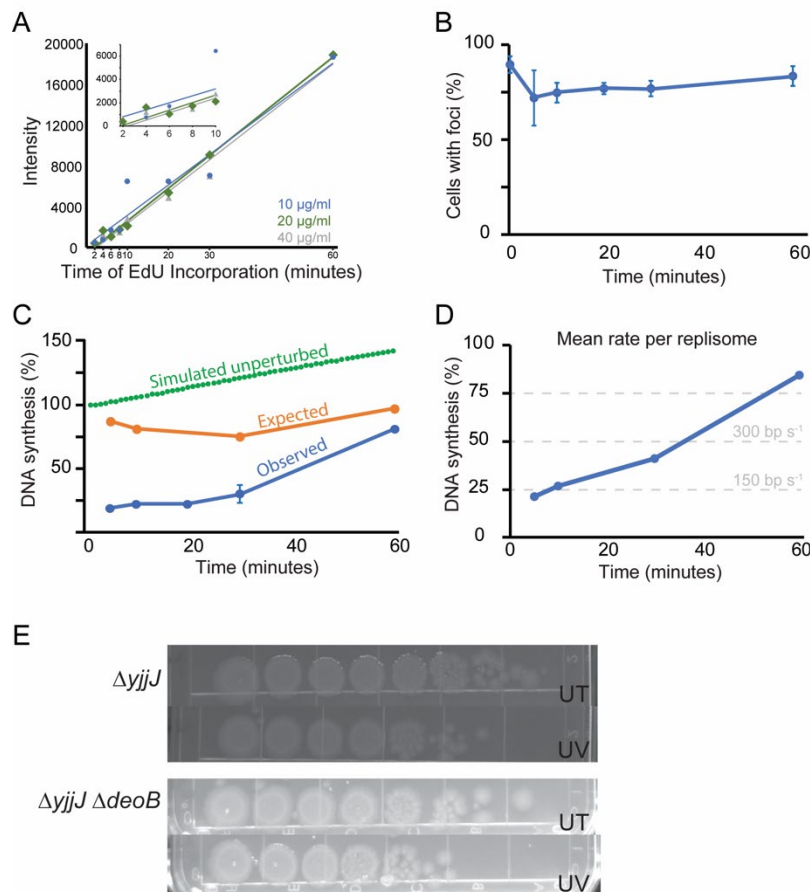
Supplementary Figure 4

Supplementary Figure A2.2.4. Recruitment of ϵ after UV. (A) Average number of foci per cell for YPet-DnaB and ϵ -mTagRFP before (0 minutes) and at various times after treatment. Independent set of experiments to those in Fig. 2C. The samples were imaged before and after exposing to a dose of 25 J/m² of UV through a quartz slide. Error bars represent SE. (B) Average number of foci for ϵ -YPet in a Δ recF background. Pictures were taken 5 minutes after exposure. Error bars represent SE.



Supplementary Figure 5

Supplementary Figure A2.2.5. Replisome components remain in vicinity to each other after UV exposure. (A) Distribution of apparent distances between a mCherry- β focus and the closest ϵ -mNeonGreen focus in a cell. The untreated sample is compared with the results at 10, 30 and 60 minutes after UV. The median (M) of each population is shown. (B) Distribution of distances between a mCherry- β focus and the closest YPet-DnaB focus in a cell. (C) Cumulative distribution function plots of the distances between YPet-DnaB focus and the closest ϵ -mTagRFP focus, mCherry- β focus and the closest YPet-DnaB focus, and mCherry- β focus and the closest ϵ -mNeonGreen focus, all in cells. In each panel, the untreated sample is compared with the results at 10, 30 and 60 minutes after UV.



Supplementary Figure 6

Supplementary Figure A2.2.6. Persistence of DNA synthesis after UV. (A) EdU incorporation control of a strain carrying $\Delta yjjG$ where 3 different concentrations of EdU (10, 20 and 40 $\mu\text{g/ml}$) were tested. For each concentration, a pulse of 2, 4, 6, 8, 10, 20, 30, 60 were done to determine the linear increase of EdU over time. Inset shows a zoomed in view of 2, 4, 6, 8 and 10 is what is shown in inset. (B) A 4-minute pulse of EdU, followed by fixation and coupling of fluorescence through click chemistry. Cells were sampled at various times after UV. Percentage of $\Delta yjjG$ cells with at least one focus for EdU before (0 minutes) and at various times after UV. Error bars represent SE. (C) Estimated normalized DNA synthesis at various times after UV (Observed), as measured by the integrated intensity of all spots in a cell. Compared to the expected synthesis if all remaining DnaB foci in Figs. 1 and 2 were fully functional replisomes (Expected), and to the expected synthesis in cells with fully functional replisomes and no replisome disassembly (Simulated unperturbed). Error bars represent SE. (D) Mean rate per replisome obtained by re-normalizing the ‘Observed’ data using the ‘Expected’ data in C. The estimated rates in bp s^{-1} are shown as reference. (E) Serial 10-fold dilutions of liquid bacterial cultures plated on LB. Plates were exposed to 25 J/m^2 of UV exposure.

A2.3 Supplemental Tables

Table A2.3.1. Stains used for this study.

Strain	Relevant genotype	Source
AB1157	<i>thr-1, araC14, leuB6(Am), DE(gpt-proA)62, lacY1, tsx-33, qsr'-0, glnV44(AS), galK2(Oc), LAM-, Rac-0, hisG4(Oc), rfbC1, mgl-51, rpoS396(Am), rpsL31(strR), kdgK51, xylA5, mtl-1, argE3(Oc), thi-1</i>	<i>Dewitt and Adelberg, 1962</i>
AW1	<i>dnaQ-mtagRFP kan frt-ypet-dnaB</i>	This study
AW13	<i>dnaQ-ypet frt, ΔrecF::kan</i>	This study
NPS25	<i>Placq-lacI PLLac-s-dCas9 cat::ΔattB, oriC13 sgRNA cm, ypet-dnaB kan</i>	This study
NPS26	<i>ΔsspB::frt, nocus-PBAD-sspB frt, holC-degron kan</i>	This study
NPS28	<i>Placq-lacI PLLac-s-dCas9 cat::ΔattB, oriC13 sgRNA cm, dnaQ-ypet kan</i>	This study
NPS30	<i>ΔdeoB ΔyjjG</i>	This study
NPS31	<i>ΔsspB::frt, nocus-PBAD-sspB frt, ypet-dnaB frt, holC- degron kan</i>	This study
RRL27	<i>holC-ypet kan</i>	<i>Reyes-Lamothe et al. (2008)</i>
RRL32	<i>ssb-ypet kan</i>	<i>Reyes-Lamothe et al. (2008)</i>
RRL93	<i>dnaC2, thr::tn10 dnaQ-ypet kan</i>	<i>Reyes-Lamothe et al. (2008)</i>
RRL183	<i>frt pBAD-sspB</i>	<i>Reyes-Lamothe et al. (2010)</i>
RRL187	<i>frt dnaQ-ypet</i>	<i>Reyes-Lamothe et al. (2008)</i>
RRL196	<i>frt ypet-dnaN</i>	<i>Reyes-Lamothe et al. (2010)</i>
RRL203	<i>frt dnaG-ypet</i>	<i>Reyes-Lamothe et al. (2010)</i>
RRL280	<i>dnaX(τ)-ypet kan</i>	<i>Reyes-Lamothe et al. (2010)</i>
RRL368	<i>frt ypet-dnaB</i>	<i>Reyes-Lamothe et al. (2010)</i>
RRL369	<i>frt ypet-dnaC</i>	This study
RRL388	<i>frt mCherry-dnaN</i>	This study
RRL396	<i>mCherry-dnaN kan frt ypet- dnaB</i>	This study
RRL497	<i>dnaC2, thr::tn10 ypet-dnaB</i>	<i>Reyes-Lamothe et al. (2008)</i>
RRL551	<i>priA-mNeonGreen kan</i>	This study

TB80	<i>ΔsspB::frt, nocus-PBAD-sspB frt, dnaQ-ypet frt, holC- degron kan</i>	This study
VV13	<i>kan dnaQ-mNeonGreen frt mCherry-dnaN</i>	This study
WM6	<i>frt dnaQ-mMaple</i>	<i>Beattie et al. (2017)</i>

Table A2.3.2. Plasmids used for this study

Plasmid	Description
pROD44	Plasmid containing N-terminal YPet with kanamycin resistance
pROD84	Plasmid containing N-terminal mCherry with kanamycin resistance
pROD166	Plasmid containing sgRNA with target to oriC
pTB35	Plasmid containing dCas9 under PLlac with constitutive lacI. For integration at attB with chloramphenicol resistance
pVV04	Plasmid containing C-terminal mNeonGreen with kanamycin resistance

Table A2.3.3. Primers used for this study.

Primer	Sequence	Description
λ priA-F	cggattcccgtaaggtgaaatgggtgctggatgttgatccgattgag ggtTCGGCTGGCTCCGCTGCTGG	Forward primer to mNeonGreen attachment to priA by lambda red
λ priA-R	aaagtgtgatgaatattgaatcttcgatccgctcgcacgtgagcg gtCTTATGAATATCCTCCTTAG	Reverse primer to mNeonGreen attachment to priA by lambda red
dnaN-NF	tatcaaagaagattttcaaatatcagaacattgtcatcgtaaacc TGTAGGCTGGAGCTGCTTCG	Forward primer to mCherry attachment to dnaN by lambda red
dnaN-NR	acctgtttagcggtttaataaatgctcacgttctacggtaaattcat CGCGCTGCCAGAACCAGC	Reverse primer to mCherry attachment to dnaN by lambda red
NdnaC_F	acggtcagcgaacctgacagccaaattccaccaggattcagaggg taacgTGTAGGCTGGAGCTGCTTCG	Forward primer to YPet attachment to dnaC by lambda red
NdnaC_F	gcaggcatcatttttgcaggcgttgcacaggtcgccaacgttttca tCGCGCTGCCAGAACCAGC	Reverse primer to YPet attachment to dnaC by lambda red
TB200	ataaatactgcatgaatattgatactatcatgaccagaggtgtgtcaa caTTTCGCTAAGGATGATTTCTGG	For primer to insert sgRNA into argE by lambda red
TB201	cggatgcgggcgagcgccttatccggcctacgttttaatgccagc aTATCCTCCTTAGTTCCTATTCC	Rev primer to insert sgRNA into argE by lambda red

Table A2.3.4. Number of repeats and total cell count for each Figure.

Figure	Strain	Treatment	Number of Repeats	Total Number of Cells	Average \pm SE	P-Value		
1								
C	RRL368	UT	3	196	1.58 \pm 0.06	0.30		
		10 J/m ²	3	323	1.51 \pm 0.08			
		25 J/m ²	3	191	1.27 \pm 0.09	3.11E-05		
		50 J/m ²	3	321	1.21 \pm 0.07	1.01E-06		
	RRL187	UT	3	296	1.52 \pm 0.02	5.71E-03		
		10 J/m ²	3	370	1.69 \pm 0.04			
		25 J/m ²	3	300	1.88 \pm 0.04	3.46E-06		
		50 J/m ²	3	351	1.95 \pm 0.02	1.03E-06		
		E	RRL368	UT	3	1294	1.59 \pm 0.02	5.16E-10
				25 J/m ²	3	2088	1.27 \pm 0.06	
RRL203	UT		3	1419	1.56 \pm 0.08	0.14		
	25 J/m ²		3	1709	1.48 \pm 0.11			
RRL196	UT		3	1511	1.89 \pm 0.06	1.72E-08		
	25 J/m ²		3	1490	2.55 \pm 0.13			
RRL187	UT		3	1766	1.59 \pm 0.06	1.12E-17		
	25 J/m ²		3	2599	2.06 \pm 0.06			
RRL280	UT		3	1036	1.57 \pm 0.08	5.81E-09		
	25 J/m ²		3	1201	2.02 \pm 0.09			
RRL27	UT	3	2014	1.55 \pm 0.03	4.80E-14			
	25 J/m ²	3	1261	2.16 \pm 0.08				
RRL32	UT	3	1868	1.58 \pm 0.06	1.20E-10			
	25 J/m ²	3	1104	2.42 \pm 0.11				
2								
C	AW1	UT	3	449	1.52 \pm 0.07	4.74E-03		
		dnaQ	3	387	1.77 \pm 0.06			
		30 Minutes	3	452	2.02 \pm 0.10			
		60 Minutes	3	382	1.87 \pm 0.06			
	AW1	dnaB	UT	3	449	1.61 \pm 0.11	1.97E-05	
			10 Minutes	3	387	1.20 \pm 0.05		
		30 Minutes	3	452	1.09 \pm 0.07	4.29E-07		
		60 Minutes	3	382	1.39 \pm 0.08	4.59E-03		
		F	RRL551	UT	3	318	0.07 \pm 0.02	1.52E-14
				10 Minutes	3	369	0.47 \pm 0.07	
30 Minutes	3			407	0.71 \pm 0.06			
60 Minutes	3			368	1.00 \pm 0.05			
RRL369	UT		2	352	0.19 \pm 0.05	8.89E-08		
	10 Minutes		2	384	0.64 \pm 0.05			
		30 Minutes	2	426	0.78 \pm 0.04	8.86E-10		
		60 Minutes	2	422	0.92 \pm 0.03	1.57E-12		

3						
B	NPS30	UT	2	220		
		5 Minutes	2	252		
		10 Minutes	2	258		
		20 Minutes	2	204		
		30 Minutes	2	342		
		60 Minutes	2	290		
4						
A	NPS25	UT	3	735	1.27±0.04	1.43E-07
		25 J/m ²	3	1041	0.93±0.04	
		UT IPTG	3	1572	0.64±0.05	4.81E-01
		25 J/m ² IPTG	3	1773	0.58±0.07	
	NPS28	UT	3	661	1.33±0.03	3.24E-10
		25 J/m ²	3	1198	1.77±0.04	
		UT IPTG	3	902	0.29±0.02	1.73E-12
		25 J/m ² IPTG	3	1350	1.25±0.07	
C	RRL497	UT 30°C	3	306	1.61±0.11	0.45
		25 J/m ² 30°C	3	294	1.20±0.05	
		UT 37°C	2	561	1.09±0.07	0.20
		25 J/m ² 37°C	2	739	1.39±0.08	
	RRL93	UT 30°C	3	566	1.49±0.20	4.20E-03
		25 J/m ² 30°C	3	258	1.97±0.15	
		UT 37°C	2	561	0.11±0.02	1.17E-14
		25 J/m ² 37°C	2	739	0.80±0.04	
E	NPS31	UT	3	1051	1.31±0.04	2.62E-05
		25 J/m ²	3	913	0.92±0.06	
		UT ARA	3	615	1.39±0.04	4.00E-07
		25 J/m ² ARA	3	719	1.00±0.04	
	TB80	UT	3	1036	1.61±0.02	1.62E-06
		25 J/m ²	3	770	1.91±0.04	
		UT ARA	3	1079	1.23±0.04	9.04E-10
		25 J/m ² ARA	3	1229	0.63±0.05	
5						
B	WM6	UT	2	219		
		25 J/m ²	2	223		
C	WM6	UT	2	146		
		25 J/m ²	2	233		
S2						
B	RRL32	UT	1			
S4						
A	AW1	UT	2	1699		
		5 Minutes	2	201		
		10 Minutes	2	247		
		15 Minutes	2	347		
		20 Minutes	2	305		

		25 Minutes	2	283		
		30 Minutes	2	185		
		35 Minutes	2	222		
		40 Minutes	2	303		
		45 Minutes	2	313		
		50 Minutes	2	205		
		55 Minutes	2	209		
		60 Minutes	2	196		
B	AW13	UT	2	275	1.41	2.95E-03
		25 J/m ²	2	233	2.07	
S5						
A	RRL396	UT	3	352		
		10 Minutes	3	437		
		30 Minutes	3	538		
		60 Minutes	3	480		
B	VV13	UT	3	235		
		10 Minutes	3	589		
		30 Minutes	3	544		
		60 Minutes	3	484		
S6						
A	VC1	10 µg/ml 2	2	234		
		10 µg/ml 4	2	234		
		10 µg/ml 6	2	254		
		10 µg/ml 8	2	222		
		10 µg/ml 10	2	230		
		10 µg/ml 20	2	372		
		10 µg/ml 30	2	260		
		10 µg/ml 60	2	248		
		20 µg/ml 2	2	230		
		20 µg/ml 4	2	266		
		20 µg/ml 6	2	288		
		20 µg/ml 8	2	288		
		20 µg/ml 10	2	208		
		20 µg/ml 20	2	276		
		20 µg/ml 30	2	240		
		20 µg/ml 60	2	262		
		40 µg/ml 2	2	322		
		40 µg/ml 4	2	250		
		40 µg/ml 6	2	290		
		40 µg/ml 8	2	374		
		40 µg/ml 10	2	284		
		40 µg/ml 20	2	336		
		40 µg/ml 30	2	266		
		40 µg/ml 60	2	282		
B	VC1	UT	2	405		

		5 Minutes	2	324
		10 Minutes	2	352
		20 Minutes	2	444
		30 Minutes	2	467
		60 Minutes	2	357

A2.4. References

1. Reyes-Lamothe R, Possoz C, Danilova O, & Sherratt DJ (2008) Independent positioning and action of *Escherichia coli* replisomes in live cells. *Cell* 133(1):90-102.
2. Datsenko KA & Wanner BL (2000) One-step inactivation of chromosomal genes in *Escherichia coli* K-12 using PCR products. *Proc Natl Acad Sci U S A* 97(12):6640-6645.
3. Wang X, Lesterlin C, Reyes-Lamothe R, Ball G, & Sherratt DJ (2011) Replication and segregation of an *Escherichia coli* chromosome with two replication origins. *Proc Natl Acad Sci U S A* 108(26):E243-250.
4. Julou T, *et al.* (2013) Cell-cell contacts confine public goods diffusion inside *Pseudomonas aeruginosa* clonal microcolonies. *Proc Natl Acad Sci U S A* 110(31):12577-12582.
5. Uphoff S, Reyes-Lamothe R, Garza de Leon F, Sherratt DJ, & Kapanidis AN (2013) Single-molecule DNA repair in live bacteria. *Proc Natl Acad Sci U S A* 110(20):8063-8068.
6. Beattie TR, *et al.* (2017) Frequent exchange of the DNA polymerase during bacterial chromosome replication. *Elife* 6.
7. Tokunaga M, Imamoto N, & Sakata-Sogawa K (2008) Highly inclined thin illumination enables clear single-molecule imaging in cells. *Nat Methods* 5(2):159-161.
8. Schindelin J, *et al.* (2012) Fiji: an open-source platform for biological-image analysis. *Nat Methods* 9(7):676-682.
9. Koch AL & Schaechter M (1962) A model for statistics of the cell division process. *J Gen Microbiol* 29:435-454.

Chapter 6

1. Beattie, T.R. and R. Reyes-Lamothe, *A Replisome's journey through the bacterial chromosome*. 2015. **6**.
2. Beattie, T.R., N. Kapadia, E. Nicolas, S. Uphoff, A.J. Wollman, M.C. Leake, and R. Reyes-Lamothe, *Frequent exchange of the DNA polymerase during bacterial chromosome replication*. eLife, 2017. **6**.
3. Lewis, J.S., L.M. Spenkelink, S. Jergic, E.A. Wood, E. Monachino, N.P. Horan, K.E. Duderstadt, M.M. Cox, A. Robinson, N.E. Dixon, and A.M.v. Oijen, *Single-molecule visualization of fast polymerase turnover in the bacterial replisome*. eLife, 2017. **6**: p. e23932.
4. Monachino, E., S. Jergic, J.S. Lewis, Z.Q. Xu, A.T.Y. Lo, V.L. O'Shea, J.M. Berger, N.E. Dixon, and A.M. van Oijen, *A Primase-Induced Conformational Switch Controls the Stability of the Bacterial Replisome*. Mol Cell, 2020. **79**(1): p. 140-154 e7.
5. Spenkelink, L.M., J.S. Lewis, S. Jergic, Z.-Q. Xu, A. Robinson, N.E. Dixon, and A.M.v. Oijen, *Recycling of single-stranded DNA-binding protein by the bacterial replisome*. bioRxiv, 2018: p. 486555.
6. Reyes-Lamothe, R., D.J. Sherratt, and M.C. Leake, *Stoichiometry and architecture of active DNA replication machinery in Escherichia coli*. 2010. **328**(5977).
7. Wolak, C., H.J. Ma, N. Soubry, S.J. Sandler, R. Reyes-Lamothe, and J.L. Keck, *Interaction with single-stranded DNA-binding protein localizes ribonuclease HI to DNA replication forks and facilitates R-loop removal*. Molecular Microbiology, 2020.
8. Yao, N.Y., R.E. Georgescu, J. Finkelstein, and M.E. O'Donnell, *Single-molecule analysis reveals that the lagging strand increases replisome processivity but slows replication fork progression*. Proceedings of the National Academy of Sciences of the United States of America, 2009. **106**(32): p. 13236-41.
9. Tanner, N.A., J.J. Loparo, S.M. Hamdan, S. Jergic, N.E. Dixon, and A.M. van Oijen, *Real-time single-molecule observation of rolling-circle DNA replication*. Nucleic Acids Res, 2009. **37**(4): p. e27.
10. Fijalkowska, I.J., R.M. Schaaper, and P. Jonczyk, *DNA replication fidelity in Escherichia coli: a multi-DNA polymerase affair*. FEMS Microbiol Rev, 2012. **36**(6): p. 1105-21.
11. Hanawalt, P.C., *THE U.V. SENSITIVITY OF BACTERIA: ITS RELATION TO THE DNA REPLICATION CYCLE*. Photochemistry and Photobiology, 1966. **5**(1): p. 1-12.
12. Kreuzer, K.N., *DNA damage responses in prokaryotes: regulating gene expression, modulating growth patterns, and manipulating replication forks*. Cold Spring Harb Perspect Biol, 2013. **5**(11): p. a012674.
13. Meneghini, R. and P.C. Hanawalt, *Postreplication repair in human cells: on the presence of gaps opposite dimers and recombination*. 1975. **5B**.
14. Rupp, W.D. and P. Howard-Flanders, *Discontinuities in the DNA synthesized in an excision-defective strain of Escherichia coli following ultraviolet irradiation*. 1968. **31**(2).
15. Kolakofsky, D., *A short biased history of RNA viruses*. RNA, 2015. **21**(4): p. 667-9.
16. Dahm, R., *Discovering DNA: Friedrich Miescher and the early years of nucleic acid research*. Hum Genet, 2008. **122**(6): p. 565-81.
17. Griffith, F., *The Significance of Pneumococcal Types*. J Hyg (Lond), 1928. **27**(2): p. 113-59.

18. Avery, O.T. and W.F. Goebel, *Chemoimmunological Studies on the Soluble Specific Substance of Pneumococcus : I. The Isolation and Properties of the Acetyl Polysaccharide of Pneumococcus Type I.* J Exp Med, 1933. **58**(6): p. 731-55.
19. Avery, O.T., C.M. Macleod, and M. McCarty, *Studies on the Chemical Nature of the Substance Inducing Transformation of Pneumococcal Types : Induction of Transformation by a Desoxyribonucleic Acid Fraction Isolated from Pneumococcus Type Iii.* J Exp Med, 1944. **79**(2): p. 137-58.
20. McCarty, M., *Discovering genes are made of DNA.* Nature, 2003. **421**(6921): p. 406.
21. Kresge, N., R.D. Simoni, and R.L. Hill, *Chargaff's Rules: the Work of Erwin Chargaff.* Journal of Biological Chemistry, 2005. **280**(24): p. 172-174.
22. Wilkins, M.H.F. and J.T. Randall, *Crystallinity in sperm heads: Molecular structure of nucleoprotein in vivo.* Biochimica et Biophysica Acta, 1953. **10**: p. 192-193.
23. Franklin, R.E., A. Klug, J.T. Finch, and K.C. Holmes, *On the structure of some ribonucleoprotein particles.* Discussions of the Faraday Society, 1958. **25**.
24. Watson, J.D. and F.H. Crick, *Molecular structure of nucleic acids; a structure for deoxyribose nucleic acid.* Nature, 1953. **171**(4356): p. 737-8.
25. Meselson, M. and F.W. Stahl, *The Replication of DNA in Escherichia Coli.* Proc Natl Acad Sci U S A, 1958. **44**(7): p. 671-82.
26. Cairns, J., *The bacterial chromosome and its manner of replication as seen by autoradiography.* Journal of Molecular Biology, 1963. **6**(3): p. 208-IN5.
27. Paweletz, N., *Walther Flemming: pioneer of mitosis research.* Nat Rev Mol Cell Biol, 2001. **2**(1): p. 72-5.
28. Morgan, T.H., *Sex Limited Inheritance in Drosophila.* Science, 1910. **32**(812): p. 120-2.
29. Drlica, K. and A.J. Bendich, *Chromosome, Bacterial,* in *Encyclopedia of Microbiology.* 2009.
30. Hacker, W.C., S. Li, and A.H. Elcock, *Features of genomic organization in a nucleotide-resolution molecular model of the Escherichia coli chromosome.* Nucleic Acids Res, 2017. **45**(13): p. 7541-7554.
31. Dorman, C.J. and M.J. Dorman, *DNA supercoiling is a fundamental regulatory principle in the control of bacterial gene expression.* Biophys Rev, 2016. **8**(Suppl 1): p. 89-100.
32. Wallden, M., D. Fange, E.G. Lundius, O. Baltekin, and J. Elf, *The Synchronization of Replication and Division Cycles in Individual E. coli Cells.* Cell, 2016. **166**(3): p. 729-739.
33. Dame, R.T., F.M. Rashid, and D.C. Grainger, *Chromosome organization in bacteria: mechanistic insights into genome structure and function.* Nat Rev Genet, 2020. **21**(4): p. 227-242.
34. Dame, R.T. and M. Tark-Dame, *Bacterial chromatin: converging views at different scales.* Curr Opin Cell Biol, 2016. **40**: p. 60-65.
35. Verma, S.C., Z. Qian, and S.L. Adhya, *Architecture of the Escherichia coli nucleoid.* PLoS Genet, 2019. **15**(12): p. e1008456.
36. Danilova, O., R. Reyes-Lamothe, M. Pinskaya, D. Sherratt, and C. Possoz, *MukB colocalizes with the oriC region and is required for organization of the two Escherichia coli chromosome arms into separate cell halves.* 2007. **65**(6).
37. Woldringh, C.L. and N. Nanninga, *Structural and physical aspects of bacterial chromosome segregation.* J Struct Biol, 2006. **156**(2): p. 273-83.

38. Cremazy, F.G., F.M. Rashid, J.R. Haycocks, L.E. Lamberte, D.C. Grainger, and R.T. Dame, *Determination of the 3D Genome Organization of Bacteria Using Hi-C*. *Methods Mol Biol*, 2018. **1837**: p. 3-18.
39. Nielsen, H.J., Y. Li, B. Youngren, F.G. Hansen, and S. Austin, *Progressive segregation of the Escherichia coli chromosome*. *Molecular Microbiology*, 2006. **61**(2): p. 383-393.
40. Wang, X., X. Liu, C. Possoz, and D.J. Sherratt, *The two Escherichia coli chromosome arms locate to separate cell halves*. *Genes Dev*, 2006. **20**(13): p. 1727-31.
41. Reyes-Lamothe, R., E. Nicolas, and D.J. Sherratt, *Chromosome replication and segregation in bacteria*. 2012. **46**.
42. Willis, L. and K.C. Huang, *Sizing up the bacterial cell cycle*. *Nat Rev Microbiol*, 2017. **15**(10): p. 606-620.
43. Schaechter, M., M.W. Bentzon, and O. Maaloe, *Synthesis of deoxyribonucleic acid during the division cycle of bacteria*. *Nature*, 1959. **183**(4669): p. 1207-8.
44. Cooper, S. and C.E. Helmstetter, *Chromosome Replication and the Division Cycle of Escherichia coli B/r*. *J. Mol. Biol*, 1968. **31**: p. 519-540.
45. Donachie, W.D., *Relationship between Cell Size and Time of Initiation of DNA Replication*. *Nature*, 1968. **219**: p. 1077-1079.
46. Si, F., D. Li, S.E. Cox, J.T. Sauls, O. Azizi, C. Sou, A.B. Schwartz, M.J. Erickstad, Y. Jun, X. Li, and S. Jun, *Invariance of Initiation Mass and Predictability of Cell Size in Escherichia coli*. *Curr Biol*, 2017. **27**(9): p. 1278-1287.
47. Zheng, H., P.Y. Ho, M. Jiang, B. Tang, W. Liu, D. Li, X. Yu, N.E. Kleckner, A. Amir, and C. Liu, *Interrogating the Escherichia coli cell cycle by cell dimension perturbations*. *Proc Natl Acad Sci U S A*, 2016. **113**(52): p. 15000-15005.
48. Reyes-Lamothe, R. and D.J. Sherratt, *The bacterial cell cycle, chromosome inheritance and cell growth*. *Nat Rev Microbiol*, 2019. **17**(8): p. 467-478.
49. Kath, J.E., S. Jergic, J.M. Heltzel, D.T. Jacob, N.E. Dixon, M.D. Sutton, G.C. Walker, and J.J. Loparo, *Polymerase exchange on single DNA molecules reveals processivity clamp control of translesion synthesis*. 2014. **111**(21).
50. Slater, S.C., M.R. Lifsics, M. O'Donnell, and R. Maurer, *holE, the gene coding for the theta subunit of DNA polymerase III of Escherichia coli: characterization of a holE mutant and comparison with a dnaQ (epsilon-subunit) mutant*. *J Bacteriol*, 1994. **176**(3): p. 815-21.
51. Zechner, E.L., C.A. Wu, and K.J. Marians, *Coordinated leading- and lagging-strand synthesis at the Escherichia coli DNA replication fork. II. Frequency of primer synthesis and efficiency of primer utilization control Okazaki fragment size*. *The Journal of biological chemistry*, 1992. **267**(6): p. 4045-53.
52. McInerney, P., A. Johnson, F. Katz, and M. O'Donnell, *Characterization of a triple DNA polymerase replisome*. *Mol Cell*, 2007. **27**(4): p. 527-38.
53. Georgescu, R.E., I. Kurth, and M.E. O'Donnell, *Single-molecule studies reveal the function of a third polymerase in the replisome*. *Nature Structural & Molecular Biology*, 2011. **19**(1): p. 113-116.
54. Moolman, M.C., S.T. Krishnan, J.W. Kerssemakers, A.v.d. Berg, P. Tulinski, M. Depken, R. Reyes-Lamothe, D.J. Sherratt, and N.H. Dekker, *Slow unloading leads to DNA-bound beta2-sliding clamp accumulation in live Escherichia coli cells*. 2014. **5**.
55. Leonard, A.C. and J.E. Grimwade, *Regulation of DnaA assembly and activity: taking directions from the genome*. *Annu Rev Microbiol*, 2011. **65**: p. 19-35.

56. Erzberger, J.P., M.L. Mott, and J.M. Berger, *Structural basis for ATP-dependent DnaA assembly and replication-origin remodeling*. Nat Struct Mol Biol, 2006. **13**(8): p. 676-83.
57. Duderstadt, K.E., K. Chuang, and J.M. Berger, *DNA stretching by bacterial initiators promotes replication origin opening*. Nature, 2011. **478**(7368): p. 209-13.
58. Fang, L., M.J. Davey, and M. O'Donnell, *Replisome assembly at oriC, the replication origin of E. coli, reveals an explanation for initiation sites outside an origin*. Mol. Cell, 1999. **4**: p. 541-553.
59. Mott, M.L., J.P. Erzberger, M.M. Coons, and J.M. Berger, *Structural synergy and molecular crosstalk between bacterial helicase loaders and replication initiators*. Cell, 2008. **135**(4): p. 623-34.
60. Arias-Palomo, E., V.L. O'Shea, I.V. Hood, and J.M. Berger, *The bacterial DnaC helicase loader is a DnaB ring breaker*. Cell, 2013. **153**(2): p. 438-48.
61. Davey, M.J., L. Fang, P. McInerney, R.E. Georgescu, and M. O'Donnell, *The DnaC helicase loader is a dual ATP/ADP switch protein*. EMBO J, 2002. **21**(12): p. 3148-59.
62. Makowska-Grzyska, M. and J.M. Kaguni, *Primase directs the release of DnaC from DnaB*. Mol Cell, 2010. **37**(1): p. 90-101.
63. Katayama, T., S. Ozaki, K. Keyamura, and K. Fujimitsu, *Regulation of the replication cycle: conserved and diverse regulatory systems for DnaA and oriC*. Nat Rev Microbiol, 2010. **8**(3): p. 163-70.
64. Kasho, K. and T. Katayama, *DnaA binding locus datA promotes DnaA-ATP hydrolysis to enable cell cycle-coordinated replication initiation*. Proc Natl Acad Sci U S A, 2013. **110**(3): p. 936-41.
65. Fujimitsu, K., T. Senriuchi, and T. Katayama, *Specific genomic sequences of E. coli promote replicational initiation by directly reactivating ADP-DnaA*. Genes Dev, 2009. **23**(10): p. 1221-33.
66. Yeeles, J.T.P., A. Janska, A. Early, and J.F.X. Diffley, *How the Eukaryotic Replisome Achieves Rapid and Efficient DNA Replication*. Mol Cell, 2017. **65**(1): p. 105-116.
67. Elshenawy, M.M., S. Jergic, Z.Q. Xu, M.A. Sobhy, M. Takahashi, A.J. Oakley, N.E. Dixon, and S.M. Hamdan, *Replisome speed determines the efficiency of the Tus-Ter replication termination barrier*. Nature, 2015. **525**(7569): p. 394-8.
68. Pham, T.M., K.W. Tan, Y. Sakumura, K. Okumura, H. Maki, and M.T. Akiyama, *A single-molecule approach to DNA replication in Escherichia coli cells demonstrated that DNA polymerase III is a major determinant of fork speed*. Molecular microbiology, 2013. **90**(3): p. 584-96.
69. Kim, S., H.G. Dallmann, C.S. McHenry, and K.J. Marians, *Coupling of a Replicative Polymerase and Helicase: A τ -DnaB Interaction Mediates Rapid Replication Fork Movement*. Cell, 1996. **84**(4): p. 643-650.
70. Soubry, N., A. Wang, and R. Reyes-Lamothe, *Replisome activity slowdown after exposure to ultraviolet light in Escherichia coli*. Proceedings of the National Academy of Sciences, 2019: p. 201819297.
71. Sinha, N.K., C.F. Morris, and B.M. Alberts, *Efficient in vitro replication of double-stranded DNA templates by a purified T4 bacteriophage replication system*. J Biol Chem, 1980. **255**(9): p. 4290-3.
72. Park, K., Z. Debyser, S. Tabor, C.C. Richardson, and J.D. Griffith, *Formation of a DNA loop at the replication fork generated by bacteriophage T7 replication proteins*. J Biol Chem, 1998. **273**(9): p. 5260-70.

73. Hamdan, S.M., J.J. Loparo, M. Takahashi, C.C. Richardson, and A.M. van Oijen, *Dynamics of DNA replication loops reveal temporal control of lagging-strand synthesis*. Nature, 2009. **457**(7227): p. 336-9.
74. Johnson, A. and M. O'Donnell, *Cellular DNA replicases: components and dynamics at the replication fork*. 2005. **74**.
75. Lewis, J.S., S. Jergic, and N.E. Dixon, *The E. coli DNA Replication Fork*. Enzymes, 2016. **39**: p. 31-88.
76. Georgescu, R.E., I. Kurth, N.Y. Yao, J. Stewart, O. Yurieva, and M. O'Donnell, *Mechanism of polymerase collision release from sliding clamps on the lagging strand*. EMBO J, 2009. **28**(19): p. 2981-91.
77. Wu, C.A., E.L. Zechner, and K.J. Marians, *Coordinated leading- and lagging-strand synthesis at the Escherichia coli DNA replication fork. I. Multiple effectors act to modulate Okazaki fragment size*. The Journal of biological chemistry, 1992. **267**(6): p. 4030-44.
78. Mangiameli, S.M., J.A. Cass, H. Merrikh, and P.A. Wiggins, *The bacterial replisome has factory-like localization*. Current Genetics, 2018. **64**(5): p. 1029-1036.
79. Mangiameli, S.M., B.T. Veit, H. Merrikh, and P.A. Wiggins, *The Replisomes Remain Spatially Proximal throughout the Cell Cycle in Bacteria*. PLoS genetics, 2017. **13**(1): p. e1006582.
80. Breier, A.M., H.U. Weier, and N.R. Cozzarelli, *Independence of replisomes in Escherichia coli chromosomal replication*. Proc Natl Acad Sci U S A, 2005. **102**(11): p. 3942-7.
81. Reyes-Lamothe, R., C. Possoz, O. Danilova, and D.J. Sherratt, *Independent positioning and action of Escherichia coli replisomes in live cells*. 2008. **133**(1).
82. Bates, D. and N. Kleckner, *Chromosome and Replisome Dynamics in E. coli: Loss of Sister Cohesion Triggers Global Chromosome Movement and Mediates Chromosome Segregation*. Cell, 2005. **121**(6): p. 899-911.
83. Tanner, N.A., G. Tolun, J.J. Loparo, S. Jergic, J.D. Griffith, N.E. Dixon, and A.M.v. Oijen, *E. coli DNA replication in the absence of free β clamps*. The EMBO Journal, 2011. **30**(9): p. 1830-1840.
84. Maisnier-Patin, S., K. Nordström, and S. Dasgupta, *Replication arrests during a single round of replication of the Escherichia coli chromosome in the absence of DnaC activity*. Molecular Microbiology, 2001. **42**(5): p. 1371-1382.
85. Moore, P.D., K.K. Bose, S.D. Rabkin, and B.S. Strauss, *Sites of termination of in vitro DNA synthesis on ultraviolet- and N-acetylaminofluorene-treated phi X174 templates by prokaryotic and eukaryotic DNA polymerases*. Proc Natl Acad Sci U S A, 1981. **78**(1): p. 110-4.
86. Mettrick, K.A. and I. Grainge, *Stability of blocked replication forks in vivo*. Nucleic acids research, 2015. **44**(2): p. 657-68.
87. Gupta, S., J.T.P. Yeeles, and K.J. Marians, *Regression of Replication Forks Stalled by Leading-strand Template Damage I. BOTH RecG AND RuvAB CATALYZE REGRESSION, BUT RuvC CLEAVES THE HOLLIDAY JUNCTIONS FORMED BY RecG PREFERENTIALLY*. Journal of Biological Chemistry, 2014. **289**(41): p. 28376-28387.
88. Yeeles, J.T. and K.J. Marians, *The Escherichia coli replisome is inherently DNA damage tolerant*. 2011. **334**(6053).
89. Pomerantz, R.T. and M. O'Donnell, *The replisome uses mRNA as a primer after colliding with RNA polymerase*. Nature, 2008. **456**(7223): p. 762-6.

90. Heller, R.C. and K.J. Marians, *Replication fork reactivation downstream of a blocked nascent leading strand*. *Nature*, 2006. **439**(7076): p. 557-62.
91. Gupta, M.K., C.P. Guy, J.T. Yeeles, J. Atkinson, H. Bell, R.G. Lloyd, K.J. Marians, and P. McGlynn, *Protein-DNA complexes are the primary sources of replication fork pausing in Escherichia coli*. *Proc Natl Acad Sci U S A*, 2013. **110**(18): p. 7252-7.
92. Heller, R.C. and K.J. Marians, *Replisome assembly and the direct restart of stalled replication forks*. 2006. **7**(12).
93. Neylon, C., A.V. Kralicek, T.M. Hill, and N.E. Dixon, *Replication termination in Escherichia coli: structure and antihelicase activity of the Tus-Ter complex*. *Microbiol Mol Biol Rev*, 2005. **69**(3): p. 501-26.
94. Dewar, J.M. and J.C. Walter, *Mechanisms of DNA replication termination*. *Nature reviews. Molecular cell biology*, 2017. **18**(8): p. 507-516.
95. Mulcair, M.D., P.M. Schaeffer, A.J. Oakley, H.F. Cross, C. Neylon, T.M. Hill, and N.E. Dixon, *A molecular mousetrap determines polarity of termination of DNA replication in E. coli*. *Cell*, 2006. **125**(7): p. 1309-19.
96. Valjavec-Gratian, M., T.A. Henderson, and T.M. Hill, *Tus-mediated arrest of DNA replication in Escherichia coli is modulated by DNA supercoiling*. *Mol Microbiol*, 2005. **58**(3): p. 758-73.
97. Duggin, I.G. and S.D. Bell, *Termination structures in the Escherichia coli chromosome replication fork trap*. *J Mol Biol*, 2009. **387**(3): p. 532-9.
98. Midgley-Smith, S.L., J.U. Dimude, T. Taylor, N.M. Forrester, A.L. Upton, R.G. Lloyd, and C.J. Rudolph, *Chromosomal over-replication in Escherichia coli recG cells is triggered by replication fork fusion and amplified if replicore symmetry is disturbed*. *Nucleic Acids Res*, 2018. **46**(15): p. 7701-7715.
99. Guy, C.P., J. Atkinson, M.K. Gupta, A.A. Mahdi, E.J. Gwynn, C.J. Rudolph, P.B. Moon, I.C. van Knippenberg, C.J. Cadman, M.S. Dillingham, R.G. Lloyd, and P. McGlynn, *Rep provides a second motor at the replisome to promote duplication of protein-bound DNA*. *Mol Cell*, 2009. **36**(4): p. 654-66.
100. Lang, K.S. and H. Merrikh, *The Clash of Macromolecular Titans: Replication-Transcription Conflicts in Bacteria*. *Annual Review of Microbiology*, 2018. **72**(1): p. 1-18.
101. Meyer, R.R. and P.S. Laine, *The single-stranded DNA-binding protein of Escherichia coli*. *Microbiological reviews*, 1990. **54**(4): p. 342-80.
102. Schwartzman, J.B., P. Hernandez, D.B. Krimer, J. Dorier, and A. Stasiak, *Closing the DNA replication cycle: from simple circular molecules to supercoiled and knotted DNA catenanes*. *Nucleic Acids Res*, 2019. **47**(14): p. 7182-7198.
103. Stracy, M., A.J.M. Wollman, E. Kaja, J. Gapinski, J.E. Lee, V.A. Leek, S.J. McKie, L.A. Mitchenall, A. Maxwell, D.J. Sherratt, M.C. Leake, and P. Zawadzki, *Single-molecule imaging of DNA gyrase activity in living Escherichia coli*. *Nucleic Acids Res*, 2019. **47**(1): p. 210-220.
104. Koster, D.A., A. Crut, S. Shuman, M.A. Bjornsti, and N.H. Dekker, *Cellular strategies for regulating DNA supercoiling: a single-molecule perspective*. *Cell*, 2010. **142**(4): p. 519-30.
105. Vos, S.M., E.M. Tretter, B.H. Schmidt, and J.M. Berger, *All tangled up: how cells direct, manage and exploit topoisomerase function*. *Nat Rev Mol Cell Biol*, 2011. **12**(12): p. 827-41.

106. Rovinskiy, N., A.A. Agbleke, O. Chesnokova, Z. Pang, and N.P. Higgins, *Rates of gyrase supercoiling and transcription elongation control supercoil density in a bacterial chromosome*. PLoS Genet, 2012. **8**(8): p. e1002845.
107. Postow, L., C.D. Hardy, J. Arsuaga, and N.R. Cozzarelli, *Topological domain structure of the Escherichia coli chromosome*. Genes Dev, 2004. **18**(14): p. 1766-79.
108. Marinus, M.G., *DNA Mismatch Repair*. EcoSal Plus, 2012. **5**(1).
109. Uphoff, S., R. Reyes-Lamothe, G.F.d. Leon, D.J. Sherratt, and A.N. Kapanidis, *Single-molecule DNA repair in live bacteria*. 2013. **110**(20).
110. Sandigursky, M., G.A. Freyer, and W.A. Franklin, *The post-incision steps of the DNA base excision repair pathway in Escherichia coli: studies with a closed circular DNA substrate containing a single U:G base pair*. Nucleic Acids Res, 1998. **26**(5): p. 1282-7.
111. Bjelland, S., N.K. Birkeland, T. Benneche, G. Volden, and E. Seeberg, *DNA glycosylase activities for thymine residues oxidized in the methyl group are functions of the AlkA enzyme in Escherichia coli*. J Biol Chem, 1994. **269**(48): p. 30489-95.
112. Kisker, C., J. Kuper, and B. Houten, *Prokaryotic Nucleotide Excision Repair*. Cold Spring Harbor Perspectives in Biology, 2013. **5**(3): p. a012591.
113. Van Houten, B., J.A. Eisen, and P.C. Hanawalt, *A cut above: discovery of an alternative excision repair pathway in bacteria*. Proc Natl Acad Sci U S A, 2002. **99**(5): p. 2581-3.
114. Reardon, J.T. and A. Sancar, *Nucleotide excision repair*. Prog Nucleic Acid Res Mol Biol, 2005. **79**: p. 183-235.
115. Simmons, L.A., S.E. Cohen, J.J. Foti, and G.C. Walker, *The SOS Regulatory Network*. EcoSal Plus, 2008. **3**(1).
116. Friedberg, E.C., G.C. Walker, W. Siede, R.D. Wood, R.A. Schultz, and T. Ellenberger, *DNA Repair and Mutagenesis*. 2005.
117. Kath, J.E., S. Chang, M.K. Scotland, J.H. Wilbertz, S. Jergic, N.E. Dixon, M.D. Sutton, and J.J. Loparo, *Exchange between Escherichia coli polymerases II and III on a processivity clamp*. Nucleic Acids Res, 2016. **44**(4): p. 1681-90.
118. Thrall, E.S., J.E. Kath, S. Chang, and J.J. Loparo, *Single-molecule imaging reveals multiple pathways for the recruitment of translesion polymerases after DNA damage*. Nature Communications, 2017. **8**(1): p. 2170.
119. Chang, S., K. Naiman, E.S. Thrall, J.E. Kath, S. Jergic, N.E. Dixon, R.P. Fuchs, and J.J. Loparo, *A gatekeeping function of the replicative polymerase controls pathway choice in the resolution of lesion-stalled replisomes*. Proc Natl Acad Sci U S A, 2019. **116**(51): p. 25591-25601.
120. Cox, M.M., M.F. Goodman, K.N. Kreuzer, D.J. Sherratt, S.J. Sandler, and K.J. Marians, *The importance of repairing stalled replication forks*. Nature, 2000. **404**(6773): p. 37-41.
121. Anderson, D.G. and S.C. Kowalczykowski, *The Translocating RecBCD Enzyme Stimulates Recombination by Directing RecA Protein onto ssDNA in a χ -Regulated Manner*. Cell, 1997. **90**(1): p. 77-86.
122. West, S.C., *The processing of recombination intermediates: Mechanistic insights from studies of bacterial proteins*. Cell, 1994. **76**(1): p. 9-15.
123. West, S.C., *Processing of recombination intermediates by the RuvABC proteins*. Annu Rev Genet, 1997. **31**: p. 213-44.
124. van Gool, A.J., R. Shah, C. Mezard, and S.C. West, *Functional interactions between the holliday junction resolvase and the branch migration motor of Escherichia coli*. EMBO J, 1998. **17**(6): p. 1838-45.

125. Whitby, M.C., L. Ryder, and R.G. Lloyd, *Reverse branch migration of holliday junctions by RecG protein: A new mechanism for resolution of intermediates in recombination and DNA repair*. Cell, 1993. **75**(2): p. 341-350.
126. Whitby, M.C., S.D. Vincent, and R.G. Lloyd, *Branch migration of Holliday junctions: identification of RecG protein as a junction specific DNA helicase*. The EMBO Journal, 1994. **13**(21): p. 5220-5228.
127. Muller, B. and S.C. West, *Processing of Holliday junctions by the Escherichia coli RuvA, RuvB, RuvC and RecG proteins*. Experientia, 1994. **50**(3): p. 216-22.
128. Chan, S.N., S.D. Vincent, and R.G. Lloyd, *Recognition and manipulation of branched DNA by the RuvA Holliday junction resolvase of Escherichia coli*. Nucleic Acids Res, 1998. **26**(7): p. 1560-6.
129. Zerbib, D., S.D. Colloms, D.J. Sherratt, and S.C. West, *Effect of DNA topology on Holliday junction resolution by Escherichia coli RuvC and bacteriophage T7 endonuclease I*. J Mol Biol, 1997. **270**(5): p. 663-73.
130. Kuzminov, A., *RuvA, RuvB and RuvC proteins: cleaning-up after recombinational repairs in E. coli*. Bioessays, 1993. **15**(5): p. 355-8.
131. Giraud-Panis, M.J. and D.M. Lilley, *Structural recognition and distortion by the DNA junction-resolving enzyme RuvA*. J Mol Biol, 1998. **278**(1): p. 117-33.
132. Harmon, F.G. and S.C. Kowalczykowski, *RecQ helicase, in concert with RecA and SSB proteins, initiates and disrupts DNA recombination*. Genes Dev, 1998. **12**(8): p. 1134-44.
133. Lovett, S.T. and R.D. Kolodner, *Identification and purification of a single-stranded-DNA-specific exonuclease encoded by the recJ gene of Escherichia coli*. Proc Natl Acad Sci U S A, 1989. **86**(8): p. 2627-31.
134. Morimatsu, K. and S.C. Kowalczykowski, *RecFOR Proteins Load RecA Protein onto Gapped DNA to Accelerate DNA Strand Exchange*. Molecular Cell, 2003. **11**(5): p. 1337-1347.
135. Henrikus, S.S., C. Henry, H. Ghodke, E.A. Wood, N. Mbele, R. Saxena, U. Basu, A.M. van Oijen, M.M. Cox, and A. Robinson, *RecFOR epistasis group: RecF and RecO have distinct localizations and functions in Escherichia coli*. Nucleic Acids Res, 2019. **47**(6): p. 2946-2965.
136. Umez, K. and R.D. Kolodner, *Protein interactions in genetic recombination in Escherichia coli. Interactions involving RecO and RecR overcome the inhibition of RecA by single-stranded DNA-binding protein*. J Biol Chem, 1994. **269**(47): p. 30005-13.
137. Shan, Q., J.M. Bork, B.L. Webb, R.B. Inman, and M.M. Cox, *RecA protein filaments: end-dependent dissociation from ssDNA and stabilization by RecO and RecR proteins*. J Mol Biol, 1997. **265**(5): p. 519-40.
138. Windgassen, T.A., S.R. Wessel, B. Bhattacharyya, and J.L. Keck, *Mechanisms of bacterial DNA replication restart*. Nucleic acids research, 2017.
139. Jones, J.M. and H. Nakai, *Escherichia coli PriA helicase: fork binding orients the helicase to unwind the lagging strand side of arrested replication forks*. J Mol Biol, 2001. **312**(5): p. 935-47.
140. Liu, J. and K.J. Marians, *PriA-directed assembly of a primosome on D loop DNA*. J Biol Chem, 1999. **274**(35): p. 25033-41.
141. Heller, R.C. and K.J. Marians, *Unwinding of the nascent lagging strand by Rep and PriA enables the direct restart of stalled replication forks*. J Biol Chem, 2005. **280**(40): p. 34143-51.

142. Bhattacharyya, B., N.P. George, T.M. Thurmes, R. Zhou, N. Jani, S.R. Wessel, S.J. Sandler, T. Ha, and J.L. Keck, *Structural mechanisms of PriA-mediated DNA replication restart*. Proc Natl Acad Sci U S A, 2014. **111**(4): p. 1373-8.
143. Cadman, C.J. and P. McGlynn, *PriA helicase and SSB interact physically and functionally*. Nucleic Acids Res, 2004. **32**(21): p. 6378-87.
144. Lopper, M., R. Boonsombat, S.J. Sandler, and J.L. Keck, *A hand-off mechanism for primosome assembly in replication restart*. Mol Cell, 2007. **26**(6): p. 781-93.
145. Kornberg, T. and M.L. Gefter, *Deoxyribonucleic acid synthesis in cell-free extracts. IV. Purification and catalytic properties of deoxyribonucleic acid polymerase III*. J Biol Chem, 1972. **247**(17): p. 5369-75.
146. Sinha, R.P. and D.P. Hader, *UV-induced DNA damage and repair: a review*. 2002. **1**(4).
147. Yeeles, J.T. and K.J. Marians, *Dynamics of leading-strand lesion skipping by the replisome*. 2013. **52**(6).
148. McInerney, P. and M. O'Donnell, *Replisome fate upon encountering a leading strand block and clearance from DNA by recombination proteins*. J Biol Chem, 2007. **282**(35): p. 25903-16.
149. Pages, V. and R.P. Fuchs, *Uncoupling of leading- and lagging-strand DNA replication during lesion bypass in vivo*. Science, 2003. **300**(5623): p. 1300-3.
150. Higuchi, K., T. Katayama, S. Iwai, M. Hidaka, T. Horiuchi, and H. Maki, *Fate of DNA replication fork encountering a single DNA lesion during oriC plasmid DNA replication in vitro*. Genes Cells, 2003. **8**(5): p. 437-49.
151. Jeiranian, H.A., B.J. Schalow, C.T. Courcelle, and J. Courcelle, *Fate of the replisome following arrest by UV-induced DNA damage in Escherichia coli*. 2013. **110**(28).
152. Rudolph, C.J., A.L. Upton, and R.G. Lloyd, *Replication fork stalling and cell cycle arrest in UV-irradiated Escherichia coli*. 2007. **21**(6).
153. Echols, H. and M.F. Goodman, *Mutation induced by DNA damage: a many protein affair*. Mutation Research/DNA Repair, 1990. **236**(2-3): p. 301-311.
154. Belle, J.J., A. Casey, C.T. Courcelle, and J. Courcelle, *Inactivation of the DnaB Helicase Leads to the Collapse and Degradation of the Replication Fork: a Comparison to UV-Induced Arrest* v. Journal of Bacteriology, 2007. **189**(15): p. 5452-5462.
155. Chalfie, M., Y. Tu, G. Euskirchen, W.W. Ward, and D.C. Prasher, *Green fluorescent protein as a marker for gene expression*. Science, 1994. **263**(5148): p. 802-5.
156. Hummert, J., K. Yserentant, T. Fink, J. Euchner, and D.-P. Herten, 2020.
157. Sekar, R.B. and A. Periasamy, *Fluorescence resonance energy transfer (FRET) microscopy imaging of live cell protein localizations*. J Cell Biol, 2003. **160**(5): p. 629-33.
158. Badrinarayanan, A., C. Lesterlin, R. Reyes-Lamothe, and D. Sherratt, *The Escherichia coli SMC Complex, MukBEF, Shapes Nucleoid Organization Independently of DNA Replication*. Journal of Bacteriology, 2012. **194**(17).
159. Mazza, D., A. Abernathy, N. Golob, T. Morisaki, and J.G. McNally, *A benchmark for chromatin binding measurements in live cells*. Nucleic Acids Res, 2012. **40**(15): p. e119.
160. Stracy, M., C. Lesterlin, S. Uphoff, P. Zawadzki, and A.N. Kapanidis, *Single-Molecule Imaging of Transcription, Chromosome Organization, and DNA Repair in Live Bacteria*. Biophysical Journal, 2016. **110**(3): p. 20a-21a.
161. Shen, H., L.J. Tauzin, R. Baiyasi, W. Wang, N. Moringo, B. Shuang, and C.F. Landes, *Single Particle Tracking: From Theory to Biophysical Applications*. Chem Rev, 2017. **117**(11): p. 7331-7376.

162. McEvoy, A.L., H. Hoi, M. Bates, E. Platonova, P.J. Cranfill, M.A. Baird, M.W. Davidson, H. Ewers, J. Liphardt, and R.E. Campbell, *mMaple: a photoconvertible fluorescent protein for use in multiple imaging modalities*. PLoS One, 2012. **7**(12): p. e51314.
163. Wang, S., J.R. Moffitt, G.T. Dempsey, X.S. Xie, and X. Zhuang, *Characterization and development of photoactivatable fluorescent proteins for single-molecule-based superresolution imaging*. Proceedings of the National Academy of Sciences, 2014. **111**(23): p. 8452-8457.
164. Elf, J. and I. Barkefors, *Single-Molecule Kinetics in Living Cells*. Annual review of biochemistry, 2019. **88**: p. 635-659.
165. Henrikus, S.S., E.A. Wood, J.P. McDonald, M.M. Cox, R. Woodgate, M.F. Goodman, A.M. van Oijen, and A. Robinson, *DNA polymerase IV primarily operates outside of DNA replication forks in Escherichia coli*. PLoS Genet, 2018. **14**(1): p. e1007161.
166. Robinson, A., J.P. McDonald, V.E. Caldas, M. Patel, E.A. Wood, C.M. Punter, H. Ghodke, M.M. Cox, R. Woodgate, M.F. Goodman, and A.M. van Oijen, *Regulation of Mutagenic DNA Polymerase V Activation in Space and Time*. PLoS Genet, 2015. **11**(8): p. e1005482.
167. Suksombat, S., R. Khafizov, A.G. Kozlov, T.M. Lohman, and Y.R. Chemla, *Structural dynamics of E. coli single-stranded DNA binding protein reveal DNA wrapping and unwrapping pathways*. Elife, 2015. **4**.
168. Wu, C.A., E.L. Zechner, J.A. Reems, C.S. McHenry, and K.J. Marians, *Coordinated leading- and lagging-strand synthesis at the Escherichia coli DNA replication fork. V. Primase action regulates the cycle of Okazaki fragment synthesis*. The Journal of biological chemistry, 1992. **267**(6): p. 4074-83.
169. Glover, B.P. and C.S. McHenry, *The $\chi\psi$ Subunits of DNA Polymerase III Holoenzyme Bind to Single-stranded DNA-binding Protein (SSB) and Facilitate Replication of an SSB-coated Template*. Journal of Biological Chemistry, 1998. **273**(36): p. 23476-23484.
170. Kelman, Z., A. Yuzhakov, J. Andjelkovic, and M. O'Donnell, *Devoted to the lagging strand—the χ subunit of DNA polymerase III holoenzyme contacts SSB to promote processive elongation and sliding clamp assembly*. The EMBO Journal, 1998. **17**(8): p. 2436-2449.
171. Downey, C.D. and C.S. McHenry, *Chaperoning of a replicative polymerase onto a newly assembled DNA-bound sliding clamp by the clamp loader*. Mol Cell, 2010. **37**(4): p. 481-91.
172. Harami, G.M., Z.J. Kovacs, R. Pancsa, J. Palinkas, V. Barath, K. Tarnok, A. Malnasi-Csizmadia, and M. Kovacs, *Phase separation by ssDNA binding protein controlled via protein-protein and protein-DNA interactions*. Proc Natl Acad Sci U S A, 2020. **117**(42): p. 26206-26217.
173. Datsenko, K.A. and B.L. Wanner, *One-step inactivation of chromosomal genes in Escherichia coli K-12 using PCR products*. Proceedings of the National Academy of Sciences of the United States of America, 2000. **97**(12): p. 6640-5.
174. Nguyen, A.W. and P.S. Daugherty, *Evolutionary optimization of fluorescent proteins for intracellular FRET*. Nat Biotechnol, 2005. **23**(3): p. 355-60.
175. Shaner, N.C., R.E. Campbell, P.A. Steinbach, B.N. Giepmans, A.E. Palmer, and R.Y. Tsien, *Improved monomeric red, orange and yellow fluorescent proteins derived from Discosoma sp. red fluorescent protein*. Nat Biotechnol, 2004. **22**(12): p. 1567-72.
176. Shaner, N.C., G.G. Lambert, A. Chammas, Y. Ni, P.J. Cranfill, M.A. Baird, B.R. Sell, J.R. Allen, R.N. Day, M. Israelsson, M.W. Davidson, and J. Wang, *A bright monomeric green*

- fluorescent protein derived from Branchiostoma lanceolatum*. Nat Methods, 2013. **10**(5): p. 407-9.
177. Thomason, L.C., N. Costantino, and D.L. Court, *E. coli genome manipulation by PI transduction*. Curr Protoc Mol Biol, 2007. **Chapter 1**: p. Unit 1 17.
 178. Tinevez, J.Y., N. Perry, J. Schindelin, G.M. Hoopes, G.D. Reynolds, E. Laplantine, S.Y. Bednarek, S.L. Shorte, and K.W. Eliceiri, *TrackMate: An open and extensible platform for single-particle tracking*. Methods, 2017. **115**: p. 80-90.
 179. Julou, T., T. Mora, L. Guillon, V. Croquette, I.J. Schalk, D. Bensimon, and N. Desprat, *Cell-cell contacts confine public goods diffusion inside Pseudomonas aeruginosa clonal microcolonies*. Proceedings of the National Academy of Sciences, 2013. **110**(31): p. 12577-12582.
 180. Stylianidou, S., C. Brennan, S.B. Nissen, N.J. Kuwada, and P.A. Wiggins, *SuperSegger: robust image segmentation, analysis and lineage tracking of bacterial cells*. Molecular Microbiology, 2016. **102**(4): p. 690-700.
 181. Kapadia, N., Z.W. El-Hajj, and R. Reyes-Lamothe, *Bound2Learn: A Machine Learning Approach for Classification of DNA-Bound Proteins from Single-Molecule Tracking Experiments*. bioRxiv, 2020.
 182. Koch, A.L. and M. Schaechter, *A model for statistics of the cell division process*. J Gen Microbiol, 1962. **29**: p. 435-54.

Annex 1

Interaction with single-stranded DNA-binding protein localizes ribonuclease HI to DNA replication forks and facilitates R-loop removal

Christine Wolak, Hui Jun Ma, Nicolas Soubry, Steven J. Sandler, Rodrigo Reyes-Lamothe and James L. Keck. Interaction with single-stranded DNA-binding protein localizes ribonuclease HI to DNA replication forks and facilitates R-loop removal *Molecular Microbiology* 2020 Sep;114(3):495-509

This work contributes to the understanding of the role of RNase HI during DNA replication. RNase HI is a ribonuclease tasked with resolving R-loops. My contribution to this work was Figure 1. I imaged RNase HI and an RNase HI mutant (*rnhAK60E*) that cannot interact with SSB. I noticed that RNase HI forms foci similar to those seen with the replication fork protein. The RNase HI mutant was not able to bind DNA. I then did a colocalization analysis between RNase HI and the β -clamp. Not only did the distribution of spots per cell closely match but also the distance between the proteins were similar to distance seen between replisome components.



Interaction with single-stranded DNA-binding protein localizes ribonuclease HI to DNA replication forks and facilitates R-loop removal

Christine Wolak¹ | Hui Jun Ma² | Nicolas Soubry² | Steven J. Sandler³ |
Rodrigo Reyes-Lamothe² | James L. Keck¹

¹Department of Biomolecular Chemistry, University of Wisconsin School of Medicine and Public Health, Madison, WI, USA

²Department of Biology, McGill University, Montreal, QC, Canada

³Department of Microbiology, University of Massachusetts, Amherst, MA, USA

Correspondence

James L. Keck, Department of Biomolecular Chemistry, University of Wisconsin School of Medicine and Public Health, 420 Henry Mall, Madison, WI 53706, USA.
Email: jlkeck@wisc.edu

Funding information

National Institute of General Medical Sciences, Grant/Award Number: R01 GM098885; National Science Foundation, Grant/Award Number: DGE-1256259

Abstract

DNA replication complexes (replisomes) routinely encounter proteins and unusual nucleic acid structures that can impede their progress. Barriers can include transcription complexes and R-loops that form when RNA hybridizes with complementary DNA templates behind RNA polymerases. Cells encode several RNA polymerase and R-loop clearance mechanisms to limit replisome exposure to these potential obstructions. One such mechanism is hydrolysis of R-loops by ribonuclease HI (RNase HI). Here, we examine the cellular role of the interaction between *Escherichia coli* RNase HI and the single-stranded DNA-binding protein (SSB) in this process. Interaction with SSB localizes RNase HI foci to DNA replication sites. Mutation of *rnhA* to encode an RNase HI variant that cannot interact with SSB but that maintains enzymatic activity (*rnhAK60E*) eliminates RNase HI foci. The mutation also produces a media-dependent slow-growth phenotype and an activated DNA damage response in cells lacking Rep helicase, which is an enzyme that disrupts stalled transcription complexes. RNA polymerase variants that are thought to increase or decrease R-loop accumulation enhance or suppress, respectively, the growth phenotype of *rnhAK60E rep::kan* strains. These results identify a cellular role for the RNase HI/SSB interaction in helping to clear R-loops that block DNA replication.

KEYWORDS

DNA replication, genome maintenance, transcription

1 | INTRODUCTION

Replisomes are protein complexes that catalyze high-fidelity DNA replication at speeds approaching 1,000 bp/sec in bacteria (Chandler *et al.*, 1975; O'Donnell *et al.*, 2013). During the replication process replisomes encounter numerous impediments to their progress including protein/DNA complexes, non-duplex nucleic acid structures, and chromosomal damage (Mirkin and Mirkin, 2007). To overcome these obstacles, cells have evolved several systems that support replication on imperfect genomic templates. These include enzymes

that dissociate protein/DNA complexes and resolve unusual nucleic acid structures, repair pathways that mitigate damaged DNA, and proteins that restructure collapsed replication forks.

RNA polymerase (RNAP) and transcription-dependent nucleic acid structures called R-loops are common barriers to replisome progress (Aguilera and Garcia-Muse, 2012; Helmrich *et al.*, 2013). R-loops are structures that form when a nascent RNA hybridizes with the DNA template behind RNAP (Westover *et al.*, 2004). Bacterial replisomes move at rates that are ~10-20 times faster than RNAP and can encounter R-loops and/or RNAP in both head-on and co-directional

collisions in bacteria (Merrick *et al.*, 2012). Replication–transcription collisions occur even in eukaryotes, where replication forks move at rates similar to RNAP and most replication and transcription reactions are temporally and spatially separated (Azvolinsky *et al.*, 2009; Helmrich *et al.*, 2011). Head-on collisions can result in replication fork arrest and activation of DNA damage-dependent recombination (French, 1992; Deshpande and Newlon, 1996; Vilette *et al.*, 1996; Prado and Aguilera, 2005; Mirkin and Mirkin, 2007; Wang *et al.*, 2007). Replisome collisions with RNAP or R-loops can also lead to DNA breaks, genome rearrangements, increased mutagenesis, and activation of DNA damage responses (Huertas and Aguilera, 2003; Li and Manley, 2005; Tuduri *et al.*, 2009; Wahba *et al.*, 2011). These events can create double-strand DNA breaks (DSBs) when a switch in the DNA replication template forms a ssDNA gap that escapes repair prior to the next round of replication (Kuzminov, 2001; Pomerantz and O'Donnell, 2010).

Cells encode redundant pathways to minimize replisome encounters with RNAPs and R-loops and to repair the damage when such collisions occur. These pathways rely on DNA helicases, transcription-associated factors, nucleases, and DNA repair enzymes. One such contributor is ribonuclease HI (RNase HI), an enzyme that hydrolyzes RNA within RNA:DNA hybrids. Classical roles for RNase HI in bacteria include degradation of RNA primers used during DNA replication and suppression of origin-independent chromosomal DNA replication (Ogawa and Okazaki, 1980; Itoh and Tomizawa, 1980; Ogawa *et al.*, 1984; Alberts, 1987). A more recent role for RNase HI in removing R-loops that block replication forks has been identified (Itoh and Tomizawa, 1980; Dutta *et al.*, 2011; Merrick *et al.*, 2012). Genetic relationships link RNase HI with proteins that promote replication fork progression, that repair or restructure replication forks following R-loop-induced DNA damage, or that prevent R-loop accumulation (Itaya and Crouch, 1991a, 1991b; Drolet *et al.*, 1995; Hong *et al.*, 1995; Hraiky *et al.*, 2000; Harinarayanan and Gowrishankar, 2003; Sandler, 2005).

Through biochemical and structural studies, a stimulatory interaction formed between *E. coli* RNase HI and the single-stranded DNA-binding protein (SSB) has been identified (Petzold *et al.*, 2015). Stimulation requires docking of the intrinsically disordered C-terminus of SSB (SSB-Ct) into a binding pocket on RNase HI. This binding mechanism is shared with several other proteins that also form complexes with SSB via the SSB-Ct (Shereda *et al.*, 2008). In some cases, interactions with SSB have been shown to localize its interaction partners to DNA replication forks (Sun and Godson, 1996; Shereda *et al.*, 2008; Marceau *et al.*, 2011).

To probe possible cellular roles of the RNase HI/SSB interaction, we have compared the localization and activity of RNase HI to those of an RNase HI variant that has lost the ability to interact with SSB but that retains normal nuclease activity levels (RNase HI K60E; (Petzold *et al.*, 2015). To do this we created an RNase HI fluorescent fusion protein that forms foci in the cell and colocalizes with a subunit of the DNA replication machinery in *E. coli*. In contrast, the RNase HI K60E fusion variant failed to form foci in *E. coli*. Thus, RNase HI localizes to sites of DNA replication in vivo via the

interaction with SSB. Strains that substitute the *rnhA* gene (encodes RNase HI) with *rnhAK60E* have normal activities in RNA primer processing and in suppressing origin-independent DNA replication. However, a strain combining *rnhAK60E* with a mutation that inactivates the Rep DNA helicase, an enzyme that helps to promote replisome movement through transcription complexes (Guy *et al.*, 2009; Boubakri *et al.*, 2010), displays a plating deficiency on rich medium and an activated DNA damage response. *rpoB* mutations that produce RNAP variants that are thought to increase or decrease R-loop levels (Kogoma, 1994) enhance or suppress, respectively, the plating deficiency of *rnhAK60E rep::kan* cells. These data lead to a model in which interaction with SSB mediates RNase HI removal of transcription-dependent R-loop obstacles by localizing the enzyme to DNA replication sites.

2 | RESULTS

2.1 | Interaction with SSB localizes RNase HI to sites of DNA replication in *E. coli*

SSB is concentrated at replication sites in bacterial cells through its binding to the extended tracts of ssDNA present at DNA replication forks (Meyer and Laine, 1990; Reyes-Lamothe *et al.*, 2010; Reyes-Lamothe, 2012; Marceau, 2012). In some, but not all, instances, direct interaction with SSB also localizes SSB's interaction partner proteins to DNA replication forks (Lecoite *et al.*, 2007; Costes *et al.*, 2010; Bentchikou *et al.*, 2015). To determine whether RNase HI is localized to DNA replication sites in *E. coli*, we created a strain in which the chromosomal *rnhA* locus was replaced with an RNase HI-YPet fluorescent fusion protein and examined RNase HI-YPet focus formation using fluorescence microscopy. RNase HI-YPet foci were found in ~80% of the *E. coli* cells examined, with the majority of cells having either one or two foci (Figure 1a,b). This pattern is strikingly similar to that observed for several fluorescently tagged DNA replication proteins (Reyes-Lamothe *et al.*, 2008).

To determine whether RNase HI-YPet foci localize to DNA replication forks, the localization of RNase HI-YPet foci and a commonly used replication site marker, mCherry-fused DNA Pol III β -clamp (Reyes-Lamothe *et al.*, 2008; 2012; Liu *et al.*, 2010; Moolman *et al.*, 2014), were simultaneously measured (Figure 1a). Consistent with RNase HI-YPet foci forming at DNA replication forks, the median distance between a spot of RNase HI-YPet and the nearest mCherry- β -clamp spot is 202 nm (Figure 1c, inset). These values are slightly higher than those previously reported for replisome components with the ϵ subunit of DNA Pol III and β -clamp, which have a median distance of 128 nm (Soubry *et al.*, 2019). Consequently, we further tested for co-localization between RNase HI-YPet and β -clamp-mCherry by comparing the distribution of distances to a random distribution of spots in cells, represented by the radial distribution function $g(r)$. Values of $g(r)$ over 1 at short radial distances indicate that the two foci of the proteins overlap far more frequently than randomly distributed spots, supporting co-localization between

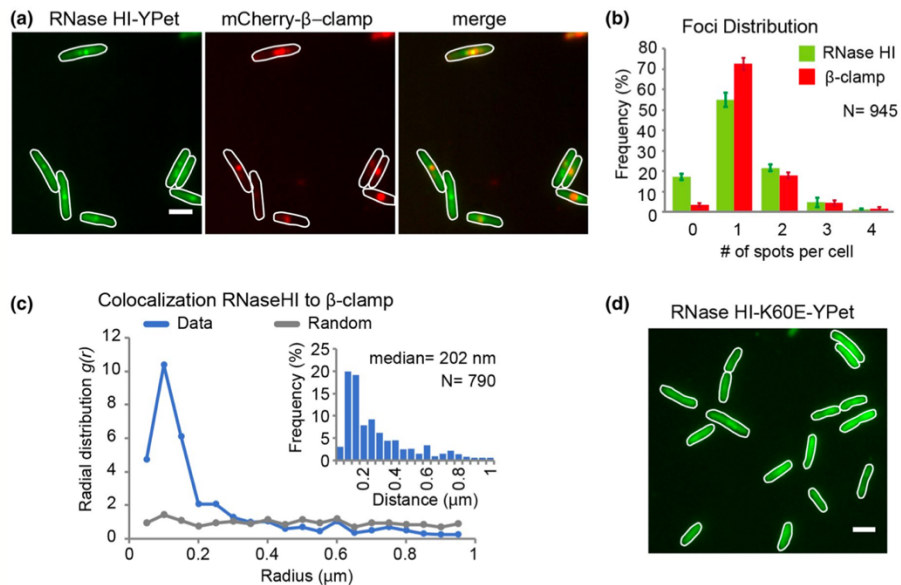


FIGURE 1 SSB-mediated localization of RNase HI to the replication fork. Fluorescence microscopy studies of *E. coli* strains expressing the fluorescent fusion proteins RNase HI-YPet and β -clamp-mCherry. (a) Representative images showing RNase HI-YPet (left), β -clamp-mCherry (middle), and a merged image showing the overlap of RNase HI-YPet and β -clamp-mCherry (right) in strain VV11. Digital contrast enhancement was used for presentation purposes. Scale bar in the right image is 2 μ m. (b) Detectable RNase HI-YPet and β -clamp-mCherry foci per cell are plotted as the frequency for the cell population. (c) Radial distribution function for RNase HI-YPet and β -clamp-mCherry representing colocalization (blue line). As comparison, $g(r)$ is plotted for a set of randomly distributed spots in cells (gray line). Inset shows the distribution of nearest-neighbor distances between spots of RNase HI-YPet and β -clamp-mCherry. (d) Representative fluorescent image showing RNase HI K60E-YPet fusion protein distributed throughout strain VV08. Imaging conditions and digital contrast enhancement used were as in Figure 1b. Scale bar is 2 μ m

RNase HI-YPet and β -clamp-mCherry (Figure 1c). In addition, we observed that 16.2% carried spots for β -clamp-mCherry but no RNase HI-YPet, compared with 2.4% of cases for cells with RNase HI-YPet spots but no β -clamp-mCherry, suggesting that RNase HI is not present at the replication fork at all times or may be present at low levels that are not detected by fluorescence microscopy in some instances.

To better understand the activity of RNase HI, we used single-molecule microscopy to measure the RNase HI copy number per cell and determine the fraction of RNase HI molecules found in foci (Figure S1). To do this, we modified *E. coli* strain AB1157 to encode RNase HI-mNeonGreen at the *rnhA* locus. mNeonGreen was used in place of Ypet as it is currently the brightest monomeric fluorescent protein in use, which maximized detection of single molecules (Shaner et al., 2013). The intensity of a single molecule of RNase HI-mNeonGreen was estimated by measuring the last bleaching step in time traces of foci (Figure S1d,e). Dividing the integrated intensity of a cell by the value of a single molecule, we estimated an average of 82 ± 40 RNase HI molecules per *E. coli* cell (Figure S1f), of which $20 \pm 13\%$ were localized in foci (Figure S1). These data suggest that in many instances there are multiple copies of RNase HI localized in foci. In addition, a significant number of RNase HI molecules are available in the diffusive pool.

Prior structural and biochemical experiments defined the SSB-binding site on RNase HI and identified a point mutation in RNase HI (K60E) that eliminated interaction without altering nuclease activity in vitro (Petzold et al., 2015). The cellular localization of RNase HI K60E-YPet was examined next to determine whether RNase HI-YPet focus formation requires interaction with SSB. Unlike RNase HI-YPet, foci were not observed for RNase HI K60E-YPet and the fluorescence signal of the variant was distributed throughout the cell (Figure 1d). This result indicates that RNase HI/SSB complex formation is necessary for recruitment and/or retention of RNase HI at DNA replication sites in *E. coli*.

2.2 | SSB-mediated localization of RNase HI is not required to suppress origin-independent replication or to degrade lagging-strand Okazaki fragment primers

RNase HI has noted activities in three major cellular processes in *E. coli*: (a) suppression of origin-independent "constitutive stable DNA replication" (cSDR), (b) degradation of lagging-strand RNA primers used during DNA replication, and (c) removal of R-loop replication barriers. To test for possible roles of SSB-mediated localization of

RNase HI in each of these activities, we created an *E. coli* strain with a mutated *rnhA* locus that encodes for the RNase HI K60E variant (*rnhAK60E*) and compared its phenotype to otherwise isogenic *rnhA* + and *rnhA::cat* *E. coli* strains (Table S1). *E. coli* with the *rnhAK60E* mutation were phenotypically indistinguishable from *rnhA* + and *rnhA::cat* cells in terms of growth rate, cell morphology, and rich medium plating efficiency (Figures 2, 3 and S2). Given the lack of a phenotypic difference for the *rnhA* point mutation, we next combined the *rnhAK60E* mutation with mutations in other genes that have established genetic relationships with *rnhA* to test whether loss of RNase HI/SSB complex formation affects the pathways in which RNase HI is involved.

We first examined whether the *rnhAK60E* mutation impacted RNase HI suppression of cSDR in *E. coli*. In cSDR, R-loops are processed by RecA, DNA polymerase I, and the primosome to allow for replication initiation away from *oriC*. RNase HI nuclease activity regulates this process by removing R-loops before the replisome can be loaded (Kogoma, 1978; von Meyenburg *et al.*, 1987). Therefore the inactivation of *rnhA* preserves R-loops and can rescue cell growth in strains carrying otherwise lethal mutations in

the *oriC*-replication initiation pathway (e.g., *dnaA* loss of function mutants) (Frey *et al.*, 1981; Kogoma and von Meyenburg, 1983; de Massy *et al.*, 1984; Lindahl and Lindahl, 1984; von Meyenburg *et al.*, 1987; Carr and Kaguni, 1996). To test whether abrogation of SSB-mediated RNase HI localization facilitates cSDR similarly to *rnhA::cat*, we introduced the *rnhAK60E* allele into *dnaA46(ts)* cells. Similarly to *rnhA* + *dnaA46(ts)*, the *rnhAK60E dnaA46(ts)* strain was unable to grow under non-permissive conditions (42°C), whereas the *rnhA::cat dnaA46(ts)* strain was able to grow at 42°C (Figure S3). This result indicates that the RNase HI K60E variant maintains sufficient activity to remove R-loops required for cSDR. Thus, SSB-mediated localization of RNase HI is not required for inhibiting R-loop-dependent replication initiation.

We next tested whether SSB-mediated RNase HI localization was important for degrading RNA primers used during canonical DNA replication. The nuclease activities of RNase HI and DNA polymerase I work together to remove RNA primers that initiate lagging-strand Okazaki fragments (Ogawa and Okazaki, 1984; Kitani *et al.*, 1985; Crouch, 1990). Inactivation of *rnhA* leads to media- and temperature-dependent impaired growth of an *E. coli*

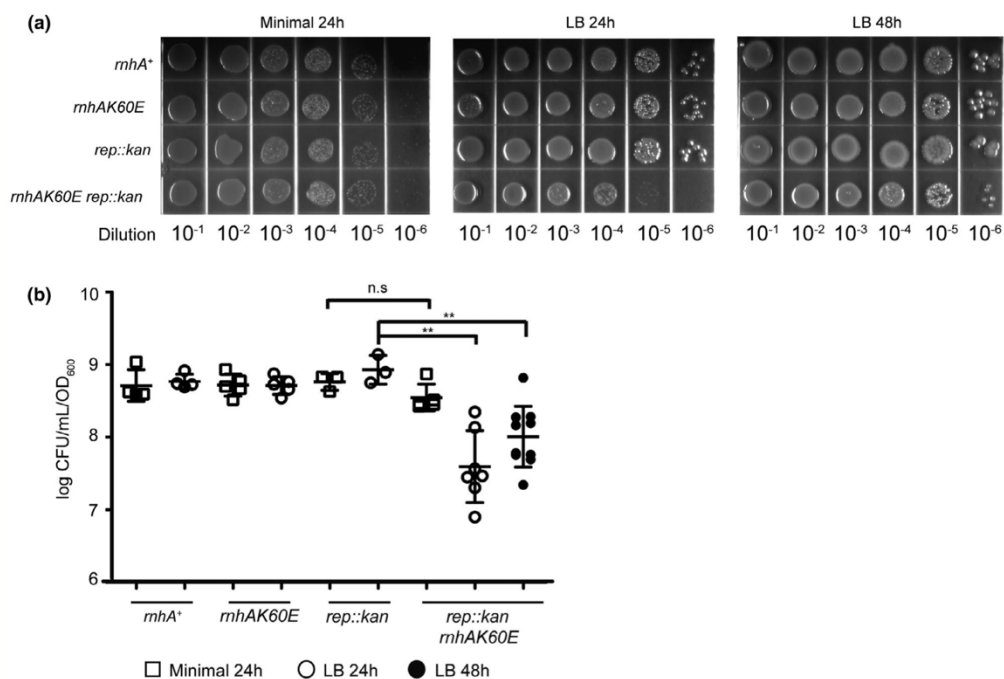
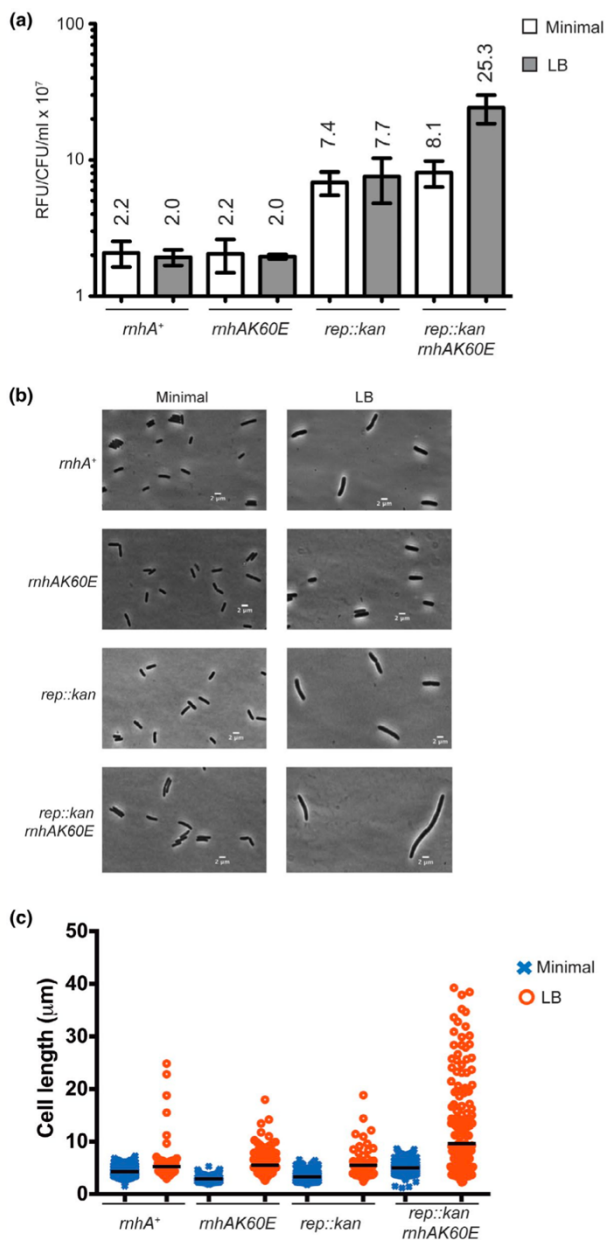


FIGURE 2 The *rnhAK60E rep::kan* strain is sensitive to growth on rich medium plates. (a) Dilutions of overnight cultures grown in minimal medium (56/2) and plated on minimal (left) or LB media (middle and right). Plates were incubated at 37°C for 24 or 48 hr. The images are representative of plating experiments performed in triplicate. Strains are CP65, CP58, CP84, and CP86 from top to bottom. (b and c) The CFU/ml of each strain (normalized to OD₆₀₀) is plotted from overnight cultures diluted and plated on minimal (squares) or LB (circles) media. Colonies were quantitated after growth at 37°C for 24 or 48 hr. Each symbol is a single culture and the mean CFU/ml for each strain is represented by a black line. Strains are CP65, CP58, CP84, and CP86 from left to right. Error bars indicate the standard deviation. ** = *p* value < .005 and n.s. = *p* value > .05 using two-tailed t-test

FIGURE 3 The *rnhAK60E rep::kan* strain has elevated SOS levels in rich medium. (a) The relative fluorescent units (RFU) from plasmid-borne GFP driven by a *recN* promoter are plotted for each strain at mid-log phase and normalized to CFU/ml at the time of data collection. Bars represent the mean RFU/CFU/ml from biological and technical replicates of strains grown in minimal medium (56/2) and LB. Error bars display the standard deviation of the mean. Mean values are written above each bar. Strains in this figure are CP127, CP128, CP129, and CP126 (from left to right). (b) Representative phase contrast images from strains grown in minimal medium (left) or LB (right). The strains were grown to early log phase and subsequently spotted on 2% agarose pads for imaging using a Nikon Eclipse Ti microscope equipped with a Photometrics CoolSNAP HQ2 charge-coupled device (CCD) camera. (c) The cell lengths captured by MATLAB of microscope images. Cells were grown in minimal medium or LB and treated as in (b)



strain carrying the *polA12(ts)* allele, which encodes a DNA polymerase I variant that has strongly reduced 5'-3' exonuclease and polymerase activities at 42°C (Uyemura and Lehman, 1976; Joyce *et al.*, 1985). To determine whether binding to SSB is required for primer-degradation by RNase HI, growth of a strain combining the *rnhAK60E* mutation with *polA12(ts)* was compared

to *rnhA* + *polA12(ts)* and *rnhA::cat polA12(ts)* strains. Growth of *rnhAK60E polA12(ts)* cells was indistinguishable from *rnhA* + *polA12(ts)* cells at 30 or 42°C in rich or minimal media (Figure S4). In contrast, the *rnhA::cat polA12(ts)* strain displayed media- and temperature-dependent growth defects as previously reported (Uyemura and Lehman, 1976; Joyce *et al.*, 1985). These data

indicate that SSB-mediated RNase HI localization is not required for Okazaki fragment RNA primer processing.

2.3 | Genetic interactions of *rnhAK60E* with DNA helicases

To examine the role of the RNase HI/SSB interaction in additional replication and repair processes, we tested the effects of combining *rnhAK60E* with deletions in several DNA replication/repair genes: *rep*, *recBCD*, *recG*, *uvrD*, or *dinG* (Table 1). These were chosen based on the reported synthetic lethal effects of *rnhA* deletion with *rep* (Sandler, 2005), *recBCD* (Itaya and Crouch, 1991a, 1991b; Kogoma et al., 1993; 1997; Hong et al., 1995), and *recG* (Hong et al., 1995) deletions and the proposed roles of UvrD and DinG helicases in DNA replication fork maintenance or repair (Kornberg and Baker, 1992; Sandler et al., 1996; Michel, 2005; Srivatsan et al., 2010; Boubakri et al., 2010; Dimude et al., 2015). Inactivation of several of these genes along with *rnhA* increases the possibility of collisions between replisomes and transcription-dependent R-loops and/or diminishes the capacity of cells to repair the resulting DNA damage from replication fork collapse (Kogoma et al., 1994; Hraiky et al., 2000; Wahba et al., 2011; Merrikh et al., 2012; Dimude et al., 2015).

We first measured the co-transduction frequencies of *rep::kan*, *recBCD::cat*, or *recG::kan* into three strains with different *rnhA* backgrounds: *rnhA+*, *rnhAK60E*, or *rnhA::cat*. *rep::kan*, *recBCD::kan*, and *recG::cat* each transduced with similar frequencies into *rnhA+* and *rnhAK60E* strains whereas they failed to transduce into *rnhA::cat* cells (Table 1). Another observation to note was that the *rnhA::cat rep::kan* synthetic lethality was dependent on transduction direction, a trait not observed with other synthetic lethal pairs (Table 1). This could be due to background differences between the *rep::kan* strain and the *rnhA* strains used in our study.

We expanded our screen to examine deletions of two other helicase genes: *uvrD::kan* and *dinG::kan*. The *uvrD::kan rnhA::cat* combination was synthetically lethal whereas the *dinG::kan rnhA::cat*, *uvrD::kan rnhAK60E*, and *dinG::kan rnhAK60E* strains were viable and had co-transduction frequencies similar to those observed with the *rnhA+* recipient (Table 1). Synthetic lethality of the *uvrD::kan rnhA::cat* is interesting considering recent data demonstrating that UvrD has a direct role in promoting replication fork movement past transcription collisions whereas DinG operates more indirectly and could reduce the chance of collisions (Hawkins et al., 2019).

These results indicate that the *rnhAK60E* mutation is not synthetically lethal with *rep*, *recBCD*, *recG*, *uvrD*, or *dinG* deletions (Table 1). Thus, loss of RNase HI localization conferred by the *rnhAK60E* mutation is not synonymous with a loss of RNase HI activity

TABLE 1 Co-transduction analysis to determine the synthetic lethality of helicase mutations with *rnhAK60E*

	Donor strain (relevant genotype)	Recipient strain (relevant genotype)	Results (screen/selection)
(a) Rep	SS9364 (<i>rep::kan ilv^r</i>)	CP70 (<i>rnhA⁺, cat ilv-500::Tn10</i>)	86/101 (Kan ^r /ilv ^r)
	SS9364 (<i>rep::kan ilv^r</i>)	CP60 (<i>rnhAK60E, cat ilv-500::Tn10</i>)	54/77 (Kan ^r /ilv ^r)
	SS9364 (<i>rep::kan ilv^r</i>)	SS9180 (<i>rnhA::cat ilv-500::Tn10</i>)	0/57 (Kan ^r /ilv ^r)
	CP165 (<i>rnhA::cat zae502::Tn10</i>)	CP65 (<i>rnhA⁺</i>)	17/56 (Cm ^r /Tc ^r)
	CP165 (<i>rnhA::cat zae502::Tn10</i>)	CP84 (<i>rep::kan</i>)	21/54 (Cm ^r /Tc ^r)
(b) RecBCD	SS6046 (<i>recBCD::cat proA⁺</i>)	JC13509 (<i>rnhA⁺ proA-</i>)	30/30 (Cm ^r /proA ⁺)
	SS6046 (<i>recBCD::cat proA⁺</i>)	CP62 (<i>rnhAK60E proA::kan</i>)	28/30 (Cm ^r /proA ⁺)
	SS6046 (<i>recBCD::cat proA⁺</i>)	SS10032 (<i>rnhA::cat del(proA)kan</i>)	0/41 (UV ^S /proA ⁺) ^a
	SS10032 (<i>rnhA::cat del(proA)kan</i>)	JC13509 (<i>rnhA⁺</i>)	6/46 (Cm ^r /Kan ^r)
	SS10032 (<i>rnhA::cat del(proA)kan</i>)	SS7329 (<i>recB270(ts) recC271(ts)</i>)	0/42 (Cm ^r /Kan ^r) ^b
(c) RecG	CP79 (<i>recG(kan ins) zic-4901::Tn10</i>)	CP63 (<i>rnhA⁺, cat</i>)	52/54 (Kan ^r /Tc ^r)
	CP79 (<i>recG(kan ins) zic-4901::Tn10</i>)	CP54 (<i>rnhAK60E, cat</i>)	44/54 (Kan ^r /Tc ^r)
	CP79 (<i>recG(kan ins) zic-4901::Tn10</i>)	CP154 (<i>rnhA::cat</i>)	0/53 (Kan ^r /Tc ^r)
	CP165 (<i>rnhA::cat zae502::Tn10</i>)	CP64 (<i>recG(kan ins)</i>)	0/12 (Cm ^r /Tet ^r)
(d) UvrD	CP95 (<i>uvrD::kan fadAB101::Tn10</i>)	CP63 (<i>rnhA⁺, cat</i>)	23/103 (Kan ^r /Tc ^r)
	CP95 (<i>uvrD::kan fadAB101::Tn10</i>)	CP54 (<i>rnhAK60E, cat</i>)	27/103 (Kan ^r /Tc ^r)
	CP95 (<i>uvrD::kan fadAB101::Tn10</i>)	SS1651 (<i>rnhA339::cat</i>)	0/104 (Kan ^r /Tc ^r)
	CP165 (<i>rnhA::cat zae502::Tn10</i>)	CP88 (<i>uvrD::kan</i>)	0/58 (Cm ^r /Tc ^r)
(e) DinG	CP96 (<i>dinG::kan zbi-29::Tn10</i>)	CP63 (<i>rnhA⁺, cat</i>)	23/31 (Kan ^r /Tc ^r)
	CP96 (<i>dinG::kan zbi-29::Tn10</i>)	CP54 (<i>rnhAK60E, cat</i>)	27/44 (Kan ^r /Tc ^r)
	CP96 (<i>dinG::kan zbi-29::Tn10</i>)	CP154 (<i>rnhA::cat</i>)	30/48 (Kan ^r /Tc ^r)

^aPCR to confirm *rnhA* locus and test *recBCD* genotype with UV sensitivity.

^bSelection at 30°C, screen at 42°C.

when combined with mutations in DNA replication and repair helicases. Nonetheless, the viability of the *rnhAK60E* variant in these helicase mutant strains allowed us to probe the role of the RNase HI/SSB interaction under other cellular conditions.

2.4 | The *rnhAK60E rep::kan* strain is sensitive to rich medium and is induced for SOS

Although the co-transduction experiments did not reveal synthetic lethal combinations between *rnhAK60E* and several different DNA repair gene deletions, a media-dependent growth defect was detected specifically with the *rnhAK60E rep::kan* strain (Figure 2). The *rnhAK60E rep::kan* strain plated with the same efficiency as wild-type, *rnhAK60E*, or *rep::kan* strains on minimal medium (normalized to OD₆₀₀ (CFU/ml/OD)) but the double mutant has an approximately 10-fold reduced plating efficiency on LB after 24 hr relative to the other strains (Figure 2). The lower plating efficiency on LB improves somewhat after 48 hr, indicating that the phenotype is due to slow growth rather than cell death (Figure 2). Interestingly, the slow growth defect of *rnhAK60E rep::kan* cells is not obvious in liquid growth curves (Figure S2). Slow growth was unique to the *rnhAK60E rep::kan* strain since the other strains that were synthetic lethal with *rnhA::cat* (*uvrD::kan*, *recG::kan*, *recBCD::cat*) plated with indistinguishable efficiencies on minimal and LB plates with the *rnhAK60E* mutation (Figure S5).

With the increased frequency of DNA replication and other stresses that arise in rich nutrient conditions, rich medium-dependent growth defects can be indicative of dysfunctional genome maintenance pathways (Boubakri *et al.*, 2010; Srivatsan *et al.*, 2010). Such problems can also lead to an increase in DNA damage that induces the SOS response, a survival mechanism used by *E. coli* to regulate the expression of DNA repair genes (Walker *et al.*, 2000; Michel, 2005; Janion, 2008). To test whether loss of RNase HI replication fork localization and/or Rep helicase activity induces the SOS response in *E. coli*, the strains were transformed with a reporter plasmid that has a *recN* promoter–GFP fusion (Chen *et al.*, 2015) and GFP levels were measured during exponential growth. *recN* is among the first group of genes to be induced during SOS, making its expression an indicator of SOS status (Finch *et al.*, 1985; Rostas *et al.*, 1987).

The SOS level of the *rnhAK60E* strain was indistinguishable from wild-type cells in minimal and rich media whereas the *rep::kan* strain had ~3.5-fold higher GFP levels in both minimal and rich media (Figure 3a). Interestingly, combining the *rnhAK60E* and *rep::kan* mutations resulted in the same GFP levels as the *rep::kan* strain in minimal medium but the GFP levels were 3.3-fold higher than *rep::kan* in rich medium. The rich medium-specific increase in SOS response for *rnhAK60E rep::kan* cells correlates with reduced plating efficiency for the strain on LB.

Cell morphologies of the strains were examined to determine whether they demonstrated signs of cell filamentation, a phenotypic consequence for the SOS response. *rnhAK60E* and *rep::kan* cells had lengths that were similar to wild-type *E. coli*; however, the *rnhAK60E rep::kan* cells were more frequently filamented (Figure 3b,c). In

minimal medium, *rnhAK60E rep::kan* cells were slightly elongated in comparison to wild-type cells whereas growth in rich medium led to much more extreme cell filamentation (*p* value < .001) (Figure 3b,c). These data show that abrogation of SSB-mediated RNase HI localization to the replication fork along with a loss of Rep helicase activity leads to an increase in DNA damage stress.

2.5 | The *rnhAK60E rep::kan* phenotype is related to transcription-dependent R-loop removal

RNase HI can remove transcription-dependent R-loops and the Rep helicase helps the replication fork progress through protein obstacles including stalled transcription complexes (Kogoma, 1978; Itoh and Tomizawa, 1980; von Meyenburg *et al.*, 1987; Guy *et al.*, 2009; Boubakri *et al.*, 2010). With the result that RNase HI is localized to the replication fork through interaction with SSB, it is possible that RNase HI and Rep collaborate to promote replisome progression when faced with R-loops and transcription complexes (Drolet *et al.*, 1995; Hraiky *et al.*, 2000; Boubakri *et al.*, 2010; Dutta *et al.*, 2011; McGlynn *et al.*, 2012). To further test this hypothesis, we examined whether changes in RNAP activity impact the growth phenotype of *rnhAK60E rep::kan* cells. Two RNAP β subunit mutations were chosen for the analysis: *rpoB2* is defective in termination whereas *rpoB8* has a slower elongation rate than wild type and is prone to termination (Jin *et al.*, 1988; 1992). A previous study showed that combining an *rnhA* deletion with *rpoB2* leads to a plating defect on rich medium and elevated SOS whereas combining an *rnhA* deletion with *rpoB8* reduces SOS levels (Kogoma, 1994). These effects are thought to arise from *rpoB2* and *rpoB8* mutant RNAPs generating more or fewer R-loops, respectively, than wild-type RNAP, and with the abundant R-loops in the *rpoB2 rnhA*-cells acting as barriers that slow replication (Kogoma, 1994).

Consistent with the model for synergy between RNAP and RNase HI/Rep, a *rnhAK60E rep::kan rpoB2* strain had a worsened plating efficiency relative to *rnhAK60E rep::kan* cells on both LB and minimal media plates (Figure 4). Even after a 48-hr incubation period the *rnhAK60E rep::kan rpoB2* CFUs on LB did not increase (Figure 4). In contrast, the *rnhAK60E rep::kan rpoB8* strain had the same plating efficiency as wild-type cells on minimal medium and LB, indicating that the *rpoB8* mutation suppressed LB growth sensitivity in *rnhAK60E rep::kan* cells. When either *rnhAK60E* or *rep::kan* were combined individually with the *rpoB* point mutations there were no significant changes in the plating efficiency relative to *rpoB2* or *rpoB8* cells (Figure S6). These data demonstrate that an RNAP variant that is thought to produce high levels of R-loops exacerbates the impact of losing RNase HI localization and Rep helicase activity whereas an RNAP variant that reduces cellular R-loop levels counteracts the mutations.

3 | DISCUSSION

E. coli RNase HI forms a direct interaction with SSB that stimulates RNase HI enzymatic activity in vitro (Petzold *et al.*, 2015). In this

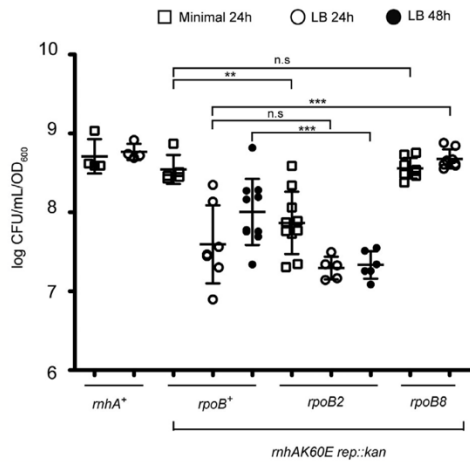


FIGURE 4 The plating efficiency of *rnhAK60E rep::kan rpoB* mutants on minimal and rich media. The CFU/ml of each strain (normalized to OD_{600}) is plotted from overnight cultures diluted and plated on minimal (squares) or LB (circles) media. Colonies were quantitated after growth at 37°C for 24 or 48 hr. Each symbol is a single culture and the mean CFU/ml for each strain is represented by a black line. The strains are CP65, CP86, CP119, and CP124 from left to right. The error bars indicate the standard deviation. Significant difference levels (p values) were determined between *rnhAK60E rep::kan* strains \pm *rpoB* mutants grown in the same medium using two-tailed t -test. * = p value < .05; ** = p value < .005; *** = p value < .0005; n.s. = p value > .05

report, the cellular roles of the RNase HI/SSB interaction have been examined. An *E. coli* RNase HI fluorescent fusion protein forms foci in cells whereas an enzymatically active variant that cannot interact with SSB (RNase HI K60E) does not form foci. RNase HI foci colocalize with a component of the replisome, consistent with SSB-dependent accumulation of the enzyme at DNA replication sites in *E. coli*. The RNase HI K60E variant supported RNase HI-mediated suppression of cSDR and lagging-strand RNA primer degradation,

indicating that localization was not required for these cellular functions. In contrast, cells encoding RNase HI K60E displayed a media-dependent plating defect and an activated SOS response when the gene encoding the Rep DNA helicase was deleted. This phenotype was linked to a deficiency in resolving transcription-derived R-loops by examining the effects of RNAP mutations that alter R-loop levels (Jin *et al.*, 1988; 1992) on *rnhAK60E rep::kan* cells. Adding *rpoB2*, which is thought to increase the abundance of R-loops (Kogoma, 1994), further increased the plating defect of *rnhAK60E rep::kan* cells whereas adding *rpoB8*, which is thought to decrease R-loop abundance, suppressed the growth phenotype. These results support a model in which SSB-dependent replication fork localization of RNase HI assists in replication progression through transcription-derived R-loops.

Roles for RNase HI in resolving replication/transcription conflicts have been proposed, but the precise mechanisms that allow RNase HI to target specific R-loop challenges to replication fork progression have not been defined (Drolet *et al.*, 1995; Hraiky *et al.*, 2000; Li and Manley, 2005; Tuduri *et al.*, 2009; El Hage *et al.*, 2010; Gan *et al.*, 2011; Dutta *et al.*, 2011; Houliard *et al.*, 2011; Wahba *et al.*, 2011). Our results support a model in which binding to SSB recruits RNase HI to sites of replication in *E. coli*, which positions the enzyme to degrade R-loop impediment. Several other cellular factors that resolve R-loop/RNAP blockages similarly rely on protein interactions for recruitment to their site of action to mediate replication progress. These include Rep, DinG, and UvrD helicases in *E. coli*, that directly associate with RNAP or with replication fork-bound proteins (Trautinger *et al.*, 2005; Baharoglu *et al.*, 2010; Boubakri *et al.*, 2010; Proshkin *et al.*, 2010; Tehranchi *et al.*, 2010; Dutta *et al.*, 2011; Washburn and Gottesman, 2011). Rep is localized to sites of replication by interaction with the replicative DnaB helicase and DinG binds to SSB (Guy *et al.*, 2009; Boubakri *et al.*, 2010; Atkinson, Gupta, & McGlynn, 2011a; Atkinson *et al.*, 2011b; Cheng *et al.*, 2012; Syeda *et al.*, 2019). UvrD associates with RNAP, which may aid in its removal of stalled transcription complexes or resolution of replication/transcription conflicts through other mechanisms (Epshtein *et al.*, 2014; Kamarthapu *et al.*, 2016; Sanders *et al.*, 2017; Hawkins *et al.*, 2019).

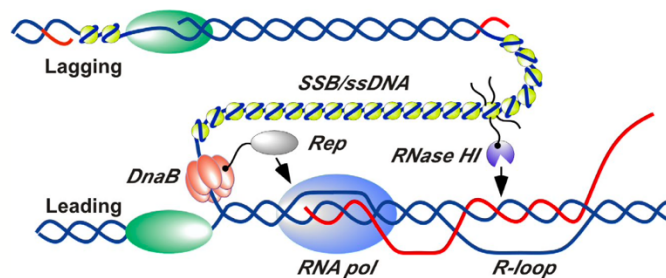


FIGURE 5 Schematic model for RNase HI and Rep helicase localization and action at sites of replication/transcription collision. RNase HI (purple) is localized to the DNA replication fork by interaction with SSB (yellow). Rep helicase (gray) is localized by interaction with DnaB (orange). SSB-Ct tails are shown explicitly for only one SSB tetramer for clarity. DNA strands are shown in blue, RNA strands are shown in red, and DNA polymerases are shown in green. Several replisome components have been omitted or separated for clarity

Our results show that simultaneous mislocalization of RNase HI and loss of Rep helicase result in defects in *E. coli* growth that are dependent on R-loop production by RNAP. Interestingly, full deletion of *rnhA* and *uvrD* is synthetically lethal as well (Table 1), but, unlike the situation with Rep, RNase HI mislocalization in the *rnhAK60E* mutant did not result in a measurable phenotype when coupled with a *uvrD* deletion (Table 1 and Figure 2). Furthermore, *dinG* was able to be deleted from an *rnhA*-deleted strain, consistent with a recent study suggesting that DinG may act less directly to resolve replication/transcription conflicts (Hawkins *et al.*, 2019). Our results suggest that RNase HI functions synergistically with Rep, and likely UvrD to a lesser extent, to promote genome duplication through R-loop-dependent fork obstacles.

How might SSB-mediated RNase HI localization help to remove R-loop obstacles to the replication fork? In *E. coli*, the lagging-strand template is exposed as ~1-2-kb-long ssDNA segments at replication forks. SSB binding to this ssDNA positions numerous SSB molecules at each site of DNA replication (Figure 5). Since each SSB tetramer has four SSB-Ct protein interaction sites, the SSB/ssDNA structures at replication forks offer abundant binding sites for partner proteins at each fork. As has been shown here, RNase HI forms foci at replication sites in a manner that requires interaction with SSB (Figure 1); several other SSB protein partners localize to the replication fork in the same manner (Sun and Godson, 1996; Glover and McHenry, 1998; Marceau *et al.*, 2011; Wessel *et al.*, 2013; Bhattacharyya *et al.*, 2014). Thus, the interaction poises RNase HI at replication forks to concentrate its nuclease activity to loci adjacent to the advancing fork. Our data collectively support a model in which this localization allows RNase HI to hydrolyze R-loops encountered ahead of the replication fork to aid in clearing RNAP complexes that would otherwise impede replication progression. With its noted roles in clearing RNAP (Guy *et al.*, 2009; Boubakri *et al.*, 2010), Rep helicase appears to cooperate with RNase HI in this activity.

We note that SSB might also coat the exposed DNA strands of R-loops and that such an arrangement could also assist with recruiting RNase HI to R-loops. Since this would also impact cSDR and no deficiency in RNase HI inhibition of cSDR was detected with the RNase HI K60E variant, this recruitment strategy does not appear to be as important as the localization to replication forks for resolving replication/transcription conflicts.

The observations described here highlight parallels between bacterial RNase HI and human RNase H1 noted in recent studies. Human RNase H1 directly interacts with Replication Protein A, the functional equivalent of bacterial SSB, forming a complex that stimulates the activity of RNase H1 *in vitro* and that is critical for suppression of R-loop forming *in vivo* (Nguyen *et al.*, 2017). Additionally, depletion of human RNase H1 leads to an accumulation of R-loops, slowed replication fork progression, and increased DNA damage (Parajuli *et al.*, 2017). It therefore appears that SSB-mediated RNase HI localization is a general phenomenon that cells have adapted to facilitate progression through R-loop challenges to replication processes in both bacterial and eukaryotic cells.

4 | EXPERIMENTAL PROCEDURES

4.1 | Bacterial strains and growth

All bacterial strains are derivatives of *E. coli* K12 and are described in Table S1. Mutations were introduced into the strain of interest by P1 transduction (Willetts *et al.*, 1969). P1 transductions were selected on 2% agar plates made with Luria broth (LB) or 56/2 minimal medium (Willetts *et al.*, 1969). M9 was supplemented with glycerol (final concentration 0.2%); 100 µg/ml of amino acids threonine, leucine, proline, histidine, and arginine; and thiamine (0.5 µg/ml). Ampicillin (10 µg/ml), tetracycline (10 µg/ml), kanamycin (50 µg/ml), chloramphenicol (25 µg/ml; 12.5 µg/ml for electroporation selection), and rifampicin (50 µg/ml) were added when required. Mutations were confirmed after new strain generations by colony PCR and sequencing.

4.2 | Strain preparation

General procedure for constructing the *rnhAK60E* chromosomal point mutation followed the λ-Red recombination method (Datsenko and Wanner, 2000). The *rnhA* gene was placed onto a pET15b with a 10-nt gap and Cm^r cassette on the 3' to generate the following product: pET15b-*rnhA*-10nt - FRT-cat- FRT. The pET15b-*rnhA* plasmid was used as a template for site-directed mutagenesis as previously described to make the K60E point mutation (Petzold *et al.*, 2015). In addition to the point mutation a restriction site polymorphism (XhoI) was inserted adjacent to K60E to allow for screening of the allele. Electrocompetent BW25113 cells with pKD46 (Datsenko and Wanner, 2000) were used to electroporate the *rnhA-cat* and *rnhAK60E-cat* DNA fragments. Cells that had incorporated the DNA were selected on LB with 12.5 µg/ml chloramphenicol (LB + Cm). Colonies were purified on LB + Cm and colony PCR was performed on Cm^r transformants to confirm the incorporation of Cm^r cassette. For cells transformed with *rnhAK60E-cat* a restriction digest with XhoI was also used to check for the point mutation. Cells with the correct product size were sequenced at the *rnhA* locus by colony PCR. P1 lysates were prepared from *rnhA-cat* and *rnhAK60E-cat* cells and introduced into JC13509 selecting for Cm^r. The protocol for P1 transduction has been described previously (Willetts *et al.*, 1969). The Cm^r transductants were again sequenced to confirm the *rnhA* genotype. The protocol for removing Cm^r was performed as described in Datsenko and Wanner (2000).

All strains used for microscopy are AB1157 derivatives. Strain carrying a wild-type copy of RNase HI fused to YPet (RRL327) or mNeonGreen (VV14) was generated through lambda red recombination as previously described (Reyes-Lamothe *et al.*, 2008). Briefly, primers L_rnhA_F (ccgcgcgatgaatccacactggaatacag-gctaccaagttgaagttTCGGCTG GCTCCGCTGCTGG) and L_rnhA_R (cgaattccgacggcgttgagccaccggcaatgtcgtaaacc acaggcTTATG AATATCCTCCTTAG) were used to amplify *ypet* and *kan^R* from

the plasmid pROD61 or *mneongreen* and *kan^R* from the plasmid pVV04. Integration into the chromosome was done using plasmid pKD46, which expresses the lambda red genes under the control of arabinose (Datsenko and Wanner, 2000). The strain carrying the *rhAK60E* allele fused to *ypet* (VV8) was generated by cloning *rhA-ypet kan* with ~500 bp of flanking regions at either side, amplified from RRL327, into a plasmid carrying an R6K gamma origin using primers *rhA_seqF5* (TTTAGACGTCGGCTATCGGTGACCTTACAG) and *rhA_seqR3* (ATCAAGTGAATGTTTCTGCGC) (resulting in pVV10). Cloning was done using an AatII site at one end and TA cloning at the other end, and ligated into a fragment containing the R6K gamma origin amplified from pKD4 (Datsenko and Wanner, 2000). The point mutation was introduced by Quick Change mutagenesis using primers *rhA_K3EF* (GCGCTGGAGGCGTTAGAAGAACATTGCGAAGTC) and *rhA_K3ER* (GACTTCGCAATGTTCTTCTAACGCCCTCCAGCGC). The resulting *rhAK60E-ypet kan* was introduced in the chromosome, replacing the wild-type copy, using primers *rhA_seqF3* (GGCTATCGGTGACCTTACAG) and *rhA_seqR3*.

The *mcherry-dnaN* fusion (RRL355) was constructed by lambda red using primers *dnaN-NF* (TATCAAAGAAGATTTTCA AATTTAATCAGAACATTGTCTATCGTAAACCTGTAGGCTGGAG CTGCTTCG) and *dnaN-NR* (ACCTGTTGTAGCGGTTTTAATAA ATGCTCACGTTCTAC GGTAATTTTCATCGCGCTGCCAGAACC AGC) and pROD84 as a template, carrying a *kan^R* *mcherry* followed by an 11-amino acid linker. The kanamycin cassette was removed by FLP recombinase expression from pCP20 (Datsenko and Wanner, 2000) resulting in strain RRL388. Fluorescent *rhA-ypet kan^R* fusion was moved into the strain carrying RRL388 by P1 transduction (resulting in strain VV11).

4.3 | Growth curves

Strains were inoculated from single colonies in overnight liquid cultures of 56/2 minimal media with antibiotic where relevant (Willets et al., 1969). After growth at 37°C for 16 hr, overnight cultures were used to inoculate 25 ml of LB or 56/2 minimal media (100-fold dilution). OD₆₀₀ was taken at t = 0 and at subsequent 30-minute time points until several time points at stationary phase were reached. Time points from three independent experiments were plotted with standard deviation using GraphPad Prism.

4.4 | CFU/ml/OD₆₀₀ determination

Strains were inoculated from single colonies in overnight liquid cultures of 56/2 minimal medium with antibiotics when relevant (Willets et al., 1969). After growth at 37°C for 16 hr the OD₆₀₀ of overnight cultures was taken. Cultures were serially diluted in sterile saline and 10 µl of the appropriate dilution was plated on LB or 56/2 minimal media. Colony counts were performed after the plates were

incubated at 37°C for 24 and 48 hr. CFU/ml/OD₆₀₀ values were determined by the following equation: [(dilution factor/volume plated) × colony count]/OD₆₀₀. CFU/ml/OD₆₀₀ values were accumulated for at least three independent cultures and plotted with standard deviation using GraphPad Prism.

4.5 | Phase contrast microscopy

Strains were inoculated from single colonies in overnight liquid cultures of 56/2 minimal medium with 100 µg/ml ampicillin (Willets et al., 1969). After growth at 37°C for 16 hr the overnight cultures were diluted 100-fold in 56/2 minimal medium or LB with ampicillin. 4 µl of cells was spotted on fresh 2% agarose pads (1XPBS) and covered with a coverslip. Cells were imaged at 25°C using an inverted Nikon Eclipse Ti microscope equipped with a Photometrics CoolSNAP HQ2 charge-coupled-device (CCD) camera (Photometrics, Tucson, AZ). Images were acquired using a ×100 oil objective (Nikon Plan Apo 100/1.40 oil Ph3 DM) and the Nikon Instruments Software (NIS)-Elements Advanced Research (AR) microscope imaging software program (Version 4.000.07) (Nikon, Melville, NY). Data were collected on the EMCCD using an exposure time of 50 ms. Data from at least 200 cells from three independent cultures were collected and analyzed using MicrobeTracker to determine average cell length for each strain in minimal and rich media (Sliusarenko et al., 2011).

4.6 | Fluorescence microscopy

Imaging was performed at room temperature on an inverted Olympus IX83 microscope using a 100× oil objective lens (Olympus Plan Apo 100X NA 1.40 oil). Images were captured using an Andor Zyla 4.2 sCMOS camera. Z-stacks were done using a NanoScanZ piezo by Prior Scientific. Excitation was done from an iChrome Multi-Laser Engine (405 nm 100 mW, 488 nm 100 mW, 561 nm 100 mW, and 640 nm 70 mW) from Topica Photonics and a 405/488/561/640 nm filter set (Chroma). Laser triggering was done through a real-time controller U-RTCE (Olympus). Experiments were done from a single-line cellTIRF illuminator (Olympus). Olympus CellSens 2.1 imaging software was used to control the microscope and lasers.

Before imaging cells were grown in LB for at least 5 hr then transferred to M9-Glycerol medium via a 1:1,000 dilution. After being grown overnight cells were diluted again in M9-Glycerol and grown to an OD₆₀₀ between 0.1 and 0.2. Cells were spotted on a 1% agarose pad in M9-Glycerol. Imaging of YPet strains was done capturing for 500 ms with 15% laser power (488 nm laser), while imaging of mCherry was done using 500 ms with 13% laser power (561 nm laser). At each field of view a z-stack of 32 pictures with a 100-nm step size was taken using bright-field illumination, which was later used for segmentation.

4.7 | Spot counting and colocalization analysis

All analyses were done using custom scripts written in MATLAB (Mathworks). A 32-frame bright-field Z-stacks was compressed to create a black and white phase contrast image for cell segmentation (Julou *et al.*, 2013). Cells were segmented using SuperSegger software (Stylianidou *et al.*, 2016). Spots were counted using a modified version of the previously developed tracking software (Uphoff *et al.*, 2013). Spots were determined using an intensity threshold then further processed using a 2D elliptical Gaussian fit. The extracted fitted parameters were x-position, y-position, x-standard deviation, y-standard deviation, intensity, and background. Co-localization analysis was done by measuring the distance between the positions of ribonuclease HI-YPet to the β -clamp-mCherry in two-color experiments. If cells had multiple foci of the same protein, then the smallest distance was recorded, and the 2 spots measured removed so their positions would not be used again in further calculations.

Colocalization was characterized using radial distribution analysis (Zawadzki *et al.*, 2015; Thrall *et al.*, 2017). The radial distribution function $g(r)$ displays the increased likelihood of ribonuclease HI-YPet at a distance r from a mCherry- β -clamp focus relative to random cellular localization. This measurement incorporates the cell shape and size of the cells analyzed in the colocalization analysis. An equivalent number of random localizations were generated within the cell outline and the distance between them and the position of a β -clamp-mCherry focus (obtained from the data for a particular cell in the analysis) measured. We also measured the distance between two randomly generated localizations in the cell. This procedure was repeated for each cell. To account for variability, we simulated the single-protein random localization and two-protein random localization distributions 100 times. We then normalized the average number of simulated localizations per bin by the number of cells to determine the probability to be found in a certain bin, obtaining the single random spot distance distribution and the two random spot distance distributions. We followed the same normalization for the measured data to obtain the measured distance distributions. Histograms were generated for the measured and random distance distributions. Numbers for individual bins in the distribution of the experimental data were divided by the number in the corresponding bins for the one random spot distribution to give $g(r)$. A $g(r)$ value of 1 indicates no enrichment relative to a random distribution. We also divided the double random spot distribution by the single random spot distribution as a control.

4.8 | Single-molecule intensity and copy number analysis

Imaging was performed at room temperature on an inverted Nikon Ti2 microscope using a 100 \times oil objective lens (CFI APO 100 \times oil TIRF NA 1.49). Images were captured using an Andor iXon EM + DU-897 EMCCD camera. Excitation was done from an OBIS 514 nm

LX 50 mW laser delivered from an OBIS Galaxy laser beam combiner (Coherent) and a zet405/514/561x custom triple excitation set (Chroma). Laser triggering was done through a real-time controller NI DAQ (National Instruments). Experiments were done using HiLo illumination setup (Tokunaga *et al.*, 2008) from a custom-made TIRF setup. Molecular Devices MetaMorph imaging software was used to control the microscope and lasers. Videos for each strain included 500 frames. Image capture was done using continuous acquisition at 10-ms frame rate (100% 515-nm laser).

Initial spot positions were manually selected using the coordinates for localized bleaching in the image recorded by the acquisition software. Tracking was then done automatically using a previously developed custom program in MATLAB (Mathworks), ADEMS code (Miller *et al.*, 2015) (freely available at <https://sourceforge.net/projects/york-biophysics/>). This program generated individual intensity traces. The change point detection algorithm, *ischange*, a built-in function in MATLAB, was then used to find abrupt changes in the spot intensity and to determine the intensity change in the last step during bleaching (representing a single molecule). The maximum numbers of steps was restricted to 10. The intensity of the last step was used as the single-molecule intensity.

An average frame projection of the videos was used to manually create single-cell outlines. Individual cells were identified along with the cell lengths in pixels, the area in pixels, and the total cell intensities for only the first frame of each video. To remove the endogenous cell background from our copy number calculations, the average pixel intensity was determined in AB1157 untagged cells. The single-pixel background intensity was multiplied by the area of each individual cell and this total background intensity was removed from the total cell intensities. This provided the total intensity of our fluorescent protein per cell. This total intensity was divided by the single-molecule intensity to give the copy number.

To determine the bound proportion, the cell background from our AB1157 measurements and the mean cell intensity for one pixel of the protein in question were removed from the first frame intensity from the single-molecule intensity analysis to get the intensity of each spot. The intensity was divided by our single-molecule intensity data to get the number of molecules bound. Finally, this number was divided by the protein copy number to get the bound proportion.

4.9 | SOS response assay

Strains were transformed with pEAW903, a pET21a plasmid with SuperGlo GFP (Qbiogene), under the control of the *E. coli recN* promoter (Ronayne *et al.*, 2016). Strains were grown overnight in M63 minimal medium +0.4% glucose supplemented with 0.2% casamino acids and ampicillin (Elbing and Brent, 2001). Overnight cultures were diluted to OD₆₀₀ 0.05 in minimal medium or LB with ampicillin and 200 μ l was added to the wells (in triplicate) of a 96-well black-side clear-bottom plate (Corning). A BioTek Synergy 2 plate reader was used for taking OD₆₀₀ and fluorescence reads

(excitation 485 nm/emission 528 nm) during the growth curve. The plate was maintained at 37°C with shaking set to "slow-continuously" and an optical adhesive cover (Applied Biosystems). Once log phase was reached, the protocol was stopped and 10 µl of cells was used for serial dilution and determining CFU/ml values. The plate was immediately returned to the plate reader and a new protocol was started to capture the growth curve through the stationary phase.

4.10 | P1 co-transduction frequency

All transductions were performed as described (Willets *et al.*, 1969). Transductions were plated on a 56/2 minimal medium with the selection markers noted in Table 1. Transductants were grown at 37°C (unless otherwise noted) and purified on the same type of media on which they were selected. Purified transductants were then patch plated on 56/2 or LB (corresponding to initial media used for selection) and grown at 37°C. Patch plates were then used for replica plating to screen for co-transduction of experimental mutation with the selectable marker. Screening for *recBCD* genotype was done using UV sensitivity. Replicate plates were exposed to UV using a Spectrolinker XL-1000 UV crosslinker (Spectronics Corp.) and plates were kept in the dark until analyzed. Co-transduction frequencies are scored out of total transductants confirmed to have the initial selection marker and genotype of recipient strain after replica plating.

ACKNOWLEDGMENTS

We thank Dr. Jeremy Schroeder and members of the Keck, Reyes-Lamothe, and Sandler laboratories for critical evaluation of the manuscript. This work was supported by a National Institutes of Health grant to JLK and SJS (R01 GM098885) and by a National Science Foundation Graduate Research Fellowship Program to CW (DGE-1256259).

AUTHOR CONTRIBUTIONS

CW and SJS performed strain preparation, genetic experiments, growth experiments, SOS assays, and phase contrast microscopy. HJM, NS, and RRL performed fluorescence microscopy experiments and the associated strain preparation. CW, RRL, SJS, and JLK conceived of experiments. CW, RRL, HJM, NS, SJS, and JLK wrote the manuscript.

DATA AVAILABILITY STATEMENT

The data that support the findings of this study are available from the corresponding author upon reasonable request.

REFERENCES

Aguilera, A. and Garcia-Muse, T. (2012) R loops: from transcription by-products to threats to genome stability. *Molecular Cell*, *46*(2), 115–124.
 Alberts, B.M. (1987) Prokaryotic DNA replication mechanisms. *Philosophical Transactions of the Royal Society of London. Series B, Biological Sciences*, *317*, 395–420.

Atkinson, J., Gupta, M.K. and McGlynn, P. (2011a) Interaction of rep and DnaB on DNA. *Nucleic Acids Research*, *39*(4), 1351–1359.
 Atkinson, J., Gupta, M.K., Rudolph, C.J., Bell, H., Lloyd, R.G. and McGlynn, P. (2011b) Localization of an accessory helicase at the replisome is critical in sustaining efficient genome duplication. *Nucleic Acids Research*, *39*(3), 949–957.
 Azvolinsky, A., Giresi, P.G., Lieb, J.D. and Zakian, V.A. (2009) Highly transcribed RNA polymerase II genes are impediments to replication fork progression in *Saccharomyces cerevisiae*. *Molecular Cell*, *34*(6), 722–734.
 Baharoglu, Z., Lestini, R., Duigou, S. and Michel, B. (2010) RNA polymerase mutations that facilitate replication progression in the rep *uvrD recF* mutant lacking two accessory replicative helicases. *Molecular Microbiology*, *77*(2), 324–336.
 Benthikou, E., Chagneau, C., Long, E., Allemant, J.F. and Michel, B. (2015) Are the SSB-interacting proteins *reco*, *RecG*, *PriA* and the DnaB-interacting protein *rep* bound to progressing replication forks in *Escherichia coli*. *PLoS One*, *10*(8), e0134892
 Bhattacharyya, B., George, N.P., Thurmes, T.M., Zhou, R., Jani, N., Wessel, S.R., *et al.* (2014) Structural mechanisms of PriA-mediated DNA replication restart. *Proceedings of the National Academy of Sciences of the United States of America*, *111*(4), 1373–1378.
 Boubakri, H., de Septenville, A.L., Viguera, E. and Michel, B. (2010) The helicases *DinG*, *Rep* and *UvrD* cooperate to promote replication across transcription units *in vivo*. *The EMBO Journal*, *29*(1), 145–157.
 Carr, K.M. and Kaguni, J.M. (1996) The A184V missense mutation of the *dnaA5* and *dnaA46* alleles confers a defect in ATP binding and thermostability in initiation of *Escherichia coli* DNA replication. *Molecular Microbiology*, *20*, 1307–1318.
 Chandler, M., Bird, R.E. and Caro, L. (1975) The replication time of the *Escherichia coli* K12 chromosome as a function of cell doubling time. *Journal of Molecular Biology*, *94*(1), 127–132.
 Chen, S.H., Byrne, R.T., Wood, E.A. and Cox, M.M. (2015) *Escherichia coli* *radD* (*yejH*) gene: a novel function involved in radiation resistance and double-strand break repair. *Molecular Microbiology*, *95*(January), 754–768.
 Cheng, Z., Caillet, A., Ren, B. and Ding, H. (2012) Stimulation of *Escherichia coli* DNA damage inducible DNA helicase *DinG* by the single-stranded DNA binding protein SSB. *FEBS Letters*, *586*(21), 3825–3830.
 Costes, A., Lecoite, F., McGovern, S., Quevillon-Cheruel, S. and Polard, P. (2010) The C-terminal domain of the bacterial SSB protein acts as a DNA maintenance hub at active chromosome replication forks. *PLoS Genetics*, *6*(12), e1001238.
 Crouch, R.J. (1990) Ribonuclease H: from discovery to 3D structure. *New Biology*, *2*(9), 771–777.
 Datsenko, K.A. and Wanner, B.L. (2000) One-step inactivation of chromosomal genes in *Escherichia coli* K-12 using PCR products. *Proceedings of the National Academy of Sciences of the United States of America*, *97*(12), 6640–6645.
 de Massy, B., Fayet, O. and Kogoma, T. (1984) Multiple origin usage for DNA replication in *sdrA*(*rnh*) mutants of *Escherichia coli* K-12. Initiation in the absence of *oriC*. *Journal of Molecular Biology*, *178*(2), 227–236.
 Deshpande, A.M. and Newlon, C.S. (1996) DNA replication fork pause sites dependent on transcription. *Science*, *272*(5264), 1030–1033.
 Dimude, J.U., Stockum, A., Midgley-Smith, S.L., Upton, A.L., Foster, H.A., Khan, A., *et al.* (2015) Consequences of replicating in the wrong orientation: bacterial chromosome duplication without an active replication origin. *mBio*, *6*(6), e01294–e01215.
 Drollet, M., Phoenix, P., Menzel, R., Masse, E., Liu, L.F. and Crouch, R.J. (1995) Overexpression of RNase H partially complements the growth defect of an *Escherichia coli* *delta topA* mutant: R-loop formation is a major problem in the absence of DNA topoisomerase I. *Proceedings*

- of the National Academy of Sciences of the United States of America, 92(8), 3526–3530.
- Dutta, D., Shatalin, K., Epshtein, V., Gottesman, M.E. and Nudler, E. (2011) Linking RNA polymerase backtracking to genome instability in *E. coli*. *Cell*, 146(4), 533–543.
- El Hage, A., French, S.L., Beyer, A.L. and Tollervey, D. (2010) Loss of Topoisomerase I leads to R-loop-mediated transcriptional blocks during ribosomal RNA synthesis. *Genes & Development*, 24(14), 1546–1558.
- Elbing, K. and Brent, R. (2001) Media preparation and bacteriological tools. *Current Protocols in Molecular Biology*. <https://doi.org/10.1002/0471140864.psa04as13>
- Epshtein, V., Kamarthapu, V., McGary, K., Svetlov, V., Ueberheide, B., Proshkin, S., et al. (2014) UvrD facilitates DNA repair by pulling RNA polymerase backwards. *Nature*, 505(7483), 372–377.
- Finch, P.W., Chambers, P. and Emmerson, P.T. (1985) Identification of the *Escherichia coli* *recN* gene product as a major SOS protein. *Journal of Bacteriology*, 164(2), 653–658.
- French, S. (1992) Consequences of replication fork movement through transcription units in vivo. *Science*, 258(5086), 1362–1365.
- Frey, J., Chandler, M. and Caro, L. (1981) The initiation of chromosome replication in a *dnaAts46* and a *dnaA+* strain at various temperatures. *Molecular and General Genetics*, 182(2), 364–366.
- Gan, W., Guan, Z., Liu, J., Gui, T., Shen, K., Manley, J.L., et al. (2011) R-loop-mediated genomic instability is caused by impairment of replication fork progression. *Genes and Development*, 25(19), 2041–2056.
- Glover, B.P. and McHenry, C.S. (1998) The chi psi subunits of DNA polymerase III holoenzyme bind to single-stranded DNA-binding protein (SSB) and facilitate replication of an SSB-coated template. *Journal of Biological Chemistry*, 273(36), 23476–23484.
- Guy, C.P., Atkinson, J., Gupta, M.K., Mahdi, A.A., Gwynn, E.J., Rudolph, C.J., et al. (2009) Rep provides a second motor at the replisome to promote duplication of protein-bound DNA. *Molecular Cell*, 36(4), 654–666.
- Harinarayanan, R. and Gowrishankar, J. (2003) Host factor titration by chromosomal R-loops as a mechanism for runaway plasmid replication in transcription termination-defective mutants of *Escherichia coli*. *Journal of Molecular Biology*, 332(1), 31–46.
- Hawkins, M., Dimude, J.U., Howard, J.A.L., Smith, A.J., Dillingham, M.S., Savery, N.J., et al. (2019) Direct removal of RNA polymerase barriers to replication by accessory replicative helicases. *Nucleic Acids Research*, 47(10), 5100–5113.
- Helmrich, A., Ballarino, M., Nudler, E. and Tora, L. (2013) Transcription-replication encounters, consequences and genomic instability. *Nature Structural & Molecular Biology*, 20(4), 412–418.
- Helmrich, A., Ballarino, M. and Tora, L. (2011) Collisions between replication and transcription complexes cause common fragile site instability at the longest human genes. *Molecular Cell*, 44(6), 966–977.
- Hong, X., Cadwell, G.W. and Kogoma, T. (1995) *Escherichia coli* RecG and RecA proteins in R-loop formation. *EMBO Journal*, 14(10), 2385–2392.
- Houlard, M., Artus, J., Léguillier, T., Vandormael-Pournin, S. and Cohen-Tannoudji, M. (2011) DNA-RNA hybrids contribute to the replication dependent genomic instability induced by *Omeg1* deficiency. *Cell Cycle*, 10(1), 108–117.
- Hraïky, C., Raymond, M.A. and Drolet, M. (2000) RNase H overproduction corrects a defect at the level of transcription elongation during rRNA synthesis in the absence of DNA topoisomerase I in *Escherichia coli*. *Journal of Biological Chemistry*, 275(15), 11257–11263.
- Huertas, P. and Aguilera, A. (2003) Cotranscriptionally formed DNA:RNA hybrids mediate transcription elongation impairment and transcription-associated recombination. *Molecular Cell*, 12(3), 711–721.
- Itaya, M. and Crouch, R.J. (1991a) Correlation of activity with phenotypes of *Escherichia coli* partial function mutants of *rnH*, the gene encoding RNase H. *Molecular & General Genetics*, 227(3), 433–437.
- Itaya, M. and Crouch, R.J. (1991b) A combination of RNase H (*rnH*) and *recBCD* or *sbcB* mutations in *Escherichia coli* K 12 adversely affects growth. *MGG Molecular & General Genetics*, 227, 424–432.
- Itoh, T. and Tomizawa, J. (1980) Formation of an RNA primer for initiation of replication of ColE1 DNA by ribonuclease H. *Proceedings of the National Academy of Sciences of the United States of America*, 77(5), 2450–2454.
- Janion, C. (2008) Inducible SOS response system of DNA repair and mutagenesis in *Escherichia coli*. *International Journal of Biological Sciences*, 4(6), 338–344.
- Jin, D.J., Burgess, R.R., Richardson, J.P. and Gross, C.A. (1992) Termination efficiency at rho-dependent terminators depends on kinetic coupling between RNA polymerase and rho. *Proceedings of the National Academy of Sciences of the United States of America*, 89(4), 1453–1457.
- Jin, D.J., Cashel, M., Friedman, D.I., Nakamura, Y., Walter, W.A. and Gross, C.A. (1988) Effects of Rifampicin resistant *rpoB* mutations on antitermination and interaction with *nusA* in *Escherichia coli*. *Journal of Molecular Biology*, 204(2), 247–261.
- Joyce, C.M., Fujii, D.M., Laks, H.S., Hughes, C.M. and Grindley, N.D. (1985) Genetic mapping and DNA sequence analysis of mutations in the *polA* gene of *Escherichia coli*. *Journal of Molecular Biology*, 186(2), 283–293.
- Julou, T., Mora, T., Guillon, L., Croquette, V., Schalk, I.J., Bensimon, D., et al. (2013) Cell-cell contacts confine public goods diffusion inside *Pseudomonas aeruginosa* clonal microcolonies. *Proceedings of the National Academy of Sciences of the United States of America*, 110(31), 12577–12582.
- Kamarthapu, V., Epshtein, V., Benjamin, B., Proshkin, S., Mironov, A., Cashel, M., et al. (2016) ppGpp couples transcription to DNA repair in *E. coli*. *Science*, 352(6288), 993–996.
- Kitani, T., Yoda, K., Ogawa, T. and Okazaki, T. (1985) Evidence that discontinuous DNA replication in *Escherichia coli* is primed by approximately 10 to 12 residues of RNA starting with a purine. *Journal of Molecular Biology*, 184(1), 45–52.
- Kogoma, T. (1994) *Escherichia coli* RNA polymerase mutants that enhance or diminish the SOS response constitutively expressed in the absence of RNase HI activity. *Journal of Bacteriology*, 176, 1521–1523.
- Kogoma, T. (1997) Stable DNA replication: interplay between DNA replication, homologous recombination, and transcription. *Microbiology and Molecular Biology Reviews*, 61(2), 212–238.
- Kogoma, T. (1978) A novel *Escherichia coli* mutant capable of DNA replication in the absence of protein synthesis. *Journal of Molecular Biology*, 121(1), 55–69.
- Kogoma, T., Barnard, K.G. and Hong, X. (1994) RecA, Tus protein and constitutive stable DNA replication in *Escherichia coli* *rnhA* mutants. *Molecular & General Genetics*, 244, 557–562.
- Kogoma, T., Hong, X., Cadwell, G.W., Barnard, K.G. and Asai, T. (1993) Requirement of homologous recombination functions for viability of the *Escherichia coli* cell that lacks RNase HI and exonuclease V activities. *Biochimie*, 75, 89–99.
- Kogoma, T. and von Meyenburg, K. (1983) The origin of replication, *oriC*, and the *dnaA* protein are dispensable in stable DNA replication (*sdrA*) mutants of *Escherichia coli* K-12. *The EMBO Journal*, 2(3), 463–468.
- Kornberg, A. and Baker, T.A. (1992) *DNA Replication*, 2nd edition. New York, NY: W. H. Freeman.
- Kuzminov, A. (2001) Single-strand interruptions in replicating chromosomes cause double-strand breaks. *Proceedings of the National Academy of Sciences of the United States of America*, 98(15), 8241–8246.
- Lecoïnte, F., Serena, C., Velten, M., Costes, A., McGovern, S., Meile, J.C., et al. (2007) Anticipating chromosomal replication fork arrest: SSB targets repair DNA helicases to active forks. *EMBO Journal*, 26(19), 4239–4251.
- Li, X. and Manley, J.L. (2005) Inactivation of the SR protein splicing factor ASF/SF2 results in genomic instability. *Cell*, 122(3), 365–378.

- Lindahl, G. and Lindahl, T. (1984) Initiation of DNA replication in *Escherichia coli*: RNase H-deficient mutants do not require the dnaA function. *Molecular & General Genetics*, 196(2), 283–289.
- Liu, X., Wang, X., Reyes-Lamothe, R. and Sherratt, D. (2010) Replication-directed sister chromosome alignment in *Escherichia coli*. *Molecular Microbiology*, 75(5), 1090–1097.
- Marceau, A.H. (2012) Functions of single-strand DNA-binding proteins in DNA replication, recombination, and repair. *Methods in Molecular Biology*, 922, 1–21.
- Marceau, A.H., Soon, B., Massoni, S.C., George, N.P., Sandler, S.J., Marians, K.J., et al. (2011) Structure of the SSB-DNA polymerase III interface and its role in DNA replication. *EMBO Journal*, 30, 4236–4247.
- McGlynn, P., Savery, N.J. and Dillingham, M.S. (2012) The conflict between DNA replication and transcription. *Molecular Microbiology*, 85(1), 12–20.
- Merrick, H., Zhang, Y., Grossman, A.D. and Wang, J.D. (2012) Replication-transcription conflicts in bacteria. *Nature Reviews Microbiology*, 10(7), 449–458.
- von Meyenburg, K., Boye, E., Skarstad, K., Koppes, L. and Kogoma, T. (1987) Mode of initiation of constitutive stable DNA replication in RNase H-defective mutants of *Escherichia coli* K-12. *Journal of Bacteriology*, 169(6), 2650–2658.
- Meyer, R.R. and Laine, P.S. (1990) The single-stranded DNA-binding protein of *Escherichia coli*. *Microbiological Reviews*, 54(4), 342–380.
- Michel, B. (2005) After 30 years of study, the bacterial SOS response still surprises us. *PLoS Biology*, 3(7), 1174–1176.
- Miller, H., Zhou, Z., Wollman, A.J. and Leake, M.C. (2015) Superresolution imaging of single DNA molecules using stochastic photoblinking of minor groove and intercalating dyes. *Methods*, 88, 81–88.
- Mirkin, E.V. and Mirkin, S.M. (2007) Replication fork stalling at natural impediments. *Microbiology and Molecular Biology Reviews*, 71(1), 13–35.
- Moolman, M.C., Krishnan, S.T., Kerssemakers, J.W.J., van den Berg, A., Tulinski, P., Depken, M., et al. (2014). Slow unloading leads to DNA-bound β 2-sliding clamp accumulation in live *Escherichia coli* cells. *Nature Communications*, 5, 5820.
- Nguyen, H.D., Yadav, T., Giri, S., Saez, B., Graubert, T.A. and Zou, L. (2017) Functions of replication protein A as a sensor of R loops and a regulator of RNaseH1. *Molecular Cell*, 65(5), 832–847.e4.
- O'Donnell, M., Langston, L. and Stillman, B. (2013) Principles and concepts of DNA replication in bacteria, archaea, and eukarya. *Cold Spring Harbor Perspectives in Biology*, 5(7), a010108.
- Ogawa, T. and Okazaki, T. (1980) Discontinuous DNA replication. *Annual Review of Biochemistry*, 49, 421–457.
- Ogawa, T. and Okazaki, T. (1984) Function of RNase H in DNA replication revealed by RNase H defective mutants of *Escherichia coli*. *Molecular & General Genetics*, 193(2), 231–237.
- Ogawa, T., Pickett, G.G., Kogoma, T. and Kornberg, A. (1984) RNase H confers specificity in the dnaA-dependent initiation of replication at the unique origin of the *Escherichia coli* chromosome in vivo and in vitro. *Proceedings of the National Academy of Sciences of the United States of America*, 81(4), 1040–1044.
- Parajuli, S., Teasley, D.C., Murali, B., Jackson, J., Vindigni, A. and Stewart, S.A. (2017) Human ribonuclease H1 resolves R-loops and thereby enables progression of the DNA replication fork. *Journal of Biological Chemistry*, 292(37), 15216–15224.
- Petzold, C., Marceau, A. H., Miller, K. H., Marqusee, S. and Keck, J. L. (2015) Interaction with single-stranded DNA binding protein stimulates *Escherichia coli* ribonuclease HI enzymatic activity. *Journal of Biological Chemistry*, 290(23), 14626–14636. <https://doi.org/10.1074/jbc.M115.655134>
- Pomerantz, R.T. and O'Donnell, M. (2010) What happens when replication and transcription complexes collide? *Cell Cycle*, 9(13), 2537–2543.
- Prado, F. and Aguilera, A. (2005) Impairment of replication fork progression mediates RNA polII transcription-associated recombination. *EMBO Journal*, 24(6), 1267–1276.
- Proshkin, S., Rahmouni, A.R., Mironov, A. and Nudler, E. (2010) Cooperation between translating ribosomes and RNA polymerase in transcription elongation. *Science*, 328(5977), 504–508.
- Reyes-Lamothe, R. (2012) Use of fluorescently tagged SSB proteins in vivo localization experiments. *Methods in Molecular Biology*, 922, 245–253.
- Reyes-Lamothe, R., Nicolas, E. and Sherratt, D.J. (2012) Chromosome replication and segregation in bacteria. *Annual Review of Genetics*, 46, 121–143.
- Reyes-Lamothe, R., Possoz, C., Danilova, O. and Sherratt, D.J. (2008) Independent positioning and action of *Escherichia coli* replisomes in live cells. *Cell*, 133(1), 90–102.
- Reyes-Lamothe, R., Sherratt, D.J. and Leake, M.C. (2010) Stoichiometry and architecture of active DNA replication machinery in *Escherichia coli*. *Science*, 328(5977), 498–501.
- Ronayne, E.A., Wan, Y.C.S., Boudreau, B.A., Landick, R. and Cox, M.M. (2016) P1 ref endonuclease: a molecular mechanism for phage-enhanced antibiotic lethality. *PLoS Genetics*, 12(1), e1005797.
- Rostas, K., Morton, S.J., Picksley, S.M. and Lloyd, R.G. (1987) Nucleotide sequence and LexA regulation of the *Escherichia coli* recN gene. *Nucleic Acids Research*, 15(13), 5041–5049.
- Sanders, K., Lin, C.L., Smith, A.J., Cronin, N., Fisher, G., Eftychidis, V., et al. (2017) The structure and function of an RNA polymerase interaction domain in the PcrA/UvrD helicase. *Nucleic Acids Research*, 45(7), 3875–3887.
- Sandler, S.J. (2005) Requirements for replication restart proteins during constitutive stable DNA replication in *Escherichia coli* K-12. *Genetics*, 169(4), 1799–1806.
- Sandler, S.J., Samra, H.S. and Clark, A.J. (1996) Differential suppression of priA2:kan phenotypes in *Escherichia coli* K-12 by mutations in priA, lexA, and dnaC. *Genetics*, 143(1), 5–13.
- Shaner, N.C., Lambert, G.G., Chamma, A., Ni, Y., Cranfill, P.J., Baird, M.A., et al. (2013) A bright monomeric green fluorescent protein derived from *Branchiostoma lanceolatum*. *Nature Methods*, 10(5), 407–409.
- Shereda, R.D., Kozlov, A.G., Lohman, T.M., Cox, M.M. and Keck, J.L. (2008) SSB as an organizer/mobilizer of genome maintenance complexes. *Critical Reviews in Biochemistry and Molecular Biology*, 43(5), 289–318.
- Sliusarenko, O., Heinritz, J., Emonet, T. and Jacobs-Wagner, C. (2011) High-throughput, subpixel precision analysis of bacterial morphogenesis and intracellular spatio-temporal dynamics. *Molecular Microbiology*, 80(3), 612–627.
- Soubry, N., Wang, A. and Reyes-Lamothe, R. (2019) Replisome activity slowdown after exposure to ultraviolet light in *Escherichia coli*. *Proceedings of the National Academy of Sciences of the United States of America*, 116(24), 11747–11753.
- Srivatsan, A., Tehrani, A., MacAlpine, D.M. and Wang, J.D. (2010) Co-orientation of replication and transcription preserves genome integrity. *PLoS Genetics*, 6(1), e1000810.
- Stylianiidou, S., Brennan, C., Nissen, S.B., Kuwada, N.J. and Wiggins, P.A. (2016) SuperSegger: robust image segmentation, analysis and lineage tracking of bacterial cells. *Molecular Microbiology*, 102(4), 690–700.
- Sun, W. and Godson, G.N. (1996) Interaction of *Escherichia coli* primase with a phage G4ori(c)-E. coli SSB complex. *Journal of Bacteriology*, 178(23), 6701–6705.
- Syeda, A.H., Wollman, A.J.M., Hargreaves, A.L., Howard, J.A.L., Brüning, J.-G., McGlynn, P., et al. (2019) Single-molecule live cell imaging of Rep reveals the dynamic interplay between an accessory replicative helicase and the replisome. *Nucleic Acids Research*, 47(12), 6287–6298.
- Tehrani, A.K., Blankschien, M.D., Zhang, Y., Halliday, J.A., Srivatsan, A., Peng, J., et al. (2010) The transcription factor DksA prevents conflicts between DNA replication and transcription machinery. *Cell*, 141(4), 595–605.

- Thrall, E.S., Kath, J.E., Chang, S. and Loparo, J.J. (2017) Single-molecule imaging reveals multiple pathways for the recruitment of translesion polymerases after DNA damage. *Nature Communications*, *8*(1), 2170.
- Tokunaga, M., Imamoto, N. and Sakata-Sogawa, K. (2008) Highly inclined thin illumination enables clear single-molecule imaging in cells. *Nature Methods*, *5*(2), 159–161.
- Trautinger, B.W., Jaktaji, R.P., Rusakova, E. and Lloyd, R.G. (2005) RNA polymerase modulators and DNA repair activities resolve conflicts between DNA replication and transcription. *Molecular Cell*, *19*(2), 247–258.
- Tuduri, S., Crabbé, L., Conti, C., Tourrière, H., Holtgreve-Grez, H., Jauch, A., et al. (2009) Topoisomerase I suppresses genomic instability by preventing interference between replication and transcription. *Nature Cell Biology*, *11*(11), 1315–1324.
- Uphoff, S., Reyes-Lamothe, R., De Leon, F.G., Sherratt, D.J. and Kapanidis, A.N. (2013) Single-molecule DNA repair in live bacteria. *Proceedings of the National Academy of Sciences of the United States of America*, *110*(20), 8063–8068.
- Uyemura, D. and Lehman, I. (1976) Biochemical characterization of mutant forms of DNA polymerase I from *Escherichia coli*. I. The polA12 mutation. *The Journal of Biological Chemistry*, *251*(13), 4078–4084.
- Vilette, D., Ehrlich, D.S. and Michel, B. (1996) Transcription-induced deletions in plasmid vectors: M13 DNA replication as a source of instability. *Molecular and General Genetics*, *252*(4), 398–403.
- Wahba, L., Amon, J.D., Koshland, D. and Vuica-Ross, M. (2011) RNase H and multiple RNA biogenesis factors cooperate to prevent RNA:DNA hybrids from generating genome instability. *Molecular Cell*, *44*(6), 978–988.
- Walker, G.C., Smith, B.T. and Sutton, M.D. (2000) The SOS response to DNA damage. In: Storz, R. and Hengge-Aronis, G. (Eds.) *Bacterial Stress Responses* (pp. 131–144. Washington D.C.: American Society of Microbiology Press.
- Wang, J.D., Berkmen, M.B. and Grossman, A.D. (2007) Genome-wide co-orientation of replication and transcription reduces adverse effects on replication in *Bacillus subtilis*. *Proceedings of the National Academy of Sciences of the United States of America*, *104*(13), 5608–5613.
- Washburn, R.S. and Gottesman, M.E. (2011) Transcription termination maintains chromosome integrity. *Proceedings of the National Academy of Sciences of the United States of America*, *108*(2), 792–797.
- Wessel, S.R., Marceau, A.H., Massoni, S.C., Zhou, R., Ha, T., Sandler, S.J., et al. (2013) PriC-mediated DNA replication restart requires PriC complex formation with the single-stranded DNA-binding protein. *Journal of Biological Chemistry*, *288*, 17569–17578.
- Westover, K.D., Bushnell, D.A. and Kornberg, R.D. (2004) Structural basis of transcription: separation of RNA from DNA by RNA polymerase II. *Science*, *303*(5660), 1014–1016.
- Willets, N.S., Clark, A.J. and Low, B. (1969) Genetic location of certain mutations conferring recombination deficiency in *Escherichia coli*. *Journal of Bacteriology*, *97*(1), 244–249.
- Zawadzki, P., Stracy, M., Ginda, K., Zawadzka, K., Lesterlin, C., Kapanidis, A.N., et al. (2015) The localization and action of topoisomerase IV in *Escherichia coli* chromosome segregation is coordinated by the SMC complex, MukBEF. *Cell Reports*, *13*(11), 2587–2596.

SUPPORTING INFORMATION

Additional supporting information may be found online in the Supporting Information section.

How to cite this article: Wolak, Ma HJ, Soubry N, Sandler SJ, Reyes-Lamothe R, Keck JL. Interaction with single-stranded DNA-binding protein localizes ribonuclease HI to DNA replication forks and facilitates R-loop removal. *Mol Microbiol.* 2020;114:495–509. <https://doi.org/10.1111/mmi.14529>